UNIVERSIDADE FEDERAL DE MINAS GERAIS

Faculdade de Medicina

Programa de Pós-Graduação em Ciências Aplicadas à Cirurgia e Oftalmologia

Ricardo Gonçalves Alvim

A IMUNOTERAPIA COMBINADA COM AGONISTA OX40 E INIBIDOR DE PD-1 MELHORA A EFICÁCIA DA TERAPIA FOTODINÂMICA VASCULAR (VTP) EM UM MODELO DE TUMOR UROTELIAL

Belo Horizonte, Minas Gerais

2024

Ricardo Gonçalves Alvim

A IMUNOTERAPIA COMBINADA COM AGONISTA OX40 E INIBIDOR DE PD-1 MELHORA A EFICÁCIA DA TERAPIA FOTODINÂMICA VASCULAR (VTP) EM UM MODELO DE TUMOR UROTELIAL

Tese apresentada ao Programa de Pós-Graduação em Ciências Aplicadas à Cirurgia e Oftalmologia, da Faculdade de Medicina da Universidade Federal de Minas Gerais, como requisito parcial à obtenção do título de Doutor em Medicina.

Área de Concentração: Etiopatogenia cirúrgica

Linha de Pesquisa: Repercussões locais e sistêmicas a lesões teciduais e fármacos aplicados em cirurgia.

Orientador: Prof. Augusto Barbosa Reis

Belo Horizonte, Minas Gerais
2024

AL475i

Alvim, Ricardo Gonçalves.
A Imunoterapia combinada com Agonista OX40 e Inibidor de PD-1 melhora a eficácia da Terapia Fotodinâmica Vascular (VTP) em um modelo de Tumor Urotelial [recurso eletrônico]. / Ricardo Gonçalves Alvim. - - Belo Horizonte: 2024.
100f.: il.
Formato: PDF.
Requisitos do Sistema: Adobe Digital Editions.

Orientador (a): Augusto Barbosa Reis.
Área de concentração: Etiopatogenia Cirúrgica.
Tese (doutorado): Universidade Federal de Minas Gerais, Faculdade de Medicina.

1. Carcinoma de Células de Transição. 2. Técnicas de Ablação. 3. Neoplasias da Próstata. 4. Imunoterapia. 5. Dissertação Acadêmica. I. Reis, Augusto Barbosa. II. Universidade Federal de Minas Gerais, Faculdade de Medicina. III. Título.

NLM: QW 940

Bibliotecário responsável: Fabian Rodrigo dos Santos CRB-6/2697

UNIVERSIDADE FEDERAL DE MINAS GERAIS

FACULDADE DE MEDICINA - CENTRO DE PÓS-GRADUAÇÃO
PROGRAMA DE PÓS-GRADUAÇÃO EM CIÊNCIAS APLICADAS À CIRURGIA E À OFTALMOLOGIA

ATA DE DEFESA DE TESE

Às treze horas do dia vinte e três de setembro de dois mil e vinte e quatro, na Faculdade de Medicina, na sala 526, realizou-se a sessão pública para a defesa da Tese de **RICARDO GONÇALVES ALVIM**. A presidência da sessão coube ao Prof. Augusto Barbosa Reis (orientador). Inicialmente, o presidente fez a apresentação da Comissão Examinadora assim constituída: Prof. Augusto Barbosa Reis (Orientador) - UFMG, Prof. Geraldo Felício da Cunha Júnior - Hospital Semper, Prof. Renato Beluco Corradi Fonseca - Hospital Luxemburgo, Prof. Bruno Mello Rodrigues dos Santos - UFMG e Prof. Daniel Xavier Lima - UFMG. Em seguida, o candidato fez a apresentação do trabalho que constitui sua Tese de Doutorado, intitulada: A IMUNOTERAPIA COMBINADA COM AGONISTA OX40 E INIBIDOR DE PD-1 MELHORA A EFICÁCIA DA TERAPIA FOTODINÂMICA VASCULAR (VTP) EM UM MODELO DE TUMOR UROTELIAL. Seguiu-se a arguição pelos examinadores e logo após, a Comissão reuniu-se, sem a presença do candidato e do público e decidiu considerar aprovado a Tese de Doutorado. O resultado final foi comunicado publicamente ao candidato pelo presidente da Comissão. Nada mais havendo a tratar, o presidente encerrou a sessão e lavrou a presente ata que, depois de lida, se aprovada, será assinada pela Comissão Examinadora.

Belo Horizonte, 23 de setembro de 2024.

Assinatura dos membros da banca examinadora:

Documento assinado eletronicamente por **Bruno Mello Rodrigues dos Santos**, **Professora do Magistério Superior**, em 24/09/2024, às 16:05, conforme horário oficial de Brasília, com fundamento no art. 5º do Decreto nº 10.543, de 13 de novembro de 2020.

Documento assinado eletronicamente por **Geraldo Felício da Cunha Júnior**, **Usuário Externo**, em 24/09/2024, às 17:38, conforme horário oficial de Brasília, com fundamento no art. 5º do Decreto nº 10.543, de 13 de novembro de 2020.

Documento assinado eletronicamente por **Daniel Xavier Lima**, **Professor do Magistério Superior**, em 24/09/2024, às 22:59, conforme horário oficial de Brasília, com fundamento no art. 5º do Decreto nº 10.543, de 13 de novembro de 2020.

Documento assinado eletronicamente por **Renato Beluco Corradi Fonseca**, **Usuário Externo**, em 25/09/2024, às 15:33, conforme horário oficial de Brasília, com fundamento no art. 5º do Decreto nº 10.543, de 13 de novembro de 2020.

Documento assinado eletronicamente por **Augusto Barbosa Reis**, **Chefe de divisão**, em 03/10/2024, às 09:05, conforme horário oficial de Brasília, com fundamento no art. 5º do Decreto nº 10.543, de 13 de novembro de 2020.

Reitora

Professora Sandra Regina Goulart Almeida

Vice-Reitor

Professor Alessandro Fernandes Moreira

Pró-Reitora de Pós-Graduação

Professora Isabela Almeida Pordeus

Pró-Reitor de Pesquisa

Professor Fernando Marcos dos Reis

FACULDADE DE MEDICINA

Diretora da Faculdade de Medicina

Professora Alamanda Kfoury Pereira

Vice-Diretora da Faculdade de Medicina

Professora Cristina Gonçalves Alvim

Coordenadora do Centro de Pós-Graduação

Professora Ana Cristina Simões e Silva

Subcoordenadora do Centro de Pós-Graduação

Professora Tereza Cristina de Abreu Ferrari

Coordenação do Programa de Pós-Graduação em Cirurgia e à Oftalmologia

Coordenadora: Professora Vivian Resende

Subcoordenador: Professor Tulio Pinho Navarro

Chefe do Departamento de Cirurgia da Faculdade de Medicina

Professor Cristiano Xavier Lima

Chefe do Departamento de Oftalmologia e de Otorrinolaringologia

Prof. Daniel Vitor de Vasconcelos

Colegiado do Programa de Pós-Graduação em Cirurgia e à Oftalmologia

Professor Alexandre Varella Giannetti

Professor Cristiano Xavier Lima

Professor Marco Antônio Percope de Andrade

Professor Daniel Vitor de Vasconcelos Santos

RESUMO

Objetivo: A terapia fotodinâmica vascular (VTP) é uma abordagem de ablação tumoral usada para tratar o câncer de próstata em estágio inicial e também pode ser eficaz para o câncer urotelial do trato urinário superior (UTUC) com base em dados pré-clínicos. No sentido de aumentar as taxas de resposta ao VTP, avaliamos sua eficácia em combinação com inibidor de PD-1 com agonista de OX40 em um modelo animal de tumor urotelial.

Projeto experimental: Em camundongos aloenxertados com células MB-49 UTUC, comparamos os efeitos do VTP combinado com o inibidor PD-1 e agonista OX40 em relação ao crescimento tumoral, sobrevida, ocorrência de metástase pulmonar e respostas imunes antitumorais.

Resultados: A combinação de VTP com inibidor de PD-1 e agonista de OX40 inibiu o crescimento do tumor e prolongou a sobrevida em um grau maior do que VTP com qualquer um dos imunoterápicos individualmente. Esses efeitos resultam do aumento da infiltração tumoral e proliferação intratumoral de células T citotóxicas e auxiliares, depleção de células Treg e supressão de células supressoras derivadas de mieloides.

Conclusões: Nossos resultados sugerem que o VTP sinergiza-se com o bloqueio de PD-1 e agonista OX40 para promover fortes respostas imunes antitumorais, produzindo eficácia terapêutica em um modelo animal de câncer urotelial.

Palavras-chave: câncer urotelial, ablação tumoral, TOOKAD, terapia focal, imunoterapia

ABSTRACT

Purpose: Vascular targeted photodynamic therapy (VTP) is a non-surgical tumor ablation approach used to treat early-stage prostate cancer and may also be effective for upper tract urothelial cancer (UTUC) based on preclinical data. Toward increasing response rates to VTP, we evaluated its efficacy in combination with concurrent PD-1 inhibitor/OX40 agonist immunotherapy in a urothelial tumor-bearing model.

Experimental design: In mice allografted with MB-49 UTUC cells, we compared the effects of combined VTP with PD-1 inhibitor/OX40 agonist with those of the component treatments on tumor growth, survival, lung metastasis, and antitumor immune responses.

Results: The combination of VTP with both PD-1 inhibitor and OX40 agonist inhibited tumor growth and prolonged survival to a greater degree than VTP with either immunotherapeutic individually. These effects result from increased tumor infiltration and intratumoral proliferation of cytotoxic and helper T cells, depletion of Treg cells, and suppression of myeloid-derived suppressor cells.

Conclusions: Our findings suggest that VTP synergizes with PD-1 blockade and OX40 agonist to promote strong antitumor immune responses, yielding therapeutic efficacy in an animal model of urothelial cancer.

Keywordds: urothelial carcinoma, tumor ablation, TOOKAD, focal therapy, immunotherapy

LISTA DE FIGURAS E GRÁFICOS

LISTA DE ABREVIATURAS

BCG: *Bacillus Calmette-Guerin*

CIS: Carcinoma In Situ

MB-49: Murine Bladder 49

MIBC: Tumor vesical músculo invasivo

MSKCC: Memorial Sloan Kettering Cancer Center

NMIBC: Tumor de bexiga não músculo-invasivo

PD-1: Program death-1

RLO: Radicais livres de oxigênio

RTU: Ressecção Transuretral

Teff: Linfócitos T Efetores

Treg: Linfócitos T Reguladores

TTUA: Tumores de Trato Urinário Alto/Superior

VPO: VTP associado a terapia com inibidor PD-1 + agonista OX-40

VTP: Terapia vascular fotodinâmica (Vascular Targeted Photodynamic Therapy)

WST 11: Water Soluble Tookad

SUMÁRIO

1. INTRODUÇÃO

O carcinoma urotelial representa o sexto tumor maligno mais comum entre os homens nos Estados Unidos e é mais prevalente entre os homens com mais de 60 anos (1). Em pacientes com tumores uroteliais pequenos de baixo grau, bem como aqueles nos quais a preservação funcional é especialmente crítica (ou seja, pacientes com rim único, função renal deficiente e/ou não elegíveis para cistectomia/nefro-ureterectomia), as terapias ablativas locais surgiram como um meio promissor de reduzir a morbidade do tratamento e priorizando a preservação renal/funcional (3,4).

A terapia VTP empregando WST11 (TOOKAD Soluble, Steba Biotech, França) foi clinicamente aprovada na Europa e no México em 2017 para câncer de próstata localizado em estágio inicial (5-7) e demonstrou eficácia em vários modelos animais de carcinoma urotelial (7,8). WST-11 é um fotossensibilizador administrado por via intravenosa e tem meia-vida de 60 minutos. A iluminação a laser confinada fornecida por meio de fibras ópticas ativa a droga localmente e induz a liberação rápida de substâncias tóxicas, principalmente radicais livres de vida curta, dentro dos vasos sanguíneos do tumor, levando à oclusão vascular e, finalmente, à necrose do tumor 48 horas após o tratamento (9).

Embora o VTP possa erradicar os tumores uroteliais, a taxa de cura no modelo de camundongo padrão é de apenas aproximadamente 30%. Para aumentar sua eficácia, o VTP foi combinado com inibidores de checkpoint imunológico capazes de induzir respostas imunológicas antitumorais por meio de uma reação inflamatória rápida e proeminente (10). A atividade do VTP com inibidores de checkpoint, como anti-PD-1 e anti-CTLA-4, foi demonstrada em estudos com animais, nos quais a taxa de resposta completa é superior a 40% (7,11). A combinação de drogas imunomoduladoras com inibidores de checkpoint imunológico tem recebido considerável atenção como forma de aumentar o benefício destes últimos, que podem induzir respostas clínicas e imunológicas potentes em uma minoria de pacientes (12).

1.1 Objetivos

Objetivo Principal

Nesse estudo, postulamos que a combinação de VTP com bloqueio de PD-1 e imunoterapia agonística OX40 aumentaria a eficácia terapêutica no câncer urotelial, induzindo imunidade antitumoral de longa duração.

Objetivos Secundários

- Avaliar a resposta imunológica (linfócitos T) local e sistêmica.
- Avaliar a prevenção de metástases.

2. REVISÃO DA LITERATURA

2.1. Epidemiologia

Os tumores uroteliais, em especial o carcinoma urotelial, representam um importante problema de saúde pública devido à sua prevalência e forte associação com fatores ambientais (1,2). Trata-se de um câncer relativamente comum, correspondendo a aproximadamente 3% de todos os cânceres diagnosticados. Dados recentes da Globocan em 2022 destacam a posição do câncer de bexiga entre os dez tipos de câncer mais comuns em nível mundial. Se considerarmos apenas pacientes do sexo masculino, o câncer de bexiga ocupa a sexta posição, sendo a nona causa mais comum de morte por câncer (39).

A incidência de tumores uroteliais varia significativamente conforme sua localização no trato urinário. Aproximadamente 90% desses tumores ocorrem na bexiga, enquanto os 10% restantes se originam no trato urinário superior (TTUA). Essa distribuição anatômica também se reflete nas diferenças de incidência entre os sexos: os tumores uroteliais da bexiga afetam os homens em uma proporção de 4:1 em relação às mulheres, enquanto nos TTUA essa proporção é de 2:1. Aproximadamente 60% dos tumores do trato urinário superior (pelve renal e ureter) são invasivos no momento do diagnóstico, enquanto essa taxa é significativamente menor nos tumores de bexiga, variando entre 15% e 25%.

2.2. Estadiamento

Os tumores confinados à mucosa e que invadem a lâmina própria são classificados como Ta e T1, respectivamente, de acordo com a classificação TNM (Tumor, Nódulo e Metástase). Tumores planos de alto grau, restritos à mucosa, são categorizados como carcinoma in situ (CIS). Esses tumores, conhecidos como tumores não músculo-invasivos da bexiga (NMIBC), podem ser tratados por meio de ressecção transuretral (RTU) da bexiga e instilações intravesicais, como veremos adiante. Em contraste, tumores que invadem a camada muscular do urotélio, o tecido perivesical e estruturas adjacentes da bexiga são classificados como T2, T3 e T4, respectivamente, sendo considerados tumores invasivos (MIBC) (Anexo B).

2.3. Tratamento

2.3.1. Câncer de Bexiga

O tratamento inicial do câncer de bexiga é comumente realizado por meio de ressecção transuretral do tumor (RTU). Esse procedimento tem como objetivo a ressecção completa de todos os tumores visualizados durante a cistoscopia. A escolha do tratamento subsequente está intimamente relacionada ao estadiamento e à histologia do tumor. Nos tumores não músculo-invasivos, particularmente aqueles maiores que 3 cm, que invadem a lâmina própria, e/ou os tumores recorrentes, ou classificados como de alto grau (incluindo carcinoma in situ), é recomendada a terapia adjuvante com BCG (Bacilo de Calmette-Guérin) ou quimioterapia (Gemcitabina/Mitomicina) intravesical (34). O objetivo dessa terapia é reduzir as taxas de progressão e recidiva tumoral.

No entanto, deve-se considerar que o uso de BCG e/ou quimioterápicos podem estar associados a efeitos colaterais, incluindo complicações graves em até 5% dos casos. Essas complicações podem limitar, e muito, seu uso.

Para pacientes que apresentam tumores músculo-invasivos ou mesmo superficiais, mas que têm um alto risco de progressão ou recidiva, a cistectomia radical acompanhada de linfadenectomia pélvica é o tratamento padrão. A cistectomia radical é reconhecida como o melhor e mais eficiente tratamento curativo disponível para esses pacientes, embora esteja associada a um índice significativo de complicações pós-operatórias. Cerca de 25-30% dos pacientes apresentam complicações graves, classificadas como Clavien-Dindo grau ≥ 3. Além disso, essa cirurgia exige a realização de derivações urinárias, que podem impactar consideravelmente a qualidade de vida dos pacientes, devido às alterações funcionais e metabólicas associadas à perda da bexiga; incluindo o risco de doença renal crônica dialítica de até 20% em 5 anos (Apêndice C).

2.3.2 Tumores do trato urinário alto

A nefroureterectomia com ressecção do cuff vesical é considerada o tratamento padrão-ouro para o manejo dos TTUA. Esta abordagem cirúrgica envolve a remoção completa do rim afetado, do ureter e de uma porção da bexiga onde o ureter se insere, garantindo a remoção abrangente do tecido tumoral e minimizando o risco de recorrência local.

No entanto, em casos selecionados, especialmente em pacientes de baixo risco, pode-se optar por uma cirurgia preservadora do rim (tratamento endoscópico principalmente), com o objetivo de preservar a função renal sem comprometer os resultados oncológicos. Essa abordagem é considerada segura e eficaz em situações em que o tumor é pequeno, de baixo grau e localizado de forma que permita uma excisão completa, mantendo a função renal.

Em pacientes de alto risco, incluindo aqueles com tumores de alto grau, grandes, multifocais ou com invasão profunda, a preservação renal é geralmente contraindicada devido ao maior risco de recorrência e progressão da doença. No entanto, a cirurgia preservadora do rim pode ser considerada em situações excepcionais, como em pacientes com insuficiência renal crônica ou com rim solitário, onde a perda da função renal pode levar à necessidade de diálise. Nesses casos, a decisão cirúrgica deve ser cuidadosamente ponderada, levando em conta a necessidade de balancear o controle oncológico rigoroso com a preservação da função renal remanescente.

2.4 Vascular Targeted Therapy (VTP) – Terapia Vascular Fotodinâmica

De maneira geral, a terapia fotodinâmica é uma modalidade de tratamento que utiliza a combinação de luz, um agente fotossensibilizador e oxigênio para destruir seletivamente células anormais como as células cancerígenas. O processo envolve três etapas principais:

1. Administração do Fotossensibilizador: Um agente fotossensibilizador, que é uma substância química que se acumula preferencialmente nas células-alvo, é administrado ao paciente. Esse agente é inicialmente inerte e não tóxico.
2. Ativação por Luz: Após a administração do fotossensibilizador, a área-alvo do corpo, onde as células anormais estão localizadas, é exposta a uma fonte de luz de uma determinada frequência que corresponde à absorção do fotossensibilizador. Essa luz ativa o fotossensibilizador.
3. Produção de Espécies Reativas de Oxigênio (RLO): A ativação do fotossensibilizador pela luz leva à geração de espécies reativas de oxigênio, que são moléculas altamente reativas que causam dano celular. Esses danos podem incluir a destruição das membranas celulares, proteínas, ácidos nucleicos ou endotélio vascular, resultando na morte das células no tecido tratado

A terapia fotodinâmica é utilizada no tratamento de vários tipos de cânceres, incluindo cânceres de pele, esôfago, pulmão e próstata, além de algumas condições não oncológicas. Ela é particularmente útil para tumores localizados, pois permite a destruição seletiva das células tumorais com danos mínimos ao tecido saudável circundante. Além disso, ela pode ser combinada com outras modalidades terapêuticas para potencializar o efeito antitumoral e promover a cura da doença.

A Terapia Fotodinâmica Vascular (VTP) é uma abordagem terapêutica inovadora que se distingue por seu mecanismo de ação focada na vasculatura tumoral. Utilizando o agente fotossensibilizante WST11 (Tookad® Solúvel, Steba Biotech, França), a VTP tem como alvo primário os vasos sanguíneos que nutrem o tumor, essencialmente interrompendo o suprimento de sangue e, consequentemente, levando à morte das células tumorais por necrose/apoptose celular.

O processo terapêutico começa com a administração intravenosa do WST11, que é um composto fotossensibilizante solúvel em água derivado da clorofila. Este agente possui uma alta afinidade pela circulação sanguínea e, diferentemente de outros fotossensibilizadores que se acumulam diretamente nas células tumorais, o WST11 permanece predominantemente no sistema vascular. Após a aplicação local de uma fonte de luz laser específica, com um comprimento de onda que corresponde à absorção máxima do WST11, esse agente é ativado e uma cascata de reações químicas é iniciada, gerando uma rápida produção de espécies reativas de oxigênio (RLO), principalmente radicais livres que são altamente citotóxicos. Estes radicais livres provocam danos oxidativos graves às células endoteliais que revestem os vasos sanguíneos do tumor. Como resultado, ocorre uma destruição seletiva da vasculatura tumoral, induzindo a interrupção do fluxo de sangue e, consequentemente a necrose tumoral/tecidual.

Além de causar necrose direta das células tumorais por privação de sangue, a VTP tem sido associada a um efeito imunológico sistêmico. A destruição da vasculatura tumoral e a subsequente morte celular liberam antígenos tumorais no sistema imunológico, que pode ser estimulado a reconhecer e destruir células tumorais remanescentes ou metastáticas em outras partes do corpo (efeito episcopal). Esse processo envolve principalmente a imunidade celular, mediada por células T, mas também a imunidade humoral, envolvendo a produção de anticorpos contra antígenos tumorais. Assim, a VTP não só combate o tumor localmente, mas também pode promover uma resposta imunológica de longa duração contra o câncer,

potencialmente prevenindo a recorrência da doença. Atualmente, o VTP é apresentado como uma forma de imunoterapia.

A aplicação da VTP no trato urinário humano era uma abordagem inédita até o início dos experimentos recentes. Primeiramente, um estudo pré-clínico utilizando modelos suínos, foi realizado focando na avaliação dos efeitos histológicos e fisiológicos da VTP nos ureteres e rins dos animais. Nesse estudo, os suínos foram submetidos à injeção intravenosa de WST11, seguida por uma sessão de iluminação com laser por um período de 10 minutos. O principal objetivo foi avaliar o impacto da terapia nos tecidos tratados e monitorar a evolução dos animais no período pós-operatório. Os resultados indicaram que a função renal e os níveis de hemoglobina permaneceram dentro dos limites normais após o tratamento (8)

As análises histológicas retiradas dos animais desse experimento mostraram regeneração do urotélio superficial nas áreas tratadas, sem evidências de obstruções sintomáticas ou hidronefrose significativa após um período de quatro semanas. Esses achados comprovaram que a VTP é uma abordagem segura e eficaz para o tratamento de tumores no trato urinário, fornecendo base para seu potencial aplicação clínica em seres humanos e estabelecendo novas perspectivas para o manejo terapêutico dessa condição.

Recentemente, um estudo de fase 1 da Terapia Fotodinâmica Vascular (VTP) com o fotossensibilizador WST11 (Tookad® Solúvel, Steba Biotech, França) para o tratamento do carcinoma urotelial foi publicado (41). Nesse estudo, 19 pacientes com carcinoma urotelial foram tratados com VTP e a segurança foi monitorada com foco em efeitos adversos. Esses efeitos foram predominantemente leves, sem eventos graves (Clavien >2) relacionados ao tratamento. A eficácia foi avaliada por biópsias e exames de imagem, revelando uma resposta positiva em alguns pacientes, com significativa redução do tamanho do tumor e resposta completa ou parcial em mais de 90% dos casos. Esses resultados iniciais indicam que a VTP é uma abordagem segura e promissora para o carcinoma urotelial, sugerindo a necessidade de estudos adicionais para validar a eficácia e refinar o protocolo de tratamento.

2.5 Imunoterapia

A terapia intravesical com Bacillus Calmette-Guérin (BCG) para o câncer de bexiga foi introduzida por Morales, Eidinger e Bruce A. em 1976. Eles observaram que o BCG poderia induzir inflamação e ativar o sistema imunológico para combater células tumorais. Desde então,

o sucesso da imunoterapia com BCG no tratamento do carcinoma urotelial gerou interesse na investigação de outros agentes imunoterápicos para o tratamento desses tumores.

Os checkpoints imunológicos são moléculas reguladoras que desempenham um papel crucial na modulação da resposta imune. Eles podem ser encontrados na superfície das células imunológicas, como os linfócitos T, e atuam como "interruptores" que podem ativar ou inibir a atividade dessas células. A função principal dos checkpoints imunológicos é garantir que a resposta imune seja equilibrada, evitando reações excessivas que podem levar a danos aos tecidos do próprio organismo. A avaliação do receptor PD-1 (Programmed Death-1) no tratamento do câncer de bexiga tem sido um campo ativo de pesquisa, especialmente com o desenvolvimento de inibidores desse checkpoint imunológico que visa melhorar a resposta imune antitumoral. Ensaios clínicos iniciais demonstraram que os inibidores de PD-1, como o pembrolizumab e o nivolumab, apresentaram uma resposta significativa em pacientes com câncer de bexiga avançado ou metastático. Em vários estudos, esses agentes mostraram taxas de resposta objetiva variando de 20% a 30%, com alguns pacientes apresentando respostas duradouras (42). Além disso, o uso desses agentes no câncer de bexiga superficial de alto grau, não responsivo ao BCG, também tem se mostrado eficaz, com taxa de resposta completa em torno de 19%, após um ano de seguimento.

Um alvo imunomodulador atraente é o receptor coestimulador de células T denominado OX40 (CD134). Ele é um membro da superfamília do receptor do fator de necrose tumoral (TNFRSF) que atua sobre as vias de sinalização de células T que promovem a sobrevivência, proliferação e produção de citocinas (13). O conceito de ativação de OX40 para o tratamento de câncer tem recebido atenção crescente devido à sua capacidade de melhorar a eficácia das respostas imunes contra células tumorais

Estudos pré-clínicos demonstraram que os anticorpos agonistas OX40 podem aumentar a imunidade antitumoral por meio da expansão das células T, levando a uma melhor sobrevida livre de progressão (14-17). O agonismo de OX40 demonstrou aumentar a eficácia dos inibidores de checkpoint em modelos de diferentes tipos de cânceres (18-21).

Até o presente momento, nenhum ensaio clínico foi publicado avaliando a eficácia desse agente no tratamento do câncer urotelial em humanos.

2.5.1 Combinações de imunoterapia

Estudos combinados mostraram respostas promissoras, mas também têm sido associados a um aumento na incidência de efeitos colaterais graves. A combinação de nivolumabe e ipilimumabe, por exemplo, demonstrou um benefício clínico em alguns pacientes com câncer de bexiga, embora o perfil de segurança precise ser cuidadosamente monitorado (42).

A combinação de quimioterapia com inibidores de PD-1/PD-L1 também tem sido estudada em câncer de bexiga, com resultados que mostram uma capacidade da quimioterapia em sensibilizar o tumor à imunoterapia, embora mais uma vez, os efeitos colaterais e a eficácia precisam ser cuidadosamente avaliados.

As combinações de imunoterapia têm o potencial de melhorar significativamente o tratamento do câncer de bexiga, oferecendo novas estratégias para superar a resistência ao tratamento e aumentar as taxas de resposta. No entanto, o desenvolvimento e a implementação dessas combinações exigem uma compreensão aprofundada dos mecanismos imunológicos envolvidos, bem como a gestão cuidadosa de efeitos colaterais e a seleção apropriada de pacientes. Esses ensaios clínicos contínuos são essenciais para validar a eficácia e a segurança dessas abordagens combinadas.

2.6 Terapia fotodinâmica e imunoterapia

A combinação da Terapia Fotodinâmica Vascular (VTP) com imunoterapia emergiu como uma abordagem inovadora no tratamento do câncer urotelial. Este método visa potencializar os efeitos antitumorais da VTP por meio da modulação do sistema imunológico, aproveitando as sinergias entre a destruição direta do tumor e a estimulação da resposta imune.

Embora o VTP possa erradicar os tumores uroteliais, a taxa de cura no modelo de camundongo padrão é em torno de 30%. Para aumentar sua eficácia, o VTP foi combinado com inibidores de checkpoint imunológico capazes de induzir respostas imunológicas antitumorais por meio de uma reação inflamatória rápida e proeminente (10). A atividade do VTP com inibidores de checkpoint, como anti-PD-1 e anti-CTLA-4, foi demonstrada em estudos com animais, nos quais a taxa de resposta completa é superior a 40% (7, 11).

3. METODOLOGIA

3.1 Aspectos Éticos

Todos os procedimentos envolvendo animais estavam de acordo com as regras éticas do MSKCC, instituição em que foram realizados os procedimentos. O projeto e o protocolo deste estudo foram aprovados pelo *Institutional Review Board* e pelo comitê institucional de cuidados dos animais (APÊNDICE A)

3.2 Cultura de células

Para realização dos experimentos foi necessário o desenvolvimento de uma linhagem celular adequada para o estudo. A linha celular tumoral utilizada nos estudos foi a *Murine Bladder 49* (MB-49). São células tumorais originadas em bexigas de camundongos machos C57BL/6, induzidas pela utilização de um carcinógeno aplicado intravesicalmente. As células MB-49 foram cultivadas em solução de *Dulbecco's modified eagle media*, suplementado com solução de soro fetal bovino a 10%, penicilina/estreptomicina a 1% e piruvato de sódio a 0,1%.

3.3 Geração de linha MB-49 expressando Luciferase

Para geração de células MB-49, que expressam luciferase (MB-49-luc), foram utilizados genes de vírus de células estaminais de camundongo (MSCV) -puromicina-Luciferase-GFP. O PMSCV-puro-Luciferase-GFP foi transferido para células de empacotamento retroviral *pantropic* GP2-293 (BD Biosciences, San Jose, CA), utilizando lipofectamina 2000 (Invitrogen, Grand Island, NY) e o retrovírus recolhido foi utilizado para infectar células MB-49. As células infectadas foram selecionadas com 0,5 μg/mL de puromicina (Invitrogen, Grand Island, NY) e o conjunto sobrevivente de células foi designado MB49/luciferase. A infecção foi realizada com 6 μg/mL de polibreno (Sigma, St. Louis, MO).

3.4 Estudos *in* vivo

Foram utilizados camundongos C57BL/6 machos de sete a oito semanas de idade (*Taconic Farms*) em todos os diferentes experimentos conduzidos (avaliação de tumor e de metástases pulmonares, sobrevida e citometria de fluxo). A escolha pela utilização de camundongos machos se deu em razão destes serem menos influenciados pelas oscilações hormonais em comparação com as fêmeas. Os camundongos da espécie C57BL/6 apresentam

sistema imune intacto e necessário para se testar os efeitos da imunoterapia. Além disso, a linhagem celular escolhida é proveniente desta espécie e a utilização de outra espécie poderia influir negativamente no desenvolvimento e uniformidade de crescimento dos tumores inoculados.

As células MB-49 marcadas com luciferase foram obtidas da American Type Culture Collection (ATCC; Manassas, VA) e cultivadas em meio RPMI suplementado com soro fetal de vitela a 10% (Life Technologies / Thermo Fisher Scientific, Waltham, MA). Antes da implantação do tumor, os camundongos foram anestesiados com isoflurano inalado, meloxicam (2 mg / kg) e buprenorfina (0,5 mg / kg), e o cabelo e a pele sobre o flanco direito foram esterilizados usando uma solução de iodopovidona e álcool etílico. Células MB-49 (50.000 células / µL) foram implantadas no flanco direito (Figura 1)

Figura 1: Modelo tumoral subcutâneo usado no experimento

Quatorze dias após a implantação do tumor, os camundongos foram avaliados quanto à formação de tumor usando imagem de bioluminescência não invasiva- IVIS. As regiões de interesse das imagens exibidas foram desenhadas com base na intensidade do sinal e quantificadas usando o software Living Image versão 2.60. O sinal específico foi calculado como a razão entre o sinal bioluminescente na região de interesse e o sinal bioluminescente em uma região de fundo que não contém tumores. Quando o volume do tumor atingiu aproximadamente 100 mm3, os animais foram atribuídos aleatoriamente aos seguintes grupos de estudo: controles (n = 5), inibidor PD-1 (n = 5), agonista OX40 (n = 5), inibidor PD-1 e agonista OX40 (n = 10), VTP (n = 10), VTP e agonista OX40 (n = 10), VTP e inibidor PD-1

(n = 10) e VTP e agonista OX40 e inibidor PD-1 (n = 10) (Figura 2). Para comparação da sobrevida e crescimento do tumor, o experimento foi repetido duas vezes, exatamente no mesmo padrão, e os resultados foram reunidos para análise estatística.

Figura 2: Divisão dos grupos do estudo

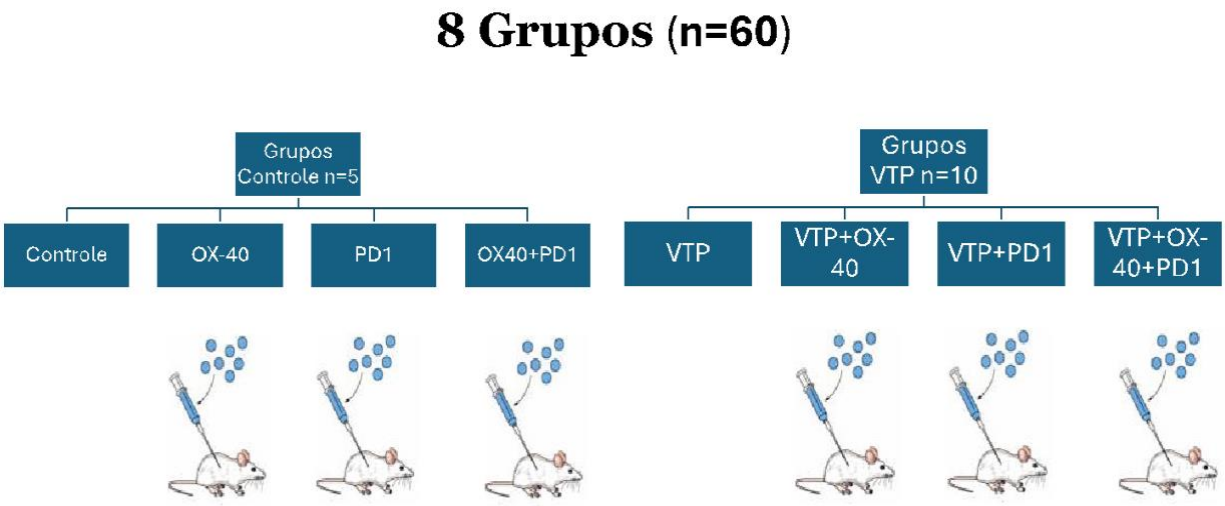

3.4.1 VTP, administração dos imunoterápicos e acompanhamento tumoral

Quinze dias após a implantação do tumor, camundongos com tumor foram anestesiados por injeção intraperitoneal (ip) de uma mistura de ketamina (150 mg / kg de peso corporal) e xilazina (10 mg / kg) mais isoflurano inalado administrado por meio de um cone nasal bem ajustado. Após a injeção retro-orbital de WST11 (9 mg / kg de peso corporal), os tumores foram iluminados com luz 753 nM fornecida via laser de diodo com uma fibra final de 600 µm (Biolitec, East Longmeadow, MA) por 10 min a 150 mW / cm2 (Figura 3).

Figura 3. Aplicação do VTP

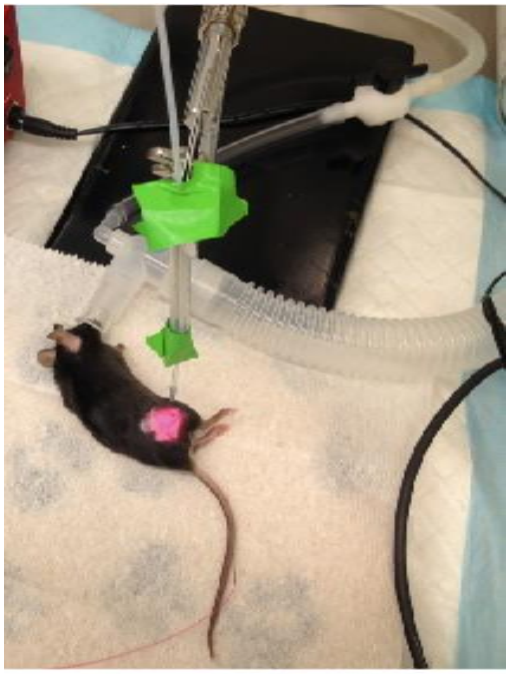

Nos subgrupos de inibidores de PD-1, InVivoPlus anti-camundongo PD-1 CD279 - Clone: 29F.1A12 (250 mg / kg, Bioxcell, West Lebanon, NH) foi injetado por via intraperitoneal (IP) nos dias 1, 4, 7, 10 , 13 e 16 após VTP. Nos subgrupos de agonistas OX40, InVivoPlus anti-camundongo OX40 CD134 - Clone: OX-86 (500 mg / kg, Bioxcell, West Lebanon, NH) foi injetado IP em uma única dose no dia 1 após VTP.

Pelo menos uma vez por semana até 90 dias após o tratamento com VTP, o volume do tumor foi medido, a saúde dos animais foi verificada e a imagem de espectro IVIS foi realizada para monitorar o tumor local e a metástase pulmonar. Quando os tumores excederam 2.000 mm3 ou metástases pulmonares foram demonstradas, os camundongos foram sacrificados por meio de 100% de dióxido de carbono a 5 PSI por um mínimo de 3 minutos. Essa prática de eutanásia está de acordo com os Métodos Recomendados para Animais de Laboratório do Centro de Recursos de Animais de Pesquisa de nossa instituição e com as Diretrizes da Associação Médica Veterinária Americana para a Eutanásia de Animais.

3.4.2 Imagem luminescente

Um dos desafios encontrados para monitorização do crescimento tumoral e desenvolvimento de metástases foi em relação a maneira como estas variáveis seriam monitoradas. Foi utilizada imaginologia bioluminescente para avaliar os camundongos dos

experimentos de avaliação de desenvolvimento de metástase e sobrevida. A opção pela bioluminescência se deu em razão de esta técnica refletir o número de células tumorais metabolicamente ativas e ser uma maneira objetiva de se mensurar o desenvolvimento de metástases pulmonares.

A imagem foi realizada com câmera sensível e refrigerada (IVIS®, Xenogen). A imagem e a quantificação dos sinais foram controladas pelo *software* de aquisição e análise *Living Image (Living Image*® – Xenogen). Os camundongos foram anestesiados (1-2,5% de isoflurano) e receberam D-luciferina (PerkinElmer Inc.), uma dose de 3 mg por animal, por injeção retro-orbital para imagens *in* vivo. Após, os camundongos foram colocados dentro da caixa de câmara resistente à luz, com exposição contínua a 1-2% de isoflurano. Os tempos de imagem foram de 1 segundo a 2 minutos. Os níveis de luz emitidos pelos tumores bioluminescentes foram detectados pelo sistema de câmara IVIS, integrados e exibidos. As regiões de interesse (ROI) das imagens exibidas foram designadas em torno dos locais do tumor e do pulmão e quantificadas como ROI/segundo usando o *software Living Image* (FIGURA 4).

Figura 4

• **Bioluminescência:** células MB49podem ser modificadas para expressar genes de bioluminescência (luciferase). Essa bioluminescência pode ser usada para monitorar a progressão local e o crescimento de metastases, por meio de imagem (IVIS).

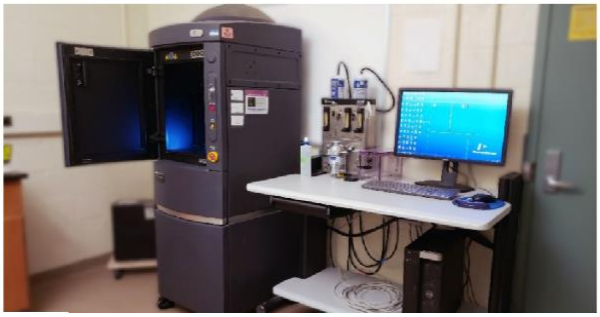

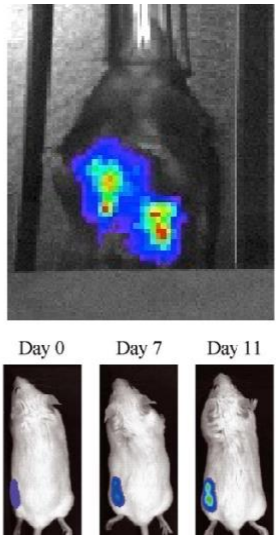

3.4.3 Imunohistoquímica

A imunohistoquímica (IHC) foi realizada para CD3, CD4, CD8 e OX40 (CD134). A IHC foi realizada em CD3, CD4 e CD8 usando um filtro automático Leica Bond RX com reagentes Bond (Leica Biosystems, Buffalo Grove, IL), incluindo um sistema de detecção de

polímero (DS9800, Novocastra Bond Polymer Refine Detection, Leica Biosystems). O cromógeno foi 3,3 diaminobenzidina tetracloreto (DAB), e os cortes foram contrastados com hematoxilina. A IHC foi realizada manualmente em OX40 (CD134) usando um sistema de detecção de avidina-biotina (Kit Vectastain Elite ABC HRP, Vector Laboratories, Burlingame, CA). O cromógeno foi 3,3 diaminobenzidina tetracloreto (DAB), e os cortes foram contrastados com hematoxilina. Os detalhes de cada marcador são mostrados na Figura 5.

As lâminas foram digitalizadas usando um scanner digital Pannoramic Flash 250 (3DHistech, Budapeste, Hungria) e uma objetiva Zeiss 20x / 0.8NA. As regiões de tecido relevantes foram denotadas e analisadas usando o Pannoramic Viewer (3DHistech, Budapest, Hungary). A coloração de CD3, CD4, CD8 e OX40 foi quantificada dentro dos tumores por contagem manual de células positivas dentro de regiões definidas.

Figura 5 – Histologia: imunohistoquimica

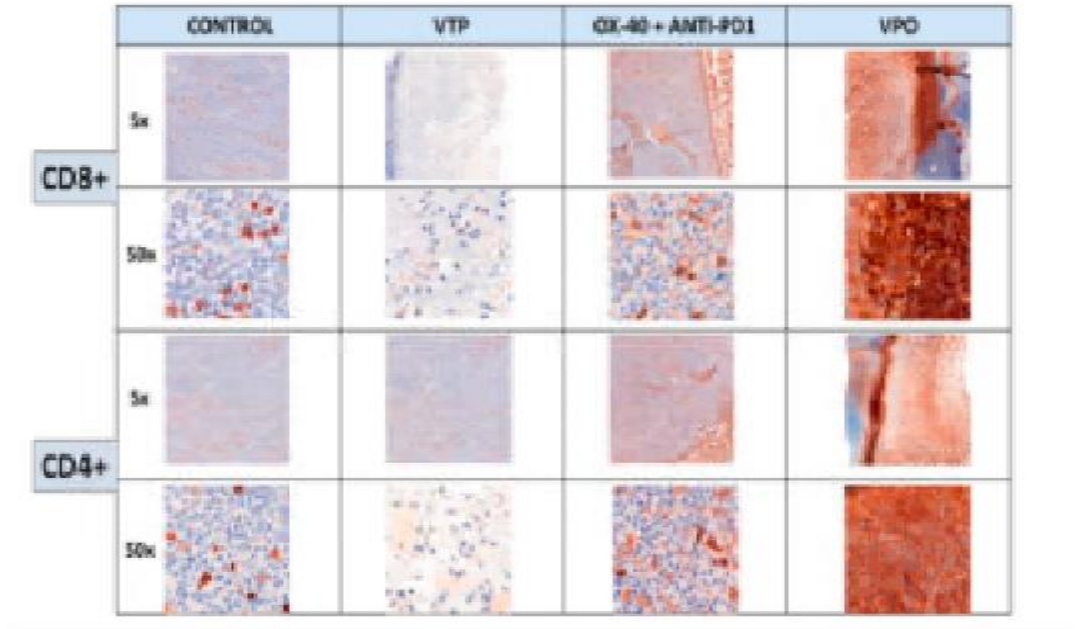

3.4.4 Experimento para avaliação de sobrevida

Os camundongos foram mantidos vivos por 90 dias. As mortes por metástases ou quando os tumores ultrapassassem o limite estabelecido pelo protocolo (2000 mm^3), foram

consideradas morte por câncer. A imagem bioluminescente foi realizada antes dos animais serem sacrificados.

3.4.5 Citometria de fluxo

As suspensões de células únicas foram preparadas a partir do baço, nódulos linfáticos ou tumores após dissociação mecânica e passagem por um filtro de náilon de 40 µm. Para todos os experimentos de citometria de fluxo, as suspensões de células únicas foram mantidas em tampão de citometria de fluxo (PBS, 2% FBS) e bloqueadas com CD16 / 32 anti-camundongo por 15 min a 4 ºC antes de incubar com os coquetéis de anticorpos apropriados no escuro por 30 min a 4 ºC. A coloração intracelular foi realizada usando reagentes Cytofix / Cytoperm (BD Biosciences, Catálogo No 554714) de acordo com as instruções do fabricante. Os anticorpos usados para o painel mieloide incluem CD45.2-FITC (BD 553772), CD11c-PE (BD 557401), CD8a-PE-Texas Red (Life Technologies MCD0817), Ly6G-PerCP-Cy5.5 (BD 560602), Ly6C -PE-Cy7 (5236982), MHC II-eFluor450 (eBioscience 48-5321-82), CD86-APC (BD 558703), CD11b-APC / eFluor 780 (eBioscience 47-0112-82). Os anticorpos usados para o painel de ativação de células T incluem Ki67-FITC (eBioscience 11-5698-82), CD62L-PE (BD 553151), GrzB-PE / Dazzle 594 (Biolegend 372216), CD8a-PerCP-Cy5.5 (BD 551162), CD44-PE / Cy7 (Biolegend 103030), CD4-V450 (BD 560468), Foxp3-APC (eBioscience 17-5773-82), CD45.2-Alexa Fluor700 (eBioscience 56-0454-82), CD25-APC / Cy7 (BD 557658). Ambos os painéis também incluem corante de viabilidade fixável eBioscience-eFluor506 (ThermoFisher 65-0866-14). As células foram quantificadas usando um analisador LSRFortessa (BD Biosciences, San Jose, CA) equipado com lasers de excitação de 350 nm, 405 nm, 488 nm, 561 nm e 640 nm.

Os dados foram coletados usando o software BD FACS Diva (BD Biosciences) e analisados usando o software FlowJo (Tree Star, Ashland, OR, EUA). Durante a aquisição, um portão CD45 + vivo foi definido de acordo com os parâmetros de dispersão, vivo / morto e coloração CD45. Um mínimo de 1-4 x105 células CD45 + vivas foram adquiridas por amostra. A compensação foi definida usando esferas UltraComp (ThermoFisher Scientific, Cat No 01-2222-41) coradas com fluorocromos individuais e células coradas com corante vivo / morto. As matrizes de compensação foram calculadas e aplicadas usando o software FlowJo. As células não coradas foram adquiridas para cada tipo de tecido analisado e os controles de fluorescência menos um (FMO) foram usados para permitir a distinção entre populações de células coradas positivamente e negativamente.

3.5 Análise estatística

A análise comparativa das medidas e sinal pulmonar no dia do sacrifício foi realizada com o teste de Mann-Whitney. Este método também foi empregado para comparar os resultados do experimento de citometria de fluxo. As variáveis avaliadas nestes experimentos são contínuas e a distribuição no gráfico não seguia a distribuição normal, o que justificou a utilização do teste em questão. A comparação entre o sinal médio pulmonar, em diferentes tempos, foi realizada com teste de ANOVA. Este método foi o escolhido, pois foram avaliadas diferentes curvas de diferentes grupos, associando variáveis categóricas e contínuas. O teste de Kruskal-Wallis foi usado para avaliar as diferenças entre todos os grupos, onde as distribuições das variáveis não eram gaussianas.

A sobrevida foi traçada utilizando o método de Kaplan-Meier e as diferenças na sobrevida entre os grupos foram comparadas aplicando o teste de *log-rank*. Este teste foi utilizado, pois houve a comparação de sobrevida de dois grupos e um entre os grupos apresentava a sua população já em óbito, apresentando um desvio para a direita. Para as avaliações estatísticas utilizou-se o *software* GraphPad Prism (GraphPad Prism® (*GraphPad Software,* San Diego, CA).

4. RESULTADOS

4.1 Resposta do tumor primário e sobrevida

A combinação de inibidor de PD-1 com agonismo de OX40 e terapia VTP suprime o crescimento do tumor e prolonga a sobrevida (Gráficos 1, 2 e 3)

Para avaliar o efeito terapêutico antitumoral da combinação do tratamento de VTP com a imunoterapia, camundongos com aloenxerto MB-49 foram tratados com VTP no dia 15 após a implantação do tumor e injetados no dia seguinte com anticorpos agonistas OX40 e inibidores de PD-1, conforme descrito acima. Cinco de 80 camundongos (6,25%) tratados com VTP morreram nas primeiras 72 horas, relacionados à toxicidade de VTP, e foram excluídos do estudo. Em comparação com os controles, os grupos de agentes imunomoduladores sem a terapia focal por VTP (apenas agonista OX40, apenas inibidor de PD-1 e dupla combinação: PD-1 e OX-40) não atrasaram significativamente o crescimento (Gráfico 1a). Já o tratamento com VTP reduziu o crescimento do tumor em comparação ao controle e os grupos tratados apenas com imunoterápicos (gráfico 1b). Quatorze dias após a ablação com VTP, 42% (8 de 19) dos camundongos não exibiram tumores ($p = 0,04$). Enquanto o tratamento com agente único (inibidor de PD-1 ou agonista OX-40) apresentou um efeito bem limitado, um camundongo (10%) no grupo tratado com ambas as drogas apresentou regressão tumoral completa e sobreviveu até o final do estudo (Gráfico 2). A combinação de VTP com inibidor de PD-1 e agonista OX40 (VPO) reduziu a carga tumoral em comparação com camundongos tratados apenas com VTP ou VTP associado a um único agente ($p <0,0001$). O tratamento com VPO aumentou significativamente a sobrevida para 60% em 90 dias em comparação com 25% em camundongos tratados com VTP sozinho, 31,25% naqueles que receberam VTP e inibidor de PD-1, 20% para VTP e agonista OX40 ($p <0,0001$). Todos os animais não tratados com VTP, exceto um no grupo OX40 + PD1, morreram cerca de 50 dias após a injeção de células tumorais (Gráfico 2).

Embora o tratamento com VTP tenha meelhorado significativamente as taxas de resposta do tumor primário, ele não preveniu a disseminação metastática pulmonar (Gráfico 3), sugerindo mecanismos de escape adicionais. Entre a coorte final de 60 camundongos que foram submetidos ao estudo de imagem IVIS, 10 (16,6%) tiveram metástases pulmonares detectadas por imagens de bioluminescência. Os únicos grupos sem um sinal pulmonar positivo foram os animais pertencentes ao grupo VPO e OX40 com inibidor de PD-1. Apesar de nenhuma

diferença estatística demonstrada, provavelmente devido ao pequeno número de metástases (limitação do modelo), este achado interessante sugere que a adição de ambos os agentes imunomoduladores ao tratamento com VTP pode ajudar a proteger contra metástases e corrobora com o aumento significativo da sobrevida no grupo VPO em relação aos demais grupos.

Gráfico 1a

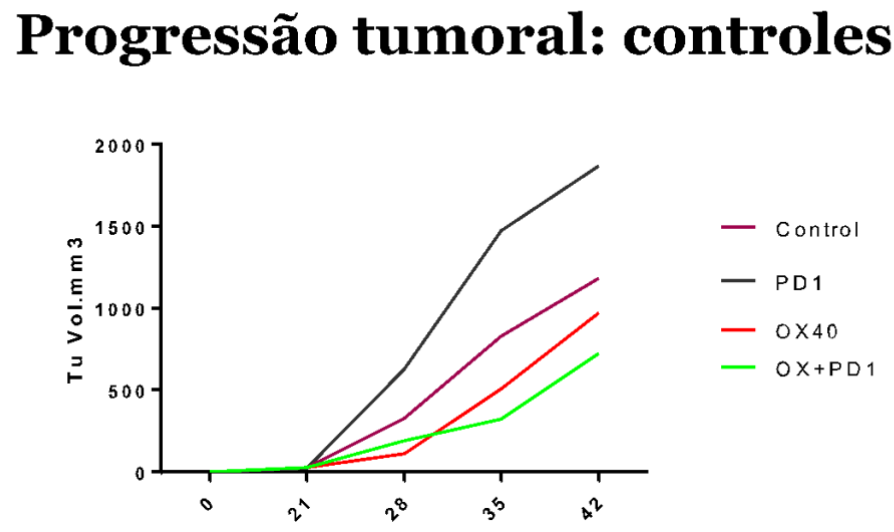

Gráfico 1b

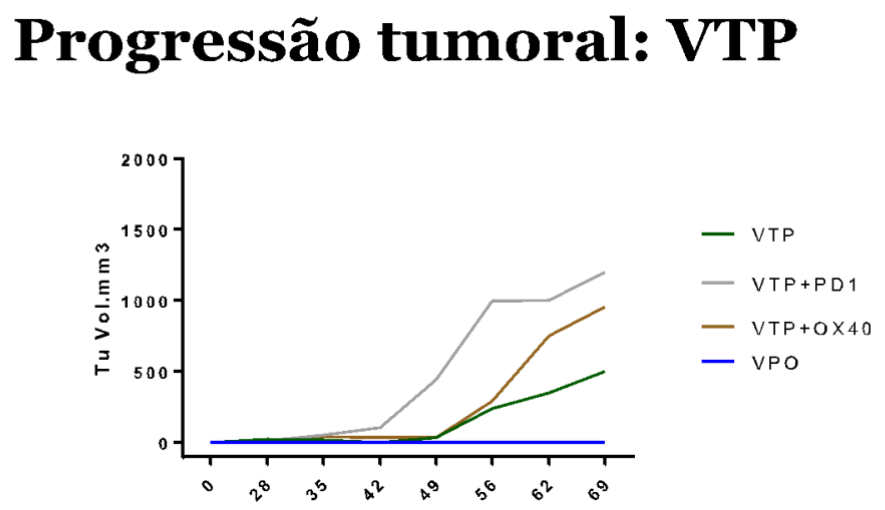

Gráfico 2

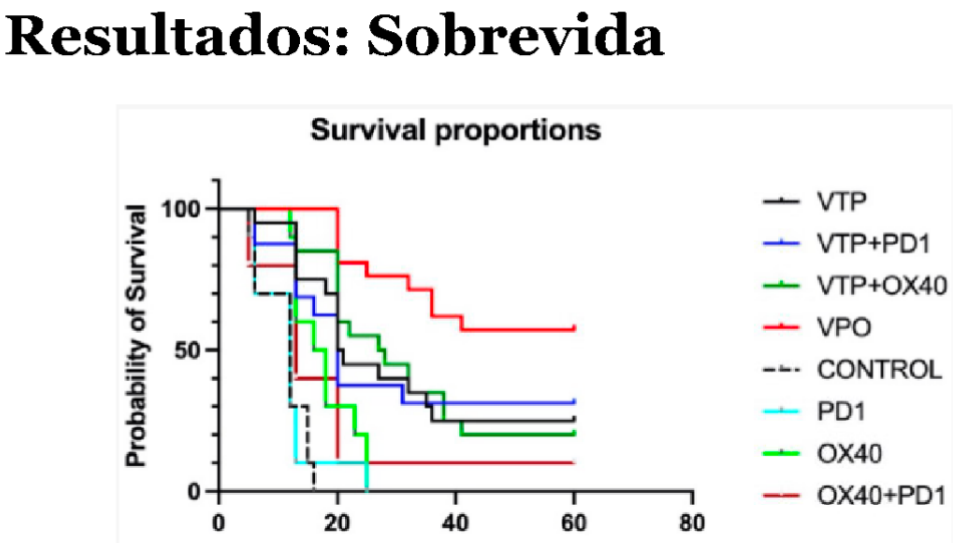

Gráfico 3

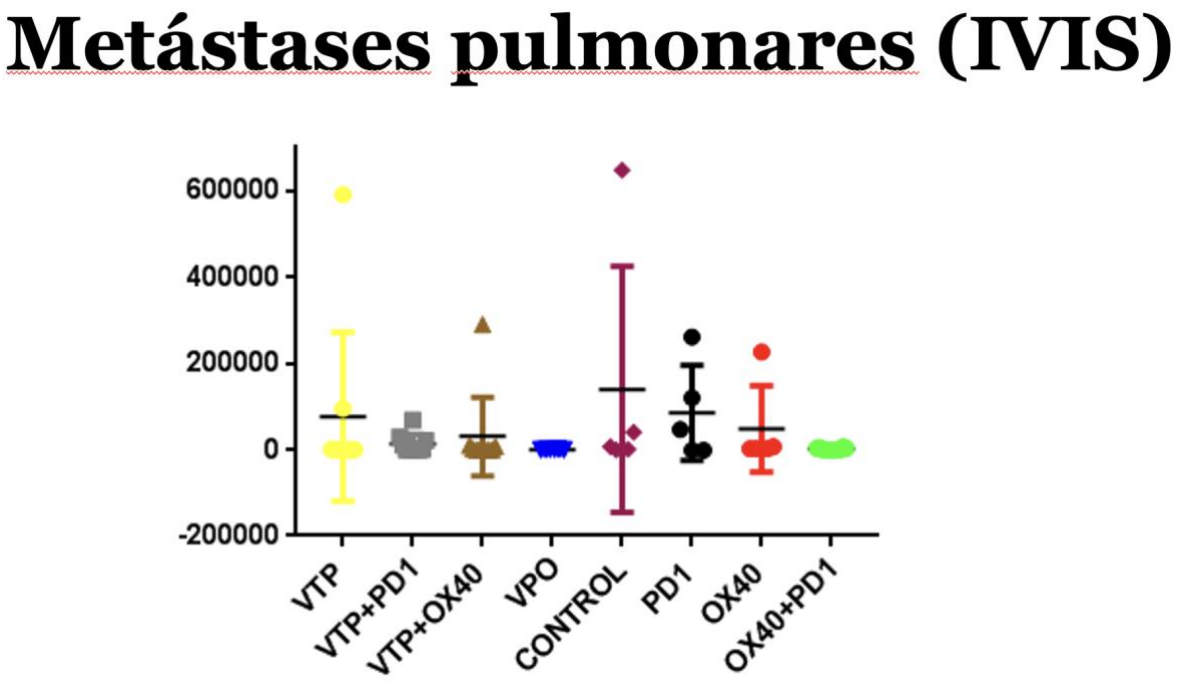

4.2 Resposta imunológica do tumor primário: linfócitos

A terapia combinada com VTP seguida por inibidor de PD-1 e tratamento com agonista OX40 aumenta a infiltração de células T no tecido tumoral urotelial (Gráficos 4a e 4b).

Como o objetivo da imunoterapia contra o câncer é eliciar respostas de células T específicas fortes e duráveis capazes de eliminar os tumores malignos, comparamos o recrutamento de células T entre os grupos de tratamento no dia 7 após o tratamento com VTP por citometria de fluxo multicolorida. Como observado em controles, esses tumores normalmente contêm poucas células T CD8 + e CD4 + e abundantes células Treg CD4 + Foxp3 + CD25 + (Gráfico 4a). Após o tratamento com VTP, CD4 + e CD8 + diminuíram. De acordo com a resposta terapêutica observada após tratamento combinado de VTP com agonista de OX40 / inibidor de PD-1, esta combinação levou a um aumento nas células T CD8 + e CD4 + intratumorais em comparação com VTP sozinho, no setimo dia pós-tratamento (Gráfico 4b). A imunohistoquímica nesse dia confirmou a presença de altos números de linfócitos T CD8 + e CD4 + em tumores tratados com VPO comparados com o grupo VTP sozinho. A quantificação da intensidade do sinal de CD4 e CD8 em tumores indicou que esse aumento foi significativo ($p < 0,01$; Gráfico 2b). O exame cuidadoso das secções do tumor revelou que a maioria das células T infiltrantes foram recrutadas na periferia do tumor.

À luz desses dados, caracterizamos ainda os fenótipos de células T CD8 + e CD4 +. Descobrimos que ambas as populações de células T CD8 + e CD4 + eram mais proliferativas no sétimo dia (5 a 10 vezes) nos camundongos tratados com VPO em comparação com VTP sozinho (conforme evidenciado pela abundante co-expressão do marcador de proliferação Ki67 – Gráfico 2b). Também observamos um aumento significativo da expressão de proliferação (Ki67) dentro da população CD45 + em tumores tratados com VPO ($p < 0,01$, Gráfico 4b). Esses marcadores de proliferação celular podem ser usados como substitutos para a ativação de células T, uma vez que a ativação é necessária para a proliferação. Em seguida, avaliamos a expressão da granzima B, que está associada à atividade citotóxica das células T CD8 +. A expressão de Granzima B foi regulada positivamente na população CD8 + de tumores tratados com VPO em comparação com tumores tratados com VTP apenas (Grafico 4b).

No geral, o aumento na infiltração e proliferação de linfócitos T CD8 + e CD4 + e a ativação de células T CD8 + citotóxicas associadas à combinação de agonista OX40 e inibidor de PD-1 com VTP indicam que esta abordagem terapêutica promove imunidade antitumoral

Gráficos 4a e 4b: Citometria: Avaliação do perfil de linfócitos T nos grupos controles e tratados por VTP

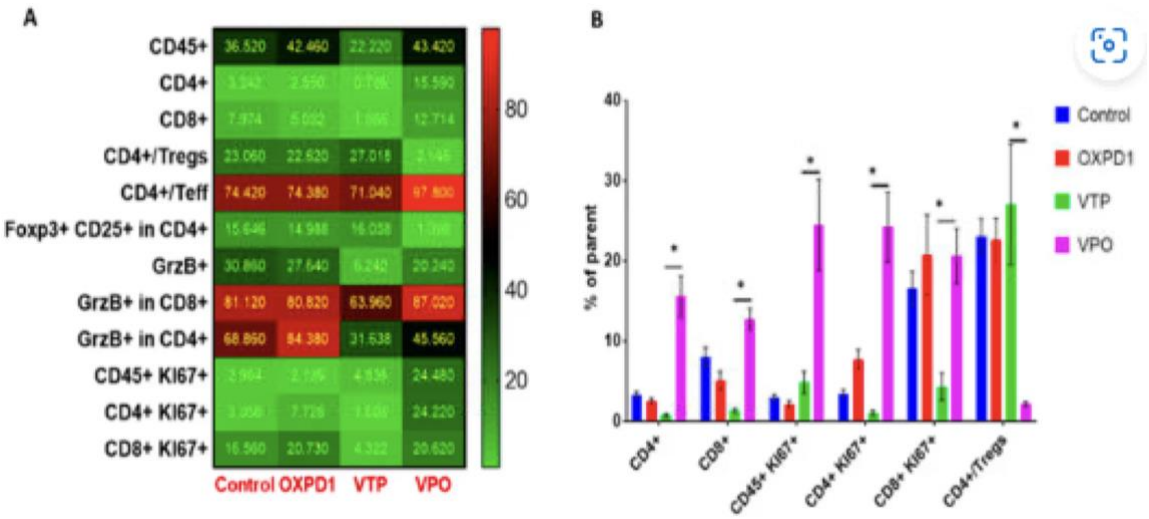

4.3 Resposta imunológica ao tumor primário: imunossupressão

A imunoterapia combinada com inibidor PD-1 / agonista OX40 diminui a imunossupressão em tumores tratados com VTP (Gráfico 5).

Avaliamos a eficácia dos inibidores de PD-1 combinada com ativação do coestimulador OX40 no bloqueio da imunossupressão em aloenxertos MB-49, quantificando populações de células regulatórias, incluindo células T regulatórias (Tregs), células supressoras derivadas de mieloide (MDSCs) e macrófagos associados a tumores (TAMs). A adição de bloqueio de PD-1 e ativação de OX40 ao VTP reduziu o número de Tregs em tumores no sétimo dia pós-VTP . Os tumores tratados com VPO continham drasticamente menos Tregs em comparação com os controles e aqueles tratados com VTP apenas. Além disso, descobrimos que os TAMs foram significativamente reduzidos em tumores tratados com VPO em comparação com tumores tratados com VTP, enquanto as DCs com apresentação cruzada de CD8 + CD11c + foram significativamente elevadas em tumores tratados com VPO em

comparação com VTP sozinho ou imunomoduladores (agonista OX40 e inibidor PD-1) sem VTP (Gráfico 5; p <0,01). No geral, essas descobertas sugerem que a combinação da inibição de PD-1 e ativação de OX40 com VTP reduz o número de células imunossupressoras. Como a depleção de Tregs foi correlacionada com respostas antitumorais aumentadas, isso está de acordo com nossos achados de aumento do acúmulo de células T intratumorais e maior sobrevida nos camundongos tratados com VPO.

Gráfico 5: Citometria: painel de células imunossupressoras

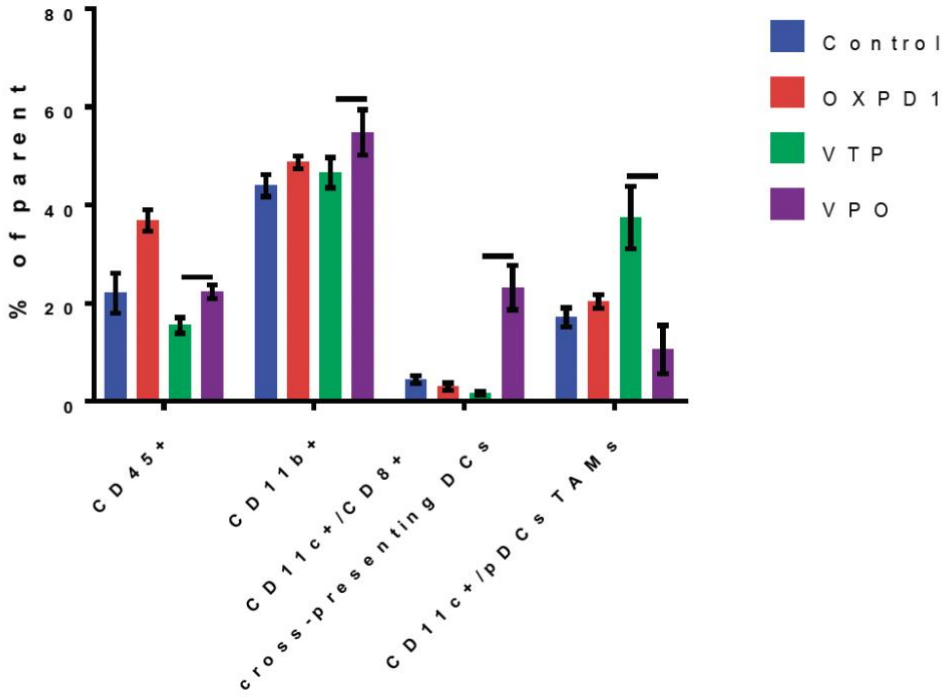

5. DISCUSSÃO

Nosso estudo destaca a imunoterapia combinada como um meio potencial para aumentar a eficácia do tratamento com VTP. Nós mostramos que essa combinação reduz a carga do tumor e aumenta a sobrevida em um grau maior do que VTP ou os imunomoduladores sozinhos em um modelo animal de câncer urotelial. Demonstramos ainda que esses efeitos antitumorais ocorrem principalmente de uma maneira dependente de células T, ou seja, enriquecimento de células T citotóxicas e auxiliares na área do tumor e depleção de células Treg. Esse efeito levou ao aumento de células T intratumorais e ao aumento da sua proliferação. A combinação tripla também atua por meio de um mecanismo independente de células T para promover imunidade antitumoral, pois reduz o número de MDSCs intratumorais. A eficácia desta combinação se encaixa bem com evidências anteriores mostrando que os cânceres uroteliais são doenças malignas altamente imunogênicas. Essa imunogenicidade é conhecida há décadas, desde a descoberta de que o bacilo Calmette-Guerin retarda o crescimento do câncer de bexiga ao invocar a atividade imunológica (22). Da mesma forma, os inibidores de checkpoint imunológico têm se mostrado benéficos como terapia de resgate no câncer urotelial metastático (23-27). As respostas imunológicas também estão correlacionadas com a agressividade dos tumores mesmo na ausência de imunoterapias, uma vez que o número de células T CD8 + foi recentemente descrito como um preditor de sobrevivência no carcinoma invasivo muscular e urotelial avançado (28,29).

O benefício de combinar VTP com bloqueio de PD-1 / PD-L1 e agonismo de OX40 (VPO) pode se estender a outros cânceres. O'Shaughnessy et al. mostraram recentemente que adicionar anti-PD-1 ou anti-PD-L1 ao VTP reduz a metástase e melhora a sobrevida num modelo animal de cancer renal (11). Assim como Preise et al., que mostraram que o VTP induz imunidade antitumoral com reação cruzada entre cânceres de cólon e mama (10).

Nosso estudo expande o conjunto de terapias com as quais o agonismo de OX40 demonstrou ter um efeito adicional. Os anticorpos estimuladores de OX40 mostraram aumentar a eficácia de vários tratamentos que estimulam indiretamente as respostas imunes, incluindo dasatinibe (em um modelo de tumor de mastocitoma mutante c-KIT P815 (30), dabrafenibe e trametinibe (em BRAFV600E - melanoma mutante) (31) e radioterapia (32-34).

Descobrimos que a combinação de VTP mais inibição de PD-1 mais tratamento com agonista OX40 (VPO) inibe a supressão imunológica, reduzindo a prevalência intratumoral de células T reguladoras (Tregs), macrófagos associados a tumor (TAMs) e, especialmente, células supressoras derivadas de mieloide (MDSCs). Os MDSCs têm sido o foco de intensa pesquisa nos últimos anos; um grande número dessas células imunossupressoras tem sido correlacionado com a agressividade tumoral e mau prognóstico, incluindo no câncer urotelial (35,36). Nosso laboratório demonstrou recentemente que alvejar MDSCs usando anti-CSF1R em combinação com VTP não só diminuiu o número de MDSCs e TAMs intratumorais, mas também aumentou a infiltração de células T CD8 +, diminuindo o crescimento do tumor e melhorando a sobrevida geral em um modelo de câncer de próstata (37). Assim sendo, a redução de TAMs e MDSCs pela combinação VPO pode ter sido um fator chave para sua eficácia no nosso estudo.

O forte recrutamento de células T induzido pelo tratamento com VPO é um achado importante de nosso estudo. Assim, a adição de VTP pode superar uma limitação dessas imunoterapias, que geralmente são mais eficazes em camundongos com pequenos tumores. Este efeito nas células T confirma a postulação de Aspeslagh et al., de que as terapias que aumentam a liberação do antígeno, um efeito conhecido do VTP (38), poderiam melhorar a potência da estimulação OX40 (13). Especulamos que a resposta inflamatória aguda induzida pelo VTP atua como um impulsionador imunológico, liberando antígenos aos quais reagem com as células T estimuladas e desinibidas pela imunoterapia.

6. CONCLUSÃO

Em síntese, fornecemos evidências de que o agonismo de OX40 associado a imunoterapia com inibidor de PD-1 é uma abordagem valiosa que melhora a eficácia de VTP em um modelo de câncer urotelial. A manipulação simultânea dessas duas vias imunes maximiza a eficácia do VTP no controle local do tumor e melhora a sobrevida. Este estudo, portanto, indica que a adição de imunoterapia ao tratamento com VTP é uma estratégia terapêutica eficaz para reduzir a imunossupressão no microambiente tumoral e, em última análise, aumentar a imunidade antitumoral

REFERÊNCIAS BIBLIOGRÁFICAS

1. Raman JD, Messer J, Sielatycki JA, Hollenbeak CS. Incidence and survival of patients with carcinoma of the ureter and renal pelvis in the USA, 1973-2005. BJU international 2011;107(7):1059-64 doi 10.1111/j.1464-410X.2010.09675.x.

2. Siegel RL, Miller KD, Jemal A. Cancer Statistics, 2017. CA: a cancer journal for clinicians 2017;67(1):7-30 doi 10.3322/caac.21387.

3. Kurohane K, Tominaga A, Sato K, North JR, Namba Y, Oku N. Photodynamic therapy targeted to tumor-induced angiogenic vessels. Cancer letters 2001;167(1):49-56.

4. Chen B, Pogue BW, Hoopes PJ, Hasan T. Vascular and cellular targeting for photodynamic therapy. Critical reviews in eukaryotic gene expression 2006;16(4):279-305.

5. Noweski A, Roosen A, Lebdai S, Barret E, Emberton M, Benzaghou F, *et al.* Medium-term Follow-up of Vascular-targeted Photodynamic Therapy of Localized Prostate Cancer Using TOOKAD Soluble WST-11 (Phase II Trials). European urology focus 2018 doi 10.1016/j.euf.2018.04.003.

6. Azzouzi AR, Vincendeau S, Barret E, Cicco A, Kleinclauss F, van der Poel HG, *et al.* Padeliporfin vascular-targeted photodynamic therapy versus active surveillance in men with low-risk prostate cancer (CLIN1001 PCM301): an open-label, phase 3, randomised controlled trial. The Lancet Oncology 2017;18(2):181-91 doi 10.1016/s1470-2045(16)30661-1.

7. Corradi RB, LaRosa S, Jebiwott S, Murray KS, Rosenzweig B, Somma AJ, *et al.* Effectiveness of the combination of vascular targeted photodynamic therapy and anti-cytotoxic T-lymphocyte-associated antigen 4 in a preclinical mouse model of urothelial carcinoma. International journal of urology : official journal of the Japanese Urological Association 2019;26(3):414-22 doi 10.1111/iju.13878.

8. Murray KS, Winter AG, Corradi RB, LaRosa S, Jebiwott S, Somma A, *et al.* Treatment Effects of WST11 Vascular Targeted Photodynamic Therapy for Urothelial Cell Carcinoma in Swine. The Journal of urology 2016;196(1):236-43 doi 10.1016/j.juro.2016.01.107.

9. Madar-Balakirski N, Tempel-Brami C, Kalchenko V, Brenner O, Varon D, Scherz A, *et al.* Permanent occlusion of feeding arteries and draining veins in solid mouse tumors by vascular targeted photodynamic therapy (VTP) with Tookad. PloS one 2010;5(4):e10282 doi 10.1371/journal.pone.0010282.

10. Preise D, Oren R, Glinert I, Kalchenko V, Jung S, Scherz A, *et al.* Systemic antitumor protection by vascular-targeted photodynamic therapy involves cellular and humoral immunity. Cancer immunology, immunotherapy : CII 2009;58(1):71-84 doi 10.1007/s00262-008-0527-0.

11. O'Shaughnessy MJ, Murray KS, La Rosa SP, Budhu S, Merghoub T, Somma A, *et al.* Systemic Antitumor Immunity by PD-1/PD-L1 Inhibition Is Potentiated by Vascular-Targeted Photodynamic Therapy of Primary Tumors. Clinical cancer research : an official journal of the American Association for Cancer Research 2018;24(3):592-9 doi 10.1158/1078-0432.Ccr-17-0186.

12. Mahoney KM, Rennert PD, Freeman GJ. Combination cancer immunotherapy and new immunomodulatory targets. Nature reviews Drug discovery 2015;14(8):561-84 doi 10.1038/nrd4591.

13. Aspeslagh S, Postel-Vinay S, Rusakiewicz S, Soria JC, Zitvogel L, Marabelle A. Rationale for anti-OX40 cancer immunotherapy. European journal of cancer (Oxford, England : 1990) 2016;52:50-66 doi 10.1016/j.ejca.2015.08.021.

14. Sadun RE, Hsu WE, Zhang N, Nien YC, Bergfeld SA, Sabzevari H, *et al.* Fc-mOX40L fusion protein produces complete remission and enhanced survival in 2 murine tumor models. Journal of immunotherapy (Hagerstown, Md : 1997) 2008;31(3):235-45 doi 10.1097/CJI.0b013e31816a88e0.

15. Curti BD, Kovacsovics-Bankowski M, Morris N, Walker E, Chisholm L, Floyd K, *et al.* OX40 is a potent immune-stimulating target in late-stage cancer patients. Cancer research 2013;73(24):7189-98 doi 10.1158/0008-5472.Can-12-4174.

16. Pardee AD, McCurry D, Alber S, Hu P, Epstein AL, Storkus WJ. A therapeutic OX40 agonist dynamically alters dendritic, endothelial, and T cell subsets within the established tumor microenvironment. Cancer research 2010;70(22):9041-52 doi 10.1158/0008-5472.Can-10-1369.

17. Bulliard Y, Jolicoeur R, Zhang J, Dranoff G, Wilson NS, Brogdon JL. OX40 engagement depletes intratumoral Tregs via activating FcgammaRs, leading to antitumor efficacy. Immunology and cell biology 2014;92(6):475-80 doi 10.1038/icb.2014.26.

18. Messenheimer DJ, Jensen SM, Afentoulis ME, Wegmann KW, Feng Z, Friedman DJ, *et al.* Timing of PD-1 Blockade Is Critical to Effective Combination Immunotherapy with Anti-OX40. Clinical cancer research : an official journal of the American Association for Cancer Research 2017;23(20):6165-77 doi 10.1158/1078-0432.Ccr-16-2677.

19. Guo Z, Wang X, Cheng D, Xia Z, Luan M, Zhang S. PD-1 blockade and OX40 triggering synergistically protects against tumor growth in a murine model of ovarian cancer. PloS one 2014;9(2):e89350 doi 10.1371/journal.pone.0089350.

20. Redmond WL, Linch SN, Kasiewicz MJ. Combined targeting of costimulatory (OX40) and coinhibitory (CTLA-4) pathways elicits potent effector T cells capable of driving robust antitumor immunity. Cancer immunology research 2014;2(2):142-53 doi 10.1158/2326-6066.Cir-13-0031-t.

21. Filatenkov A, Baker J, Mueller AM, Kenkel J, Ahn GO, Dutt S, *et al.* Ablative Tumor Radiation Can Change the Tumor Immune Cell Microenvironment to Induce Durable Complete Remissions. Clinical cancer research : an official journal of the American Association for Cancer Research 2015;21(16):3727-39 doi 10.1158/1078-0432.CCR-14-2824.

22. Herr HW, Morales A. History of bacillus Calmette-Guerin and bladder cancer: an immunotherapy success story. The Journal of urology 2008;179(1):53-6 doi 10.1016/j.juro.2007.08.122.

23. Rosenberg JE, Hoffman-Censits J, Powles T, van der Heijden MS, Balar AV, Necchi A, *et al.* Atezolizumab in patients with locally advanced and metastatic urothelial carcinoma who have progressed following treatment with platinum-based chemotherapy: a single-arm, multicentre, phase 2 trial. Lancet (London, England) 2016;387(10031):1909-20 doi 10.1016/s0140-6736(16)00561-4.

24. Bellmunt J, de Wit R, Vaughn DJ, Fradet Y, Lee JL, Fong L, *et al.* Pembrolizumab as Second-Line Therapy for Advanced Urothelial Carcinoma. The New England journal of medicine 2017;376(11):1015-26 doi 10.1056/NEJMoa1613683.

25. Lawrence MS, Stojanov P, Polak P, Kryukov GV, Cibulskis K, Sivachenko A, *et al.* Mutational heterogeneity in cancer and the search for new cancer-associated genes. Nature 2013;499(7457):214-8 doi 10.1038/nature12213.

26. Gubin MM, Artyomov MN, Mardis ER, Schreiber RD. Tumor neoantigens: building a framework for personalized cancer immunotherapy. The Journal of clinical investigation 2015;125(9):3413-21 doi 10.1172/jci80008.

27. McGranahan N, Furness AJ, Rosenthal R, Ramskov S, Lyngaa R, Saini SK, *et al.* Clonal neoantigens elicit T cell immunoreactivity and sensitivity to immune checkpoint blockade. Science (New York, NY) 2016;351(6280):1463-9 doi 10.1126/science.aaf1490.

28. Sharma P, Shen Y, Wen S, Yamada S, Jungbluth AA, Gnjatic S, *et al.* CD8 tumor-infiltrating lymphocytes are predictive of survival in muscle-invasive urothelial

carcinoma. Proceedings of the National Academy of Sciences of the United States of America 2007;104(10):3967-72 doi 10.1073/pnas.0611618104.

29. Faraj SF, Munari E, Guner G, Taube J, Anders R, Hicks J, *et al.* Assessment of tumoral PD-L1 expression and intratumoral CD8+ T cells in urothelial carcinoma. Urology 2015;85(3):703.e1-6 doi 10.1016/j.urology.2014.10.020.

30. Yang Y, Liu C, Peng W, Lizee G, Overwijk WW, Liu Y, *et al.* Antitumor T-cell responses contribute to the effects of dasatinib on c-KIT mutant murine mastocytoma and are potentiated by anti-OX40. Blood 2012;120(23):4533-43 doi 10.1182/blood-2012-02-407163.

31. Homet Moreno B, Mok S, Comin-Anduix B, Hu-Lieskovan S, Ribas A. Combined treatment with dabrafenib and trametinib with immune-stimulating antibodies for BRAF mutant melanoma. Oncoimmunology 2016;5(7):e1052212 doi 10.1080/2162402x.2015.1052212.

32. Yokouchi H, Yamazaki K, Chamoto K, Kikuchi E, Shinagawa N, Oizumi S, *et al.* Anti-OX40 monoclonal antibody therapy in combination with radiotherapy results in therapeutic antitumor immunity to murine lung cancer. Cancer science 2008;99(2):361-7 doi 10.1111/j.1349-7006.2007.00664.x.

33. Gough MJ, Crittenden MR, Sarff M, Pang P, Seung SK, Vetto JT, *et al.* Adjuvant therapy with agonistic antibodies to CD134 (OX40) increases local control after surgical or radiation therapy of cancer in mice. Journal of immunotherapy (Hagerstown, Md : 1997) 2010;33(8):798-809 doi 10.1097/CJI.0b013e3181ee7095.

34. Niknam S, Barsoumian HB, Schoenhals JE, Jackson HL, Yanamandra N, Caetano MS, *et al.* Radiation Followed by OX40 Stimulation Drives Local and Abscopal Antitumor Effects in an Anti-PD1-Resistant Lung Tumor Model. Clinical cancer research : an official journal of the American Association for Cancer Research 2018;24(22):5735-43 doi 10.1158/1078-0432.Ccr-17-3279.

35. Yang G, Shen W, Zhang Y, Liu M, Zhang L, Liu Q, *et al.* Accumulation of myeloid-derived suppressor cells (MDSCs) induced by low levels of IL-6 correlates with poor prognosis in bladder cancer. Oncotarget 2017;8(24):38378-88 doi 10.18632/oncotarget.16386.

36. Parker KH, Beury DW, Ostrand-Rosenberg S. Myeloid-Derived Suppressor Cells: Critical Cells Driving Immune Suppression in the Tumor Microenvironment. Advances in cancer research 2015;128:95-139 doi 10.1016/bs.acr.2015.04.002.

37. Lebdai S, Gigoux M, Alvim R, Somma A, Nagar K, Azzouzi AR, *et al.* Potentiating vascular-targeted photodynamic therapy through CSF-1R modulation of myeloid cells

in a preclinical model of prostate cancer. Oncoimmunology 2019;8(6):e1581528 doi 10.1080/2162402x.2019.1581528.

38. Mroz P, Hashmi JT, Huang YY, Lange N, Hamblin MR. Stimulation of anti-tumor immunity by photodynamic therapy. Expert review of clinical immunology 2011;7(1):75-91 doi 10.1586/eci.10.81.

39. Bray, F., Laversanne, M., Sung, H., Ferlay, J., Siegel, R. L., Soerjomataram, I., & Jemal, A. (2022). Global cancer statistics 2022: GLOBOCAN estimates of incidence and mortality worldwide for 36 cancers in 185 countries. *CA: A Cancer Journal for Clinicians*. Open Access.

40. World Health Organization (WHO). *2023 Global Progress Report on Implementation of the WHO Framework Convention on Tobacco Control*. WHO; 2024. Accessed January 16, 2024.

41. Yip, W., Sjoberg, D. D., Nogueira, L. M., Tracey, A. T., Alvim, R. G., Reisz, P. A., et al. (2023). Final results of a phase I trial of WST-11 (TOOKAD Soluble) vascular-targeted photodynamic therapy for upper tract urothelial carcinoma. *Journal of Urology*, 209(5), 863–871. https://doi.org/10.1097/JU.0000000000003202

42. Powles, T., Park, S. H., Voog, E., et al. (2021). Nivolumab plus ipilimumab in muscle-invasive urothelial carcinoma: Results from the phase 3 CheckMate 901 trial. *Journal of Clinical Oncology*, 39(15_suppl), 4500-4500. https://doi.org/10.1200/JCO.2021.39.15_suppl.4500

APÊNDICE A– Protocolo e projetos aprovados pelo " Institutional Review Board" e "Animal Model of Vascular Targedted Phototherapy"

Protocol preview

PI: Coleman, Jonathan
Number: 11-02-004
Title: Animal Model of Vascular Targeted Phototherapy

General

01 **Title**
Animal Model of Vascular Targeted Phototherapy

02 **Progress Report**
Small animal studies:

Mice: We established the dose and duration of laser illumination in rodent tumor models. The effect of VTP therapy was determined in multiple prostate cancer models in both immune competent and deficient rodent models, which indicated better efficacy of VTP in immune-competent models. We plan to continue to study the effect of VTP in prostate cancer, especially in metastatic models and expand it to other urological cancers. A pilot expression study of addressing molecular changes in VTP-treated tumors revealed changes in several survival pathways. This pilot study as well as future repeats in other tumor types (360 mice) will guide us for hypothesis-driven combination therapies for the next 3 years. The combination therapy includes immune therapeutics, small molecule targeted therapies and chemotherapeutic drugs. This portion of proposal was added at the end of the current protocol (1600 mice) and only the first experiment is currently ongoing using 200 mice. We plan to perform more repeats to determine drug scheduling and routes in addition to what was proposed in cycles 1. We estimate total 4000 animals encompassing cycles 1 and 2 (in animal justification) for this aim and 3800 additional mice will be needed for cycle 2 considering 200 mice being used. We expect the bulk of this aim will be addressed in the next 3 year period.

What are your specific aims for this project?

Rodent tumor model studies:

1. To determine the effect of VTP in urological cancers in rodent models of cancer
2. To assess the molecular and immunological changes induced by VTP in tumors in rodent models of cancer.
3. To develop combination therapy to improve the outcome of VTP treatment using animal models of cancer.

Special Considerations

AU.01	**Are unanesthetized animals restrained more than momentarily?** No
AU.06	**State the nature and frequency of observations to evaluate the health and well-being of this species during the course of the research:** Animals will be examined at least once per week. Animals that have undergone a surgical procedure will be observed daily for 3 days and twice per week after 3 days. Should clinical evidence of distress be present, animals will be euthenized. Animals will be sacrified if they have a tumor larger than 1.5 cm^3, respiratory rate greater than 110% of control, weight loss greater than 10% of control, or clinically obvious deterioration of grooming habits.
AU.07	**Are adverse effects expected or is there a potential for them to occur as a result of the procedures conducted in this species?** Yes

As the individual responsible for this project, I confirm that:

- The information contained in this protocol is true and accurate and, to the best of my knowledge, conforms with MSKCC, NIH, and USDA policies on the use of animals in research and teaching.
- I have considered alternatives to the biological models used in this project, and have found these other methods unacceptable on scientific or educational grounds.
- This project does not unnecessary duplicate previous experiments.
- I have received and reviewed the RARC User's Guide.
- All individuals who will be involved with the animals used in the project have been instructed in the humane care, handling, and use of animals as well as the safe handling of hazardous agents, if utilized, and that I have reviewed their qualifications to conduct the experiments described herein.
- No change will be made to the procedures, care or housing without prior written notification to and approval by the Institutional Animal Care and Use Committee (IACUC).

I understand that failure to comply with IACUC policies and procedures will jeopardize MSKCC's Animal Welfare Assurance on file with the NIH, and may lead to revocation of my privileges to conduct animal research at MSKCC.

PI: Coleman, Jonathan

Submitted: 03/24/2014

APÊNDICE B- Estadiamento dos tumores Uroteliais

Bexiga

Table 1. Bladder Cancer TNM Staging

Primary Tumor (T)	
TX	Primary tumor cannot be assessed
T0	No evidence of primary tumor
Ta	Noninvasive papillary carcinoma
Tis	Urothelial carcinoma in situ
T1	Invades lamina propria
pT2a	Invades superficial muscularis propria
pT2b	Invades deep muscularis propria
pT3a	Microscopic perivesical invasion
pT3b	Macroscopic perivesical invasion
T4a	Extravesical tumor invades prostatic stroma, uterus, vagina
T4b	Extravesical tumor invades pelvic wall, abdominal wall
Lymph Nodes (N)	
NX	Nodes cannot be assessed
N0	No lymph node metastasis
N1	Single regional lymph node metastasis in true pelvis
N2	Multiple regional lymph node metastasis in true pelvis
N3	Lymph node metastasis to common iliac lymph nodes
Metastasis (M)	
M0	No distant metastasis
M1a	Distant metastasis limited to lymph nodes beyond the common iliacs
M1b	Non-lymph node distant metastasis

Trato urinário alto (TUA)

Table 1 TNM definitions of transitional cell carcinoma of the renal pelvis and the ureter

Primary tumor (T)	
T0a	Non-invasive papilloma
Tis	Carcinoma in situ
T1	Tumor invades subepithelial connective tissue
T2	Tumor invades the muscularis
T3 (for renal pelvis only)	Tumor invades beyond muscularis into peripelvic fat or renal parenchyma
T3 (for ureter only)	Tumor invades beyond muscularis into periureteric fat
T4	Tumor invades adjacent organs or through the kidney into perinephric fat
Regional lymph nodes (N)	
N0	No regional lymph node metastasis
N1	Metastasis in a single lymph node, ≤2 cm in greatest dimension
N2	Metastasis in a single lymph node, between 2 cm and 5 cm in greatest dimension; or multiple lymph nodes, ≤2 cm in greatest dimension
N3	Metastasis in a lymph node more than 5 cm in greatest dimension
Distant metastasis (M)	
M0	No distant metastasis
M1	Distant metastasis

APÊNDICE C- Classificação Clavien-Dido de complicações cirúrgicas

Grau	Definição
I	Qualquer desvio do curso pós-operatório normal sem necessidade de intervenção para além da administração de antieméticos, antipiréticos, analgésicos, diuréticos, eletrólitos e fisioterapia #
II	Complicação requerendo tratamento farmacológico com outros medicamentos além dos que são permitidos para as complicações de grau I.
III	Complicação requerendo intervenção cirúrgica, endoscópica ou radiológica
III-a	Intervenção sem ser sob anestesia geral
III-b	Intervenção sob anestesia geral
IV	Complicação com perigo de vida requerendo admissão em unidade de terapia intensiva
IV-a	Disfunção de órgão único (incluindo diálise)
IV-b	Disfunção multi-órgão
V	Morte do paciente

ANEXOS – Artigos publicados relacionados à pesquisa apresentada na tese.

molecules

MDPI

Article

Combined OX40 Agonist and PD-1 Inhibitor Immunotherapy Improves the Efficacy of Vascular Targeted Photodynamic Therapy in a Urothelial Tumor Model

Ricardo G. Alvim [1,2,*,†], Petrina Georgala [3,*,†], Lucas Nogueira [1,2], Alexander J. Somma [1], Karan Nagar [1], Jasmine Thomas [1], Laura Alvim [1], Amelia Riegel [1], Christopher Hughes [1], Jie Chen [1], Augusto B. Reis [2], Souhil Lebdai [1], Avigdor Scherz [4], Steven Zanganeh [5], Rui Gardner [6], Kwanghee Kim [1] and Jonathan A. Coleman [1,*]

1 Urology Service, Department of Surgery, Memorial Sloan Kettering Cancer Center, New York, NY 10065, USA; nogueirl@mskcc.org (L.N.); ajsomma@gmail.com (A.J.S.); nagark@mskcc.org (K.N.); thomasj7@mskcc.org (J.T.); laurapalvim@gmail.com (L.A.); ameliariegel@gmail.com (A.R.); hughesc@mskcc.org (C.H.); chenj4@mskcc.org (J.C.); souhil.lebdai@gmail.com (S.L.); kimk1@mskcc.org (K.K.)

2 Department of Surgery, Federal University of Minas Gerais, Belo Horizonte 30130-100, Brazil; augusto.urologia@gmail.com

3 Department of Neurosurgery, Memorial Sloan Kettering Cancer Center, New York, NY 10065, USA

4 Department of Plants and Environmental Sciences, The Weizmann Institute of Science, Rehovot 76100, Israel; avigdor.scherz@weizmann.ac.il

5 Department of Bioengineering, University of Massachusetts, Dartmouth, MA 02747, USA; steven.zanganeh@gmail.com

6 Flow Cytometry Core Facility, Memorial Sloan Kettering Cancer Center, New York, NY 10065, USA; gardnerr@mskcc.org

* Correspondence: ricardoalvim1103@gmail.com (R.G.A.); petrinageorgala@gmail.com (P.G.); colemanj@mskcc.org (J.A.C.)

† These authors contributed equally to this work.

check for updates

Citation: Alvim, R.G.; Georgala, P.; Nogueira, L.; Somma, A.J.; Nagar, K.; Thomas, J.; Alvim, L.; Riegel, A.; Hughes, C.; Chen, J.; et al. Combined OX40 Agonist and PD-1 Inhibitor Immunotherapy Improves the Efficacy of Vascular Targeted Photodynamic Therapy in a Urothelial Tumor Model. *Molecules* **2021**, *26*, 3744. https://doi.org/10.3390/molecules26123744

Academic Editors: Guangyu Zhu and Már Másson

Received: 6 April 2021
Accepted: 10 June 2021
Published: 19 June 2021

Publisher's Note: MDPI stays neutral with regard to jurisdictional claims in published maps and institutional affiliations.

Abstract: Purpose: Vascular targeted photodynamic therapy (VTP) is a nonsurgical tumor ablation approach used to treat early-stage prostate cancer and may also be effective for upper tract urothelial cancer (UTUC) based on preclinical data. Toward increasing response rates to VTP, we evaluated its efficacy in combination with concurrent PD-1 inhibitor/OX40 agonist immunotherapy in a urothelial tumor-bearing model. Experimental design: In mice allografted with MB-49 UTUC cells, we compared the effects of combined VTP with PD-1 inhibitor/OX40 agonist with those of the component treatments on tumor growth, survival, lung metastasis, and antitumor immune responses. Results: The combination of VTP with both PD-1 inhibitor and OX40 agonist inhibited tumor growth and prolonged survival to a greater degree than VTP with either immunotherapeutic individually. These effects result from increased tumor infiltration and intratumoral proliferation of cytotoxic and helper T cells, depletion of Treg cells, and suppression of myeloid-derived suppressor cells. Conclusions: Our findings suggest that VTP synergizes with PD-1 blockade and OX40 agonist to promote strong antitumor immune responses, yielding therapeutic efficacy in an animal model of urothelial cancer.

Keywords: bladder cancer; tumor ablation; TOOKAD; focal therapy; immunotherapy

1. Introduction

Urothelial carcinoma (UC) represents the fifth most common malignancy among men in the United States and is most prevalent among men over 60 years old. Between 5% and 10% of primary urothelial cancers originate from the ureter or renal pelvis and are collectively called upper tract urothelial cancers (UTUCs) [1,2].

In patients with low-grade, small UTUC tumors, as well as those in whom functional preservation is especially critical (i.e., those with a single kidney, poor renal function, or

bilateral disease), local ablative therapies have emerged as a means of reducing treatment-related morbidity. One such minimally invasive therapy is vascular targeted photodynamic (VTP) therapy, which eradicates cancer cells by targeting the vascular compartment of the tumor while preserving healthy tissue [3,4]. VTP therapy employing WST11 (TOOKAD Soluble, Steba Biotech, Luxembourg) was clinically approved in Europe and Mexico in 2017 for early-stage localized prostate cancer [5–7] and has demonstrated efficacy in multiple animal models of UTUC [7,8]. WST-11 is a photosensitizer that is administered intravenously and has a 60 min half-life, avoiding long-term toxicity. Confined laser illumination supplied via optical fibers inserted into the malignant tissue activates the circulating drug locally and induces rapid release of toxic, short-lived free radicals inside tumor blood vessels, leading to vascular occlusion and ultimately tumor necrosis 48 h post-treatment [9].

Though VTP can eradicate UTUC tumors, the cure rate in the standard mouse model is only approximately 30%. To increase its efficacy, VTP has been combined with immune checkpoint inhibitors based on the observation that it induces antitumor immune responses through a prominent and rapid inflammatory reaction [10]. The synergy of VTP with checkpoint inhibitors such as anti-PD-1 and anti-CTLA-4 has been demonstrated in animal studies, in which the complete response rate is greater than 50% [7,11].

To maximize the clinical benefit of VTP, adding another immunotherapeutic agent is a promising approach. Combining immunomodulatory drugs with immune checkpoint inhibitors has received considerable attention as a means of increasing the benefit of the latter, which can induce potent clinical and immunologic responses in a minority of patients [12]. An attractive immunomodulatory target is the T cell costimulatory receptor OX40 (CD134), a member of the tumor necrosis factor receptor superfamily (TNFRSF) that acts upon T cell signaling pathways that promote survival, proliferation, and cytokine production [13]. Preclinical studies have shown that OX40 agonist antibodies can enhance antitumor immunity through T cell expansion, leading to improved progression-free survival [14–17]. OX40 agonism has been shown to augment the efficacy of checkpoint inhibitors in models of multiple cancers [18–20].

In addition, high-dose radiation has also been shown to transform the immunosuppressive tumor microenvironment, resulting in an intense $CD8^+$ T-cell tumor infiltrate and improving the tumor ablation effect. This transformation is dependent on antigen cross-presenting $CD8^+$ dendritic cells, secretion of IFNγ, and $CD4^+$ T cells expressing CD40L, opening the concept of OX40 plus ablation therapy (VTP) can increase this effect [21].

We postulated that combining VTP with PD-1 blockade and OX40 agonistic immunotherapy would enhance the therapeutic efficacy of VTP in urothelial cancer by inducing long-lasting antitumor immunity.

2. Results

2.1. Combination of PD-1 Blockade and OX40 Agonism with VTP Therapy Suppresses Tumor Growth and Prolongs Survival

To evaluate the antitumor therapeutic effect of combining VTP treatment with the combination immunotherapy, MB-49 UTUC allograft-bearing mice were treated with VTP on day 15 following tumor implantation and injected the following day with OX40 agonist and PD-1 inhibitor antibodies, as described above. Five out of 80 mice (6.25%) treated with VTP died in the first 72 h, related to intense inflammatory reaction from the VTP treatment, and were excluded from the study. For comparison, other mice were treated with one of the component therapies or a dual combination. Compared to controls, the immunomodulatory agent groups (OX40 agonist only, PD-1 inhibitor only and dual combination) significantly delay tumor growth ($p < 0.0001$), however no difference was observed between the different schemes ($p = 0.59$; Supplementary Figure S1). Treatment of primary MB-49 tumors with VTP reduced tumor growth compared with control and immunomodulatory agent-treated animals. Fourteen days after VTP ablation, 42% (8 out 19) of VTP only-treated mice did not display tumors and the average volume was 442 mm^3, while mice in the latter treatment groups developed tumors with almost double size (average volume > 800 mm^3, $p = 0.04$, Supplementary Figure S1). While single-agent treatment with either PD-1 inhibitor or

OX-40 agonist had limited effect, one mouse (10%) treated with both drugs had a complete tumor regression and survived until the end of study (Figure 1). Combined VTP plus PD-1 inhibitor plus OX40 agonist therapy (VTP+OX40+PD-1) dramatically reduced tumor burden compared with mice treated with either VTP alone or VTP plus a single drug (Supplementary Figures S1 and S2, $p < 0.0001$). VTP+OX40+PD-1 treatment significantly increased survival to 60% at 60 days compared with 25% in mice treated with VTP alone, 31.25% in those given VTP plus PD-1 inhibitor, 20% for VTP plus OX40 agonist ($p < 0.0001$; Figure 1). All non-VTP-treated animals, but one exception in OX40 + PD1 group, died around 30 days after VTP treatment (Figure 1).

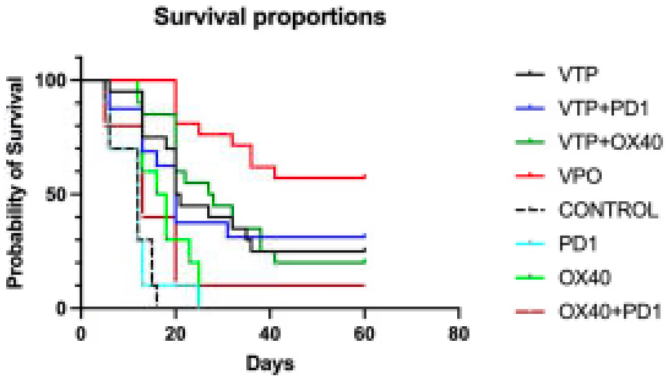

Figure 1. Combined treatment with OX40 agonist and PD1 inhibitor antibodies following VTP therapy suppresses primary tumor growth and improves survival. Percent survival of mice plotted by Kaplan-Meier methods ($p < 0.0001$).

2.2. *Combination Therapy with VTP Followed by PD-1 Inhibitor and OX40 Agonist Treatment Enhances T Cell Infiltration into Urothelial Tumor Tissue*

As the goal of cancer immunotherapy is to elicit strong, durable tumor-specific T cell responses capable of eliminating malignant tumors, we compared T cell recruitment among treatment groups at day 7 after VTP treatment by multi-color flow cytometry. As seen in controls, these tumors normally contain few $CD8^+$ and $CD4^+$ T cells and abundant $CD4^+$ $Foxp3^+CD25^+$ Treg cells (Figure 2A,B). After VTP treatment, $CD4^+$ and $CD8^+$ were decreased (Figure 2C,D). In accordance with the observed therapeutic response following combined VTP with OX40 agonist/ PD-1 inhibitor treatment (Figure 2), this combination led to a striking increase in intratumoral $CD8^+$ and $CD4^+$ T cells compared to VTP alone, at day 7 post-treatment (Figure 2). Immunohistochemistry at day 7 after treatment confirmed the presence of high numbers of $CD8^+$ and $CD4^+$ T lymphocytes in VTP+OX40+PD-1-treated tumors compared with VTP alone group (Figure 2C,E). Quantification of CD4 and CD8 signal intensity in tumors indicated that this increase was significant ($p < 0.01$; Figure 2C,D). Careful examination of tumor sections revealed that most infiltrating T cells were recruited close to the tumor boundary (Figure 2C,E).

In light of these data, we further characterized the $CD8^+$ and $CD4^+$ T cell phenotypes. We found that both $CD8^+$ and $CD4^+$ T cell populations were more proliferative at day 7, the latter by 5- to 10-fold, in VTP+OX40+PD-1-treated mice compared with VTP alone, as evidenced by abundant co-expression of the proliferation marker Ki67 (Figure 2A,B). We also observed significantly increased Ki67 expression within the $CD45^+$ population in VTP+OX40+PD-1-treated tumors ($p < 0.01$, Figures 2A,B and 3). Such markers of cellular proliferation can be used as surrogates for T cell activation, given that activation is required for proliferation. We then evaluated granzyme B expression, which is associated with the cytotoxic activity of $CD8^+$ T cells. Granzyme B expression was upregulated in the $CD8^+$ population of VTP+OX40+PD-1-treated tumors compared with VTP-treated tumors (though similar to that in control and immunomodulator-treated tumors; Figure 2B).

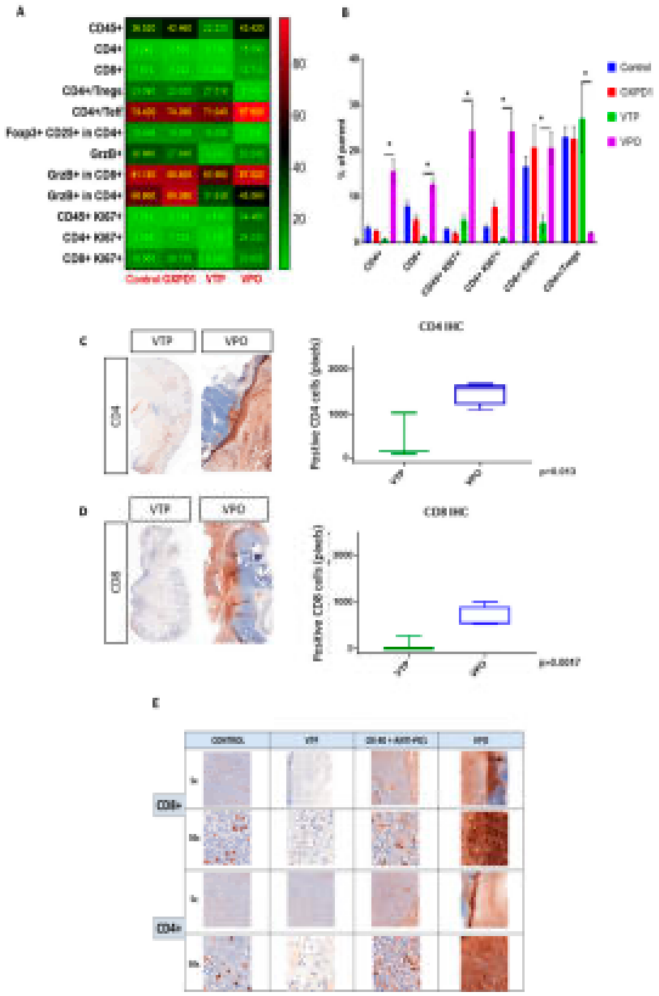

Figure 2. Adding PD-1 inhibitor and OX40 agonist to VTP therapy increases T cell infiltration and activation into MB-49 UTUC allografts at 7 days post-treatment and increases $CD4^+$ and $CD8^+$ T cell infiltration into MB-49 UTUC allografted tumors. (**A**) Heat map showing the mean frequency of each cell population as measured by flow cytometry in control and treated tumors. Each box represents the mean percentage of positive cells among the parent cell population, i.e., $CD45^+$ among live cells, $CD4^+$ or $CD8^+$ cells among $CD45^+$ cells, $Foxp3^+$ Tregs or Teff among $CD4^+$ cells, $CD25^+/Foxp3^+$ Tregs among $CD4^+$ cells, $GrzB^+$ among $CD45^+$ cells, $GrzB^+$ cells among $CD8^+$ or $CD4^+$ cells, $Ki67^+$ cells among $CD45^+$ cells, and $Ki67^+$ among $CD8^+$ or $CD4^+$ cells. (**B**) Frequency of positive cells among the parent cell population. Graph bars indicate mean ± SEM. * $p < 0.01$. OXPD1, OX40 agonist plus PD1 inhibitor; VTP+OX40+PD-1, VTP plus PD1 inhibitor and OX40 agonist. (**C**) A representative IHC of $CD4^+$ T lymphocytes in VTP+OX40+PD-1-treated tumors compared with VTP followed by the signal intensity comparison showing a more significant $CD4^+$ staining in VTP+OX40+PD-1 group compared to VTP alone ($p = 0.013$). (**D**) A representative IHC of $CD8^+$ T lymphocytes in VTP+OX40+PD-1-treated tumors compared with VTP followed by the signal intensity comparison showing a more significant $CD8^+$ staining in VTP+OX40+PD-1 group compared to VTP alone ($p = 0.0017$). (**E**) A representative microscopy IHC illustration of $CD8^+$ T lymphocytes and $CD4^+$ T lymphocytes difference between control, VTP, OX40 plus PD1 and VTP+OX40+PD-1 groups. In both staining, VTP+OX40+PD-1 presented a clear high intensity signal.

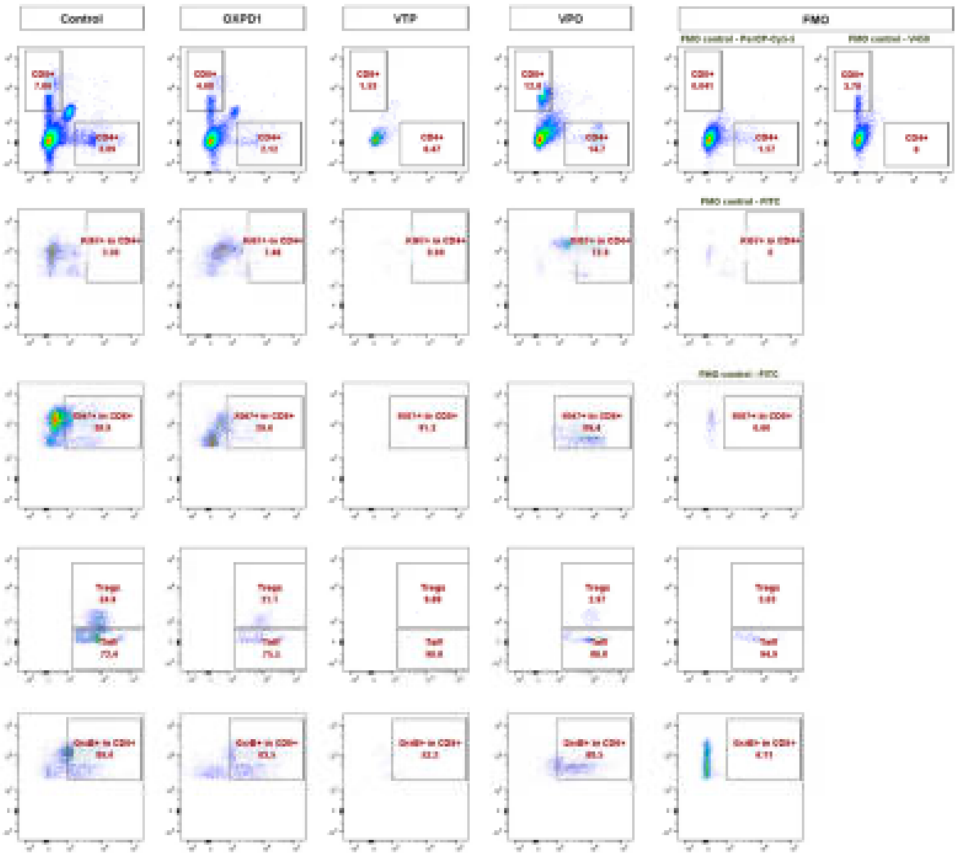

Figure 3. Adding PD-1 Inhibitor and OX40 agonist to VTP therapy increases T cell infiltration and activation compared to VTP alone, into MB-49 UTUC allografts at 7 days post-treatment. Representative flow cytometry plots showing the percentage of $CD4^+$ and $CD8^+$ cells among $CD45^+$ cells (top row), $Ki67^+$ in $CD4^+$ (second row), $Ki67^+$ in $CD8^+$ (third row), $Foxp3^+$ Tregs and $Foxp3^-$ Teff in $CD4^+$ (fourth row), and $GrzB^+$ in $CD8^+$ T cells (bottom row) in control and treated tumors analyzed 7 days after treatment. A fluorescent minus one (FMO) sample was included for each marker as a negative control for gating.

Overall, the increase in $CD8^+$ and $CD4^+$ T lymphocyte infiltration and proliferation, and activation of cytotoxic $CD8^+$ T cells associated with combining OX40 agonist and PD-1 inhibitor with VTP indicates that this therapeutic approach promotes antitumor immunity.

2.3. Combined PD-1 Inhibitor/OX40 Agonist Immunotherapy Diminishes Immunosuppression in VTP-Treated Tumors

We evaluated the efficacy of combined inhibition of the immune checkpoint PD-1 and activation of the costimulatory OX40 in blocking immunosuppression in MB-49 UTUC allografts by quantifying regulatory cell populations including regulatory T cells (Tregs), myeloid derived suppressor cells (MDSCs) and tumor-associated macrophages (TAMs). The addition of PD-1 blockade and OX40 activation to VTP reduced Treg numbers in tumors at day 7 post-VTP (Figure 2A,B); VTP+OX40+PD-1-treated tumors contained drastically fewer Tregs compared with controls and those treated with VTP or both immunomodulators. Furthermore, we found that TAMs were significantly reduced in VTP+OX40+PD-1-treated compared with VTP-treated tumors, whereas $CD8^+CD11c^+$ cross-presenting DCs were significantly elevated in VTP+OX40+PD-1-treated tumors compared to VTP alone or immunomodulators (OX40 agonist plus PD-1 inhibitor) without VTP (Figure 4A–C;

$p < 0.01$). Overall, these findings suggest that combining PD-1 inhibition and OX40 activation with VTP reduces numbers of immune-suppressive cells. As depletion of Tregs has been correlated with enhanced antitumor responses, this agrees with our findings of increased intratumoral T cell accumulation and survival in VTP+OX40+PD-1-treated mice.

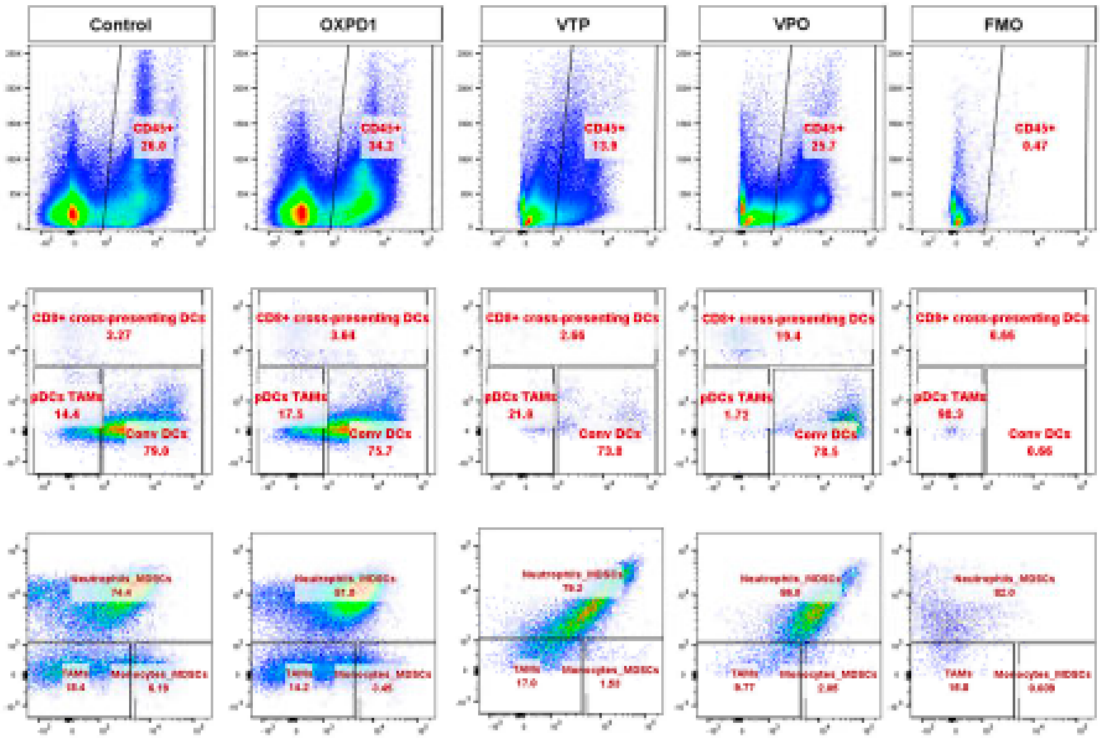

(A)

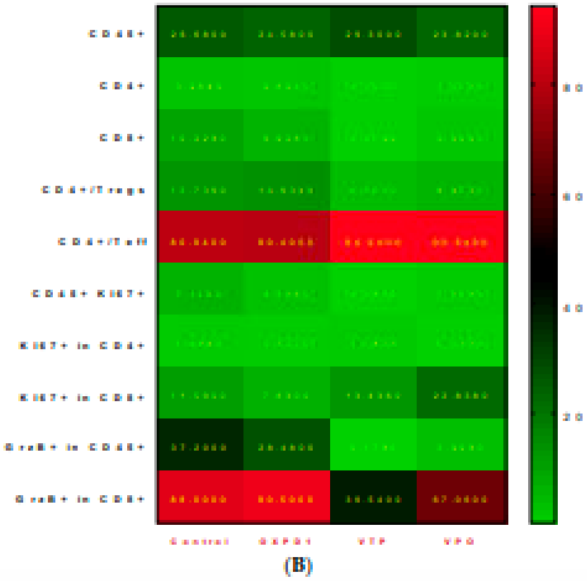

(B)

Figure 4. *Cont.*

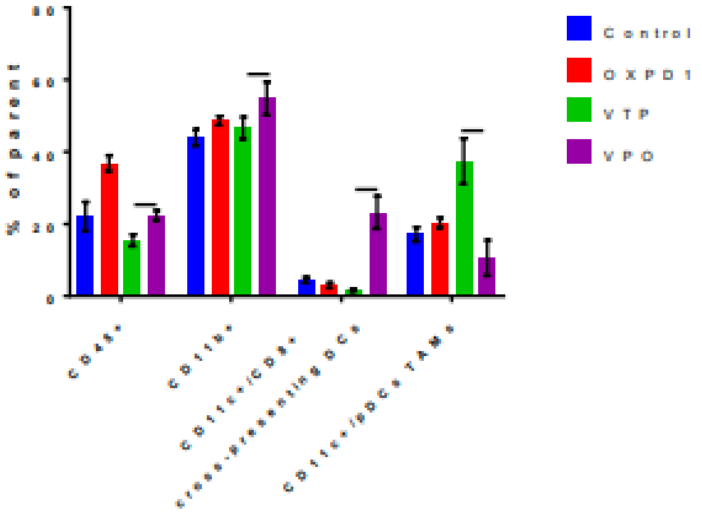

(C)

Figure 4. Combined PD-1 inhibitor/OX40 agonist therapy alters the frequency of specific myeloid cell subsets in VTP-treated tumors by day 7 post-treatment. (**A**) Representative flow cytometry plots identifying myeloid cell subsets within viable single cells. (**B**) Heat map summarizing the findings of flow cytometry analyses of tumor samples at day 7 after treatment. Values in boxes represent the mean percentage of each cell subpopulation (highlighted by row) in each experimental condition (highlighted by column). (**C**) Plot of flow cytometry data shown as the percentage of positive events among parent gated events. DCs, dendritic cells; pDCs, plasmacytoid dendritic cells; Conv DCs, conventional dendritic cells; TAMs, tumor-associated macrophages; MDSCs, myeloid-derived suppressor cells. Graph bars indicate mean ± SEM. OXPD1, OX40 agonist plus PD-1 inhibitor; VTP+OX40+PD-1, VTP plus PD-1 inhibitor and OX40 agonist.

We also performed studies using mice bearing 4T1 breast tumor cells. This is an aggressive breast cancer model with fast metastatic development, even when the primary tumor is still relatively small (<80 mm^3). However, at this time, many animals already had metastatic disease, and they died regardless of the primary tumor treated by VTP. In this validation model, outcomes were improved in the VTP+PD-1+OX40 group compared to the others, but the overall survival was not. In this study, no animal was sacrificed because of the primary tumor growth (volume > 2000 mm^3). Indeed, they died even after complete ablation of the primary tumor, showing that our timepoint for VTP treatment at two weeks was too late for disease control (supplementary Figure S3).

3. Materials and Methods

3.1. Cell Culture and Tumor Model

Luciferase-labelled MB-49 cells were obtained from the American Type Culture Collection (ATCC; Manassas, VA, USA) and cultured in RPMI medium supplemented with 10% fetal calf serum (Life Technologies/Thermo Fisher Scientific, Waltham, MA, USA). Seven- to eight-week-old male C57BL/6J mice were purchased from the National Cancer Institute (Frederick National Laboratory for Cancer Research, Frederick, MD, USA) and housed and treated according to a protocol approved by the MSKCC Institutional Animal Care and Use Committee (IACUC). Before tumor implantation, mice were anesthetized with inhaled isoflurane, meloxicam (2 mg/kg), and buprenorphine (0.5 mg/kg), and the hair and skin overlying the right flank was sterilized using a povidone-iodine and ethyl alcohol solution. MB-49 cells (50,000) were implanted in the right flank.

Fourteen days after tumor implantation, mice were assessed for tumor formation using noninvasive bioluminescence imaging. Animals were retro-orbitally injected with D-luciferin (200 mg/kg) 5 min before undergoing a 30-s scan using an IVIS Spectrum Optical

Imaging System (Xenogen, Alameda, CA, USA). Regions of interest from displayed images were drawn based on signal intensity and quantified using Living Image software version 2.60. Specific signal was calculated as the ratio of bioluminescent signal in the region of interest to the bioluminescent signal in a background region containing no tumors. When tumor volume reached approximately 100 mm^3, animals were randomly assigned to the following cohorts for future experiments: controls (n = 10), PD-1 inhibitor (n = 10), OX40 agonist (n = 10), PD-1 inhibitor plus OX40 agonist (n = 10), VTP (n = 20), VTP plus OX40 agonist (n = 20), VTP plus PD-1 inhibitor (n = 20) and VTP plus OX40 agonist and PD-1 inhibitor (n = 20) (Table 1). For survival and tumor growth comparison, the experiment was made in two steps, and the results were put together for statistical analysis.

Table 1. Therapeutic schemes received by each group.

GROUPS / INTERVENTION	PD-1	OX40	PD-1+OX40	VTP	VTP+PD-1	VTP+OX40	VTP+OX40+PD-1	CONTROL
Antibody anti OX-40		X	X			X	X	
Antibody anti-PD-1	X		X		X		X	
VTP *				X	X	X	X	
NO INTERVENTION								X

* Vascular Target Photodynamic therapy (150J).

3.2. *WST11-VTP and Immunomodulatory Treatment and Tumor Follow-Up*

Fifteen days after tumor implantation, tumor-bearing mice were anesthetized by intraperitoneal (i.p.) injection of a mixture of ketamine (150 mg/kg body weight) and xylazine (10 mg/kg) plus inhaled isoflurane administered via a tight-fitting nose cone. Following retro-orbital injection of WST11 (9 mg/kg bodyweight), tumors were illuminated with 753 nm light delivered via diode laser with a 600 µm end-fire fiber (Biolitec, East Longmeadow, MA, USA) for 10 min at 150 mW/cm^2. In the PD-1 inhibitor subgroups, InVivoPlus antimouse PD-1 CD279-Clone: 29F.1A12 (250 mg/kg, Bioxcell, West Lebanon, NH, USA) was injected intraperitoneally (IP) on days 1, 4, 7, 10, 13 and 16 after VTP. In the OX40 agonist subgroups, InVivoPlus antimouse OX40 CD134-Clone: OX-86 (500 mg/kg, Bioxcell, West Lebanon, NH, USA) was injected IP in a single dose on day 1 after VTP.

At least once a week until 60 days after VTP treatment, tumor volume was measured, the animals' health was checked, and IVIS spectrum imaging was performed to monitor local tumor and lung metastasis. When tumors exceeded 2000 mm^3 or lung metastasis developed, mice were euthanized via 100% carbon dioxide at 5 PSI for a minimum of 3 min, at a displacement rate of 30% chamber volume/minute in a cage or euthanasia chamber. These euthanasia practices are in accordance with our institution's Research Animal Resource Center's Recommended Methods of Euthanasia for laboratory Animals and the American Veterinary Medical Association Guidelines for the Euthanasia of Animals. For statistical analysis, we compared tumor volume until 30 days after tumor injection (Day 14 pos-VTP), when tumor volume in the control group reached the protocol limit (2000 mm^3).

3.3. *Immunohistochemistry*

Immunohistochemistry (IHC) was performed for CD3, CD4, CD8, and OX40 (CD134). IHC was performed on CD3, CD4, and CD8 using a Leica Bond RX automated strainer with bond reagents (Leica Biosystems, Buffalo Grove, IL, USA), including a polymer detection system (DS9800, Novocastra Bond Polymer Refine Detection, Leica Biosystems, Buffalo Grove, IL, USA). The chromogen was 3,3 diaminobenzidine tetrachloride (DAB), and sections were counterstained with hematoxylin. IHC was performed manually on OX40 (CD134) using an avidin-biotin detection system (Vectastain Elite ABC HRP Kit, Vector Laboratories, Burlingame, CA, USA). The chromogen was 3,3 diaminobenzidine

tetrachloride (DAB), and sections were counterstained with hematoxylin. Details for each marker are shown in the Supplementary Table S1.

Slides were digitally scanned using a Pannoramic Flash 250 digital scanner (3DHistech, Budapest, Hungary) and a Zeiss 20x/0.8NA objective. Relevant tissue regions were denoted and analyzed using the Pannoramic Viewer (3DHistech, Budapest, Hungary). CD3, CD4, CD8, and OX40 staining was quantified within tumors by manual counting of positive cells within defined regions of equal area.

3.4. Flow Cytometry

Single-cell suspensions were prepared from spleen, lymph nodes, or dissociated tumors after mechanical dissociation and passage through a 40 µm nylon filter. For all flow cytometry experiments, single-cell suspensions were maintained in flow cytometry buffer (PBS, 2% FBS) and blocked with rat antimouse CD16/32 for 15 min at 4 °C before incubating with the appropriate antibody cocktails in the dark for 30 min at 4 °C. Intracellular staining was performed using Cytofix/Cytoperm reagents (BD Biosciences, San Jose, Cam USA, Catalog No 554714) according to manufacturer's directions. Antibodies used for the myeloid panel include CD45.2-FITC (BD 553772), CD11c-PE (BD 557401), CD8a-PE-Texas Red (Life Technologies MCD0817), Ly6G-PerCP-Cy5.5 (BD 560602), Ly6C-PE-Cy7 (5236982), MHC II-eFluor450 (eBioscience 48-5321-82), CD86-APC (BD 558703), CD11b-APC/eFluor 780 (eBioscience 47-0112-82), and. Antibodies used for the T cell activation panel include Ki67-FITC (eBioscience 11-5698-82), CD62L-PE (BD 553151), GrzB-PE/Dazzle 594 (Biolegend 372216), CD8a-PerCP-Cy5.5 (BD 551162), CD44-PE/Cy7 (Biolegend 103030), CD4-V450 (BD 560468), Foxp3-APC (eBioscience 17-5773-82), CD45.2-Alexa Fluor700 (eBioscience 56-0454-82), CD25-APC/Cy7 (BD 557658). Both panels also included eBioscience Fixable viability dye-eFluor506 (ThermoFisher, New York, NY, USA, 65-0866-14). Cells were quantified using an LSRFortessa analyzer (BD Biosciences, San Jose, CA) equipped with 350 nm, 405 nm, 488 nm, 561 nm, and 640 nm excitation lasers. Data was collected using BD FACS Diva software (BD Biosciences) and analyzed using FlowJo software (Tree Star, Ashland, OR, USA). During acquisition, a live $CD45^+$ gate was set according to scatter parameters, live/dead and CD45 staining. A minimum of 1–4 $\times 10^5$ live CD45+ cells were acquired per sample. Compensation was set using UltraComp beads (ThermoFisher Scientific, New York, NY, USA, Cat No 01-2222-41) stained with individual fluorochromes and cells stained with live/dead dye. Compensation matrices were calculated and applied using FlowJo software. Unstained cells were acquired for each tissue type analyzed and fluorescence minus one (FMO) controls were used for gating to distinguish positively from negatively stained cell populations.

3.5. Statistical Analyses

GraphPad Prism was used for all statistical analyses. The Kruskal–Wallis test was used to assess differences among all groups and t-test was used for pairwise comparison of means between groups. A Kaplan–Meier curve was built for survival comparison. $p < 0.05$ was defined as significant.

4. Discussion

Photodynamic therapy is a minimally invasive tissue ablation modality in which a photosensitizing substance is activated through exposure to laser light radiation delivered at a specific wavelength. In the presence of oxygen, this triggers a photochemical reaction that generates oxidant species (radicals, singlet oxygen, triplet species), leading to targeted tissue destruction through direct cytotoxicity, vascular shutdown, and activation of an immune response. Our study highlights combination immunotherapy as a potential means to enhance the efficacy of VTP treatment. We show that combining VTP treatment with an immune checkpoint inhibitor and an immune costimulatory receptor agonist reduces tumor burden and enhance survival to a greater degree than VTP or the immunomodulators alone in a mouse model of urothelial cancer. We further demonstrate that these antitumor effects

occur mainly in a T cell-dependent manner, namely enrichment of cytotoxic and helper T cells in the tumor area and depletion of Treg cells, and that the increase in intratumoral T cells results in part from enhanced proliferation. The triple combination also acts via a T-cell independent mechanism to promote antitumor immunity, as it reduces numbers of intratumoral MDSCs.

The efficacy of this combination fits well with prior evidence showing that urothelial cancers are highly immunogenic malignancies. This immunogenicity has been known for decades, since the discovery that bacillus Calmette–Guerin slows the growth of bladder cancer by invoking immunological activity [22]. Similarly, immune checkpoint inhibitors have proven beneficial as salvage therapy in metastatic urothelial cancer [23,24], in accordance with its high mutation frequency [25], which presumably leads to greater neoantigen burden [26], known to correlate with checkpoint inhibitor efficacy [27]. Immune responses are also correlated with tumor aggressiveness even in the absence of immunotherapies, as numbers of $CD8^+$ T cells are recently described as predictive of survival in muscle-invasive and advanced urothelial carcinoma [28,29].

The benefit of combining VTP with PD-1/PD-L1 blockade and OX40 agonism (VTP+OX40+PD-1 treatment) may extend to other cancers, especially those in which two of the component therapies have been shown to synergize in animal models. These include lung and kidney cancer, in which O'Shaughnessy et al. showed recently that adding anti-PD-1 or anti-PD-L1 to VTP reduces metastasis and improves survival [11]. As Preise et al. showed that VTP induces antitumor immunity that is cross-reactive between colon and breast cancers, these might also respond to the combination [10].

Our study extends the range of therapies with which OX40 agonism has been shown to synergize. In addition to immune checkpoint inhibitors, OX40-stimulating antibodies have been shown to augment the effectiveness of several treatments that indirectly stimulate immune responses, including dasatinib (in a c-KIT mutant P815 mastocytoma tumor model [30], dabrafenib and trametinib (in $BRAF^{V600E}$-mutant melanoma) [31], and radiotherapy [32–34].

We found that combination VTP plus PD-1 inhibition plus OX40 agonist (VTP+OX40+PD-1) treatment inhibits immune suppression by reducing the intratumor prevalence of regulatory T cells (Tregs), tumor-associated macrophages (TAMs) and, especially, myeloid-derived suppressor cells (MDSCs). MDSCs have been the focus of intense research in recent years; high numbers of these immunosuppressive cells have been correlated with tumor aggressiveness and poor prognosis, including in urothelial cancer [35,36]. Our laboratory has recently shown that targeting MDSCs using anti-CSF1R in combination with VTP therapy not only decreased the numbers of intratumoral MDSCs and TAMs, but also increased $CD8^+$ T cell infiltration, decreasing tumor growth and improving overall survival in a prostate cancer model [37]. Thus, the reduction of TAMs and MDSCs by the VTP+OX40+PD-1 combination may have been a major contributor to its efficacy.

The strong T cell recruitment induced by VTP+OX40+PD-1 treatment—greater than that following treatment with immunomodulators in the absence of VTP—is an important finding of our study. Thus, adding VTP could overcome a limitation of these immunotherapies, which are generally more effective in mice bearing small tumors. This synergistic effect on T cells confirms Aspeslagh et al.'s postulation that therapies that increase antigen release, a known effect of VTP [38], could improve the potency of OX40 stimulation [13]. Indeed, VTP+OX40+PD-1 provided greater local tumor control compared with PD-1 inhibition and OX40 agonism, including complete remission in 66% of the animals. We speculate that the VTP-induced acute inflammatory response acts as an immune booster, releasing antigens to which immunotherapy-stimulated and deinhibited T cells react.

5. Conclusions

In summary, we provide evidence that OX40 agonism plus PD-1 inhibitor immunotherapy is a valuable combinatorial approach that improves the efficacy of VTP in a urothelial cancer model. The results presented here support the concurrent manipulation of these

two immune pathways to maximize the ability of VTP treatment to provide local tumor control and improve survival. This study, along with prior findings, indicates that the addition of immunotherapy to VTP treatment is an effective therapeutic strategy for reducing immunosuppression within tumors and ultimately enhancing antitumor immunity.

Supplementary Materials: The following are available online: Table S1: Immunohistochemistry (IHC) for CD3, CD4, CD8. Figure S1: Growth patterns individed by VTP and no VTP groups. Figure S2: Metastatic signaling by IVIS following VTP Figure S3: Survival outcomes after VTP in the 4T1 model.

Author Contributions: Conceptualization, R.G.A. and P.G.; Formal analysis, A.S.; Investigation, A.J.S., K.N., J.T., C.H., J.C., A.B.R., S.L., S.Z., R.G. and K.K.; Supervision, J.A.C.; Writing–original draft, L.N.; Writing–review & editing, L.A. and A.R. All authors have read and agreed to the published version of the manuscript.

Funding: This study was supported in part by the NIH/NCI Cancer Center Support Grant (P30 CA008748) and the Thompson Family Foundation.

Institutional Review Board Statement: Not applicable.

Informed Consent Statement: Not applicable.

Acknowledgments: The authors would like to thank Sebastien Monette for his support and assistance with this project.

Conflicts of Interest: The authors declare no conflict of interest.

Sample Availability: Samples are not available from authors.

References

1. Raman, J.D.; Messer, J.; Sielatycki, J.A.; Hollenbeak, C.S. Incidence and survival of patients with carcinoma of the ureter and renal pelvis in the USA, 1973–2005. *BJU Int.* **2011**, *107*, 1059–1064. [CrossRef]
2. Siegel, R.L.; Miller, K.D.; Jemal, A. Cancer Statistics, 2017. *CA Cancer J. Clin.* **2017**, *67*, 7–30. [CrossRef] [PubMed]
3. Kurohane, K.; Tominaga, A.; Sato, K.; North, J.R.; Namba, Y.; Oku, N. Photodynamic therapy targeted to tumor-induced angiogenic vessels. *Cancer Lett.* **2001**, *167*, 49–56. [CrossRef]
4. Chen, B.; Pogue, B.W.; Hoopes, P.J.; Hasan, T. Vascular and cellular targeting for photodynamic therapy. *Crit. Rev. Eukaryot. Gene Expr.* **2006**, *16*, 279–305. [CrossRef] [PubMed]
5. Noweski, A.; Roosen, A.; Lebdai, S.; Barret, E.; Emberton, M.; Benzaghou, F.; Apfelbeck, M.; Gaillac, B.; Gratzke, C.; Stief, C.; et al. Medium-term Follow-up of Vascular-targeted Photodynamic Therapy of Localized Prostate Cancer Using TOOKAD Soluble WST-11 (Phase II Trials). *Eur. Urol. Focus.* **2019**, *5*, 1022–1028. [CrossRef]
6. Azzouzi, A.R.; Vincendeau, S.; Barret, E.; Cicco, A.; Kleinclauss, F.; van der Poel, H.G.; Stief, C.G.; Rassweiler, J.; Salomon, G.; Solsona, E.; et al. Padeliporfin vascular-targeted photodynamic therapy versus active surveillance in men with low-risk prostate cancer (CLIN1001 PCM301): An open-label, phase 3, randomised controlled trial. *Lancet Oncol.* **2017**, *18*, 181–191. [CrossRef]
7. Corradi, R.B.; LaRosa, S.; Jebiwott, S.; Murray, K.S.; Rosenzweig, B.; Somma, A.J.; Gomez, R.S.; Scherz, A.; Kim, K.; Coleman, J.A. Effectiveness of the combination of vascular targeted photodynamic therapy and anti-cytotoxic T-lymphocyte-associated antigen 4 in a preclinical mouse model of urothelial carcinoma. *Int. J. Urol.* **2019**, *26*, 414–422. [CrossRef]
8. Murray, K.S.; Winter, A.G.; Corradi, R.B.; LaRosa, S.; Jebiwott, S.; Somma, A.; Takaki, H.; Srimathveeravalli, G.; Lepherd, M.; Monette, S.; et al. Treatment Effects of WST11 Vascular Targeted Photodynamic Therapy for Urothelial Cell Carcinoma in Swine. *J. Urol.* **2016**, *196*, 236–243. [CrossRef] [PubMed]
9. Madar-Balakirski, N.; Tempel-Brami, C.; Kalchenko, V.; Brenner, O.; Varon, D.; Scherz, A.; Salomon, Y. Permanent occlusion of feeding arteries and draining veins in solid mouse tumors by vascular targeted photodynamic therapy (VTP) with Tookad. *PLoS ONE* **2010**, *5*, e10282. [CrossRef]
10. Preise, D.; Oren, R.; Glinert, I.; Kalchenko, V.; Jung, S.; Scherz, A.; Salomon, Y. Systemic antitumor protection by vascular-targeted photodynamic therapy involves cellular and humoral immunity. *Cancer Immunol. Immunother.* **2009**, *58*, 71–84. [CrossRef]
11. O'Shaughnessy, M.J.; Murray, K.S.; La Rosa, S.P.; Budhu, S.; Merghoub, T.; Somma, A.; Monette, S.; Kim, K.; Corradi, R.B.; Scherz, A. Systemic Antitumor Immunity by PD-1/PD-L1 Inhibition Is Potentiated by Vascular-Targeted Photodynamic Therapy of Primary Tumors. *Clin. Cancer Res.* **2018**, *24*, 592–599. [CrossRef] [PubMed]
12. Mahoney, K.M.; Rennert, P.D.; Freeman, G.J. Combination cancer immunotherapy and new immunomodulatory targets. *Nat. Rev. Drug Discov.* **2015**, *14*, 561–584. [CrossRef] [PubMed]
13. Aspeslagh, S.; Postel-Vinay, S.; Rusakiewicz, S.; Soria, J.C.; Zitvogel, L.; Marabelle, A. Rationale for anti-OX40 cancer immunotherapy. *Eur. J. Cancer* **2016**, *52*, 50–66. [CrossRef] [PubMed]

14. Sadun, R.E.; Hsu, W.E.; Zhang, N.; Nien, Y.C.; Bergfeld, S.A.; Sabzevari, H.; Lutsiak, M.E.; Khawli, L.; Hu, P.; Epstein, A.L. Fc-mOX40L fusion protein produces complete remission and enhanced survival in 2 murine tumor models. *J. Immunother.* **2008**, *31*, 235–245. [CrossRef]
15. Curti, B.D.; Kovacsovics-Bankowski, M.; Morris, N.; Walker, E.; Chisholm, L.; Floyd, K.; Walker, J.; Gonzalez, I.; Meeuwsen, T.; Fox, B.A. OX40 is a potent immune-stimulating target in late-stage cancer patients. *Cancer Res.* **2013**, *73*, 7189–7198. [CrossRef] [PubMed]
16. Pardee, A.D.; McCurry, D.; Alber, S.; Hu, P.; Epstein, A.L.; Storkus, W.J. A therapeutic OX40 agonist dynamically alters dendritic, endothelial, and T cell subsets within the established tumor microenvironment. *Cancer Res.* **2010**, *70*, 9041–9052. [CrossRef]
17. Bulliard, Y.; Jolicoeur, R.; Zhang, J.; Dranoff, G.; Wilson, N.S.; Brogdon, J.L. OX40 engagement depletes intratumoral Tregs via activating FcgammaRs, leading to antitumor efficacy. *Immunol. Cell Biol.* **2014**, *92*, 475–480. [CrossRef]
18. Messenheimer, D.J.; Jensen, S.M.; Afentoulis, M.E.; Wegmann, K.W.; Feng, Z.; Friedman, D.J.; Gough, M.J.; Urba, W.J.; Fox, B.A. Timing of PD-1 Blockade Is Critical to Effective Combination Immunotherapy with Anti-OX40. *Clin. Cancer Res.* **2017**, *23*, 6165–6177. [CrossRef]
19. Guo, Z.; Wang, X.; Cheng, D.; Xia, Z.; Luan, M.; Zhang, S. PD-1 blockade and OX40 triggering synergistically protects against tumor growth in a murine model of ovarian cancer. *PLoS ONE* **2014**, *9*, e89350. [CrossRef]
20. Redmond, W.L.; Linch, S.N.; Kasiewicz, M.J. Combined targeting of costimulatory (OX40) and coinhibitory (CTLA-4) pathways elicits potent effector T cells capable of driving robust antitumor immunity. *Cancer Immunol. Res.* **2014**, *2*, 142–153. [CrossRef]
21. Filatenkov, A.; Baker, J.; Mueller, A.M.; Kenkel, J.; Ahn, G.O.; Dutt, S.; Zhang, N.; Kohrt, H.; Jensen, K.; Dejbakhsh-Jones, S.; et al. Ablative Tumor Radiation Can Change the Tumor Immune Cell Microenvironment to Induce Durable Complete Remissions. *Clin. Cancer Res.* **2015**, *21*, 3727–3739. [CrossRef]
22. Herr, H.W.; Morales, A. History of bacillus Calmette-Guerin and bladder cancer: An immunotherapy success story. *J. Urol.* **2008**, *179*, 53–56. [CrossRef]
23. Rosenberg, J.E.; Hoffman-Censits, J.; Powles, T.; van der Heijden, M.S.; Balar, A.V.; Necchi, A.; Dawson, N.; O'Donnell, P.H.; Balmanoukian, A.; Loriot, Y.; et al. Atezolizumab in patients with locally advanced and metastatic urothelial carcinoma who have progressed following treatment with platinum-based chemotherapy: A single-arm, multicentre, phase 2 trial. *Lancet* **2016**, *387*, 1909–1920. [CrossRef]
24. Bellmunt, J.; de Wit, R.; Vaughn, D.J.; Fradet, Y.; Lee, J.L.; Fong, L.; Vogelzang, N.J.; Climent, M.A.; Petrylak, D.P.; Choueiri, T.K.; et al. Pembrolizumab as Second-Line Therapy for Advanced Urothelial Carcinoma. *N. Engl. J. Med.* **2017**, *376*, 1015–1026. [CrossRef] [PubMed]
25. Lawrence, M.S.; Stojanov, P.; Polak, P.; Kryukov, G.V.; Cibulskis, K.; Sivachenko, A.; Carter, S.L.; Stewart, C.; Mermel, C.H.; Roberts, S.A.; et al. Mutational heterogeneity in cancer and the search for new cancer-associated genes. *Nature* **2013**, *499*, 214–218. [CrossRef] [PubMed]
26. Gubin, M.M.; Artyomov, M.N.; Mardis, E.R.; Schreiber, R.D. Tumor neoantigens: Building a framework for personalized cancer immunotherapy. *J. Clin. Investig.* **2015**, *125*, 3413–3421. [CrossRef] [PubMed]
27. McGranahan, N.; Furness, A.J.; Rosenthal, R.; Ramskov, S.; Lyngaa, R.; Saini, S.K.; Jamal-Hanjani, M.; Wilson, G.A.; Birkbak, N.J.; Hiley, C.T.; et al. Clonal neoantigens elicit T cell immunoreactivity and sensitivity to immune checkpoint blockade. *Science* **2016**, *351*, 1463–1469. [CrossRef] [PubMed]
28. Sharma, P.; Shen, Y.; Wen, S.; Yamada, S.; Jungbluth, A.A.; Gnjatic, S.; Bajorin, D.F.; Reuter, V.E.; Herr, H.; Old, L.J.; et al. CD8 tumor-infiltrating lymphocytes are predictive of survival in muscle-invasive urothelial carcinoma. *Proc. Natl. Acad. Sci. USA* **2007**, *104*, 3967–3972. [CrossRef] [PubMed]
29. Faraj, S.F.; Munari, E.; Guner, G.; Taube, J.; Anders, R.; Hicks, J.; Meeker, A.; Schoenberg, M.; Bivalacqua, T.; Drake, C.; et al. Assessment of tumoral PD-L1 expression and intratumoral CD8+ T cells in urothelial carcinoma. *Urology* **2015**, *85*, 703.e1–703.e6. [CrossRef]
30. Yang, Y.; Liu, C.; Peng, W.; Lizée, G.; Overwijk, W.W.; Liu, Y.; Woodman, S.E.; Hwu, P. Antitumor T-cell responses contribute to the effects of dasatinib on c-KIT mutant murine mastocytoma and are potentiated by anti-OX40. *Blood* **2012**, *120*, 4533–4543. [CrossRef]
31. Homet Moreno, B.; Mok, S.; Comin-Anduix, B.; Hu-Lieskovan, S.; Ribas, A. Combined treatment with dabrafenib and trametinib with immune-stimulating antibodies for BRAF mutant melanoma. *Oncoimmunology* **2016**, *5*, e1052212. [CrossRef] [PubMed]
32. Yokouchi, H.; Yamazaki, K.; Chamoto, K.; Kikuchi, E.; Shinagawa, N.; Oizumi, S.; Hommura, F.; Nishimura, T.; Nishimura, M. Anti-OX40 monoclonal antibody therapy in combination with radiotherapy results in therapeutic antitumor immunity to murine lung cancer. *Cancer Sci.* **2008**, *99*, 361–367. [CrossRef] [PubMed]
33. Gough, M.J.; Crittenden, M.R.; Sarff, M.; Pang, P.; Seung, S.K.; Vetto, J.T.; Hu, H.M.; Redmond, W.L.; Holland, J.; Weinberg, A.D. Adjuvant therapy with agonistic antibodies to CD134 (OX40) increases local control after surgical or radiation therapy of cancer in mice. *J. Immunother.* **2010**, *33*, 798–809. [CrossRef] [PubMed]
34. Niknam, S.; Barsoumian, H.B.; Schoenhals, J.E.; Jackson, H.L.; Yanamandra, N.; Caetano, M.S.; Li, A.; Younes, A.I.; Cadena, A.; Cushman, T.R.; et al. Radiation Followed by OX40 Stimulation Drives Local and Abscopal Antitumor Effects in an Anti-PD1-Resistant Lung Tumor Model. *Clin. Cancer Res.* **2018**, *24*, 5735–5743. [CrossRef]

35. Yang, G.; Shen, W.; Zhang, Y.; Liu, M.; Zhang, L.; Liu, Q.; Lu, H.H.; Bo, J. Accumulation of myeloid-derived suppressor cells (MDSCs) induced by low levels of IL-6 correlates with poor prognosis in bladder cancer. *Oncotarget* **2017**, *8*, 38378–38388. [CrossRef]
36. Parker, K.H.; Beury, D.W.; Ostrand-Rosenberg, S. Myeloid-Derived Suppressor Cells: Critical Cells Driving Immune Suppression in the Tumor Microenvironment. *Adv. Cancer Res.* **2015**, *128*, 95–139. [CrossRef] [PubMed]
37. Lebdai, S.; Gigoux, M.; Alvim, R.; Somma, A.; Nagar, K.; Azzouzi, A.R.; Cussenot, O.; Merghoub, T.; Wolchok, J.D.; Scherz, A.; et al. Potentiating vascular-targeted photodynamic therapy through CSF-1R modulation of myeloid cells in a preclinical model of prostate cancer. *Oncoimmunology* **2019**, *8*, e1581528. [CrossRef]
38. Mroz, P.; Hashmi, J.T.; Huang, Y.Y.; Lange, N.; Hamblin, M.R. Stimulation of anti-tumor immunity by photodynamic therapy. *Expert Rev. Clin. Immunol.* **2011**, *7*, 75–91. [CrossRef]

THE JOURNAL of UROLOGY®
www.auajournals.org/journal/juro

Final Results of a Phase I Trial of WST-11 (TOOKAD Soluble) Vascular-targeted Photodynamic Therapy for Upper Tract Urothelial Carcinoma

Wesley Yip[1], Daniel D. Sjoberg[2], Lucas M. Nogueira,[1] Andrew T. Tracey,[1] Ricardo G. Alvim,[1] Peter A. Reisz,[1] Quinlan Demac,[3] Nicole E. Benfante,[3] Rand W. Vanden Berg,[1] Kwanghee Kim,[3] Hikmat Al-Ahmadie,[4] Oscar Lin,[4] Bernard H. Bochner,[1] Guido Dalbagni,[1] S. Machele Donat,[1] Eugene J. Pietzak,[1] A. Ari Hakimi,[1] David B. Solit,[5] Avigdor Scherz,[6] Dean F. Bajorin,[5] and Jonathan A. Coleman[1]*

[1]Urology Service, Department of Surgery, Memorial Sloan Kettering Cancer Center, New York, New York
[2]Department of Epidemiology & Biostatistics, Memorial Sloan Kettering Cancer Center, New York, New York
[3]Department of Surgery, Memorial Sloan Kettering Cancer Center, New York, New York
[4]Department of Pathology, Memorial Sloan Kettering Cancer Center, New York, New York
[5]Genitourinary Oncology Service, Department of Medicine, Memorial Sloan Kettering Cancer Center, New York, New York
[6]Weizmann Institute of Science, Rehovot, Israel

Submitted October 15, 2022; accepted January 24, 2023; published February 1, 2023.

Support: Funding received from the Thompson Family Foundation, NIH/NCI Cancer Center Support Grant P30 CA008748, and Ruth L. Kirschstein National Research Service Award T32CA082088. The study sponsors had no role in the design of the study; in the analysis and interpretation of data; in the writing of the report; and in the decision to submit the paper for publication.

Conflict of Interest: None.

Ethics Statement: This study received Institutional Review Board approval (IRB No. 18-148).

Author Contributions: Conception and design: WY, DJS, LNM, AJT, RWVB, SMD, AS, DJB, JAC; Data analysis and interpretation: WY, DJS, LNM, AJT, DD, RWVB, KK, HA-A, GD, AAH, DBS, DJB, JAC; Data acquisition: WY, LNM, AJT, REA, PNR, DD, NEB, HA-A, DL, DJB, LJP, DJS, JAC; Critical revision of the manuscript for scientific and factual content: WY, DJS, LNM, AJT, REA, PNR, DD, NEB, RWVB, HA-A, DL, DJB, GD, SMD, LJP, AAH, DBS, AS, DJB, JAC; Drafting the manuscript: WY, DJS, LNM, KK, DJS, JAC; Statistical analysis: DJS, LNM, DD, RWVB; Supervision: WY, DJS, AJT, PNR, NEB, KK, HA-A, DL, DJB, GD, SMD, LJP, AAH, DBS, AS, DJB, JAC.

Data Availability: Deidentified participant data and related study documents will be made available to other researchers with publication upon request through a formal signed data sharing agreement process.

*Correspondence: Urology Service, Department of Surgery, Memorial Sloan Kettering Cancer Center, 1275 York Ave, New York, NY 10065 (telephone: 646-422-4432; email: colemanj@mskcc.org).

Purpose: Vascular-targeted photodynamic therapy with the intravascular photosensitizing agent padeliporfin (WST-11/TOOKAD-Soluble) has demonstrated therapeutic efficacy as an ablative treatment for localized cancer with potential adaptation for endoscopic management of upper tract urothelial carcinoma. This Phase I trial (NCT03617003) evaluated the safety of vascular-targeted photodynamic therapy with WST-11 in upper tract urothelial carcinoma.

Materials and Methods: Nineteen patients underwent up to 2 endoscopic vascular-targeted photodynamic therapy treatments, with follow-up for up to 6 months. Patients who had residual or recurrent upper tract urothelial carcinoma (any grade/size) failing prior endoscopic treatment or unable or unwilling to undergo surgical resection were eligible for inclusion. The primary endpoint was to identify the maximally tolerated dose of laser light fluence. A dose escalation model was employed, with increasing light fluence (100-200 mW/cm) using a modified continual reassessment method. The secondary endpoint was treatment efficacy, defined by absence of visible tumor and negative urine cytology 30 days posttreatment.

Results: Fourteen (74%) patients received the maximally tolerated dose of 200 mW/cm, 2 (11%) of whom experienced a dose-limiting toxicity. The initial 30-day treatment response rate was 94% (50% complete, 44% partial). Eight patients underwent a second treatment, with a final observed 68% complete response rate. Leading toxicities were flank pain (79%) and hematuria (84%), which were transient. No ureteral strictures associated with treatment were identified during follow-up.

Conclusions: Vascular-targeted photodynamic therapy with WST-11 has an acceptable safety profile with strong potential as an effective, kidney-sparing endoscopic management option for upper tract urothelial carcinoma. The recently initiated multicenter Phase 3 ENLIGHTED trial (NCT04620239) is expected to provide further evidence on this therapy.

Key Words: phototherapy, ureteroscopy, urogenital neoplasms

THE JOURNAL OF UROLOGY®

https://doi.org/10.1097/JU.0000000000003202
Vol. 209, 863-871, May 2023
Printed in U.S.A.

Upper tract urothelial carcinoma (UTUC) accounts for 5% of all urothelial neoplasms[1] and 10% of renal tumors,[2] with approximately two-thirds occurring in the renal pelvis.[3] Radical nephroureterectomy as extirpative management is associated with significant morbidity, including the development of chronic kidney disease or end-stage renal disease in up to 80% of patients.[4] In cases of low-grade tumors with minimal risk of metastatic progression, and even some early high-grade superficial tumors, this surgery is drastically overutilized.[5] As such, there is increased interest in organ-sparing approaches, including endoscopic management techniques, to preserve renal function. Endoscopic approaches are technically challenging and are associated with a 60% rate of recurrence.[6] Multiple treatments are often necessary, which increases the risk of procedure-related complications such as perforation, bleeding, infection, and strictures.[6] Up to 20% of patients undergoing endoscopic management of UTUC will eventually require nephrectomy, and 30% will recur in the bladder.[7] There is a clear unmet need to improve kidney-sparing endoscopic management techniques for patients with UTUC.

Photodynamic therapy, which utilizes a photosensitizing drug and light application to create tissue damage, is an effective and Food and Drug Administration–approved localized treatment modality for several malignancies, including lung, esophageal, and skin cancers, as well as the endoluminal treatment of urothelial cancers.[8] In the esophagus, eg, certain obstructing tumors may not be excisable using a neodymium yttrium-aluminum-garnet (Nd:YAG) laser, but photodynamic therapy may offer palliation in lieu of total esophagectomy.[8] However, its uptake has been limited by prolonged patient light sensitivity and nonselective tissue destruction.

Padeliporfin (WST-11/TOOKAD Soluble; STEBA Biotech, Luxembourg) is a new investigational short-acting photodynamic agent to produce a novel form of vascular-targeted photodynamic treatment (VTP), which has been proven to be effective against several cancers in preclinical studies and clinical trials.[9-11] In prostate cancer, VTP has been utilized as focal therapy option for unilateral low-risk disease.[11] After intravenous administration of WST-11, near-infrared light delivered through an optical fiber illuminates the tumor tissues and activates the agent to generate reactive oxygen and nitrogen species (free radicals). Tumor vasculature then collapses, and a propagation of cytotoxic effects to surrounding tumor cells results in athermal tumor ablation, which is histologically evident as coagulative necrosis within 24-48 hours.[12-15] The cytotoxic ablative effect is highly localized and transient, as WST-11 is rapidly cleared from the circulation in minutes. As a result, patient light sensitivity is minimized.[9] Following success utilizing WST-11–mediated VTP in preclinical models,[15] we undertook a prospective Phase 1 study to evaluate this approach as an endoscopic treatment in patients with UTUC. While toxicities in prior studies were minimal (ie, hematuria, pain, dysuria),[11] the effective light dose for the treatment of UTUC has not yet been determined, and so we hypothesized that a maximum of 200 mW/cm would have a toxicity rate that does not exceed an acceptable threshold of 20%. The primary objective was to determine the maximum tolerated dose (MTD) of laser light fluence, and the secondary objective was to assess the efficacy of VTP as a primary treatment for UTUC.

MATERIALS AND METHODS

This is a single-institution, nonrandomized, open-label Phase 1 study conducted at Memorial Sloan Kettering Cancer Center, registered under ClinicalTrials.gov Identifier NCT03617003. The protocol was approved on March 19, 2018 and began accrual on August 1, 2018. The study was closed to accrual on April 21, 2021, and the final analysis was performed on June 15, 2022. After Institutional Review Board approval (MSK IRB No. 18-140), patients were enrolled based on the following inclusion criteria: confirmed tissue diagnosis of UTUC; residual or recurrent cancer following prior endoscopic treatment; and ineligibility or unwillingness to undergo surgical management by resection of the involved kidney and/or ureter. Patients were also required to have a Karnofsky Performance Status >50%, adequate organ function (including calculated creatinine clearance >40 mL/min), and could not have received any systemic therapy (ie, chemotherapy, biological therapy, and/or immunotherapy) <4 weeks prior to treatment. Patients with existing ureteral obstruction and/or existing ureteral stent were permitted. Patients were excluded if pregnant or breast-feeding, with T4 tumors involving bowel or major blood vessels, or not surgical candidates due to medical comorbidities. Patients then underwent endoscopy of the involved upper urinary system, with measurement of tumor size (by caliper or visual reference gauge) and determination of location. Visible tumors were treated with VTP based on a prescribed light dose using the escalation protocol described below. Treatment consisted of a 10-minute intravenous administration of WST-11 at a fixed dose of 4 mg/kg, followed by light activation delivered through an INTERmedic (Barcelona, Spain) diode laser (200 μm fiber, 753 nm wavelength of light) over 10 minutes. The endoscope is positioned proximal to the site of the index tumor to be treated, and the light fiber is advanced through the endoscope and positioned within the collecting system in proximity to the index tumor. The fiber is held in place for the duration of light application, then removed through the endoscope. Per protocol, a ureteral stent was utilized following the initial endoscopic treatment to mitigate the risks inherent to endoscopy, which was removed at the subsequent evaluation. Repeat endoscopic evaluations were performed at 7 and 30 days posttreatment to assess for visual evidence of

Table 1. *Patient Summary*

Characteristic	N = 13
Age, median (IQR), y	85 (80, 70)
Sex, No. (%)	
Female	6 (32)
Male	13 (68)
Race, No. (%)	
White	18 (84)
Black or African American	2 (11)
Other	1 (5.3)
BMI, median (IQR), kg/m^2	28 (26, 31)
Unknown	2
Smoking status, No. (%)	
Current	4 (22)
Former	9 (50)
None	5 (28)
Unknown	1
Prior radiation, No. (%)	0 (0)
Prior surgery, No. (%)[a]	11 (58)
Tumor grade, No. (%)	
High grade	5 (26)
Low grade	14 (74)
Laterality, No. (%)	
Left	9 (47)
Right	10 (54)
Re-treated, No. (%)	8 (42)
VTP dose received, No. (%)	
100 mW/cm	1 (5.3)
150 mW/cm	4 (21)
200 mW/cm	14 (74)
DLT, No. (%)	2 (11)
Maximum tumor diameter, median (IQR), mm	10 (5, 20)
Maximum mm tumor diameter, No. (%)	
<15	11 (58)
≥15	8 (42)
Treatment response, No. (%)	
No response	1 (5.6)
Partial response	8 (44)
Complete response	9 (50)
Unknown	1

Abbreviations: BMI, body mass index; DLT, dose-limiting toxicity; IQR, interquartile range; VTP, vascular targeted photodynamic therapy.
[a] Ureteroscopy and ablation.

Table 2. *Response Status by Dose*

Group/VTP dose received	Treatment response, No. (%)		
	No response	Partial response	Complete response
Overall			
100 mW/cm	0 (0)	0 (0)	1 (100)
150 mW/cm	0 (0)	2 (50)	2 (50)
200 mW/cm	1 (7.7)	6 (46)	6 (46)
Overall	1 (5.6)	8 (44)	9 (50)
Maximum tumor diameter <15 mm			
100 mW/cm	0 (0)	0 (0)	1 (100)
150 mW/cm	0 (0)	2 (67)	1 (33)
200 mW/cm	0 (0)	3 (43)	4 (57)
Overall	0 (0)	5 (45)	6 (55)
Maximum tumor diameter ≥15 mm			
100 mW/cm	—	—	—
150 mW/cm	0 (0)	0 (0)	1 (100)
200 mW/cm	1 (17)	3 (50)	2 (33)
Overall	1 (14)	3 (43)	3 (43)
High grade			
100 mW/cm	—	—	—
150 mW/cm	0 (0)	1 (100)	0 (0)
200 mW/cm	1 (25)	1 (25)	2 (50)
Overall	1 (20)	2 (40)	2 (40)
Low grade			
100 mW/cm	0 (0)	0 (0)	1 (100)
150 mW/cm	0 (0)	1 (33)	2 (67)
200 mW/cm	0 (0)	5 (56)	4 (44)
Overall	0 (0)	6 (46)	7 (54)

Abbreviation: VTP, vascular targeted photodynamic therapy.

abnormalities, treatment effect, and evidence of ureteral stricture. Patients were followed for up to 6 months. Patients were allowed to receive a second VTP treatment within 6 months of the first if tumors were subsequently identified at the initial target site or at a different site in the upper tract.

The primary objective of this Phase 1 study was to identify the MTD of laser light fluence rate (mW/cm) of light exposure for VTP treatment of urothelial cancer involving the upper urinary tract. The MTD was defined as the dose whose toxicity rate did not exceed an acceptable threshold of 20%. Dose-limiting toxicity (DLT) was a binary outcome where a patient either did or did not experience a DLT. All toxicities were graded according to the National Cancer Institute Common Terminology Criteria for Adverse Events v4.0. The trial was monitored using a modification of the continual reassessment method (mCRM),[16] which assumes a simple model for the probability of a DLT as a function of dose and uses the occurrence of toxicities in the patients enrolled in the trial to sequentially determine which dose to administer to a newly enrolled patient. Newly enrolled patients were assigned a dose after previously enrolled patients were assessed for DLT. The first enrolled patient received the lowest dose, and dose skipping (eg, from the lowest dose to the highest) was not permitted. Enrollment continued until 18 patients were eligible for the primary study aim to identify the MTD and the secondary aim assessing tumor response.

We studied 3 dose levels of laser light fluence: 100, 150, and 200 mW/cm. These levels were based on our preclinical large-animal studies, in which levels from 50 to 200 mW/cm were tested. Fifty mW/cm produced treatment depth limited to the lamina propria, while 200 mW/cm penetrated muscularis propria.[15] Our initial estimates of DLT probabilities were 5%, 10%, and 20% for the 3 doses, respectively. Thus, our a priori belief was that 200 mW/cm is the MTD. We assumed that the dose-toxicity followed a logistic model where a was the unknown parameter we needed to estimate in order to determine which dose was the MTD, and b was fixed at 3.

$$\Pr(\mathrm{DLT}) = \frac{e^{b+a x}}{1+e^{b+a x}}$$

A value of $a = 1.0$ indicates that our beliefs were correct, while a value of a less than (greater than) 1.0 indicates that the combinations are more (less) toxic than believed. To reflect the uncertainty in our prior probability estimates, we assumed a followed an exponential distribution (prior distribution) with a mean of 1.0. If our a priori estimates of toxicity were correct, the probability that we would correctly identify 200 mW/cm as the MTD was 75%, with an expected 62% of enrolled patients being treated at the MTD.

The secondary objective of this study was to assess the efficacy of VTP as a primary treatment for UTUC, based on the response of the target treatment site. No entry

Table 3. *Laboratory Values*

Characteristic	Baseline	Day 2	Day 7	Day 14	Day 30
Creatinine:					
No.	19	18	18	18	16
Median (IQR), mg/dl.	1.10 (0.90, 1.35)	1.10 (0.90, 1.37)	1.05 (1.00, 1.48)	1.10 (0.90, 1.40)	1.05 (0.88, 1.30)
Range:	0.80, 1.80	0.80, 1.90	0.70, 9.00	0.80, 2.00	0.70, 1.50
BUN					
No.	19	18	18	18	16
Median (IQR), mg/dl.	18.0 (16.0, 21.0)	15.5 (12.0, 17.0)	16.5 (15.2, 19.8)	18.0 (16.2, 19.0)	18.0 (15.2, 20.5)
Range:	14.0, 28.0	9.0, 27.0	13.0, 28.0	14.0, 33.0	10.0, 28.0
Calcium					
No.	19	18	18	18	16
Median (IQR), mg/dl.	9.50 (9.05, 9.60)	8.95 (8.70, 9.20)	9.35 (9.15, 9.70)	9.30 (9.00, 9.40)	9.40 (9.00, 9.53)
Range:	8.50, 10.60	8.10, 10.20	8.90, 10.40	8.70, 10.30	8.80, 10.00
eGFR (MDRD)					
No.	19	18	18	18	16
Median (IQR), ml/min/1.73 m^2	63 (50, 74)	62 (51, 67)	64 (51, 75)	66 (50, 73)	66 (56, 72)
Range:	35, 85	36, 84	6, 85	34, 85	40, 85

Abbreviations: BUN, blood urea nitrogen; eGFR, estimated glomerular filtration rate; IQR, interquartile range; MDRD, Modification of Diet in Renal Disease.

criteria were placed on tumor size or grade in this Phase 1 trial. Response was assessed at 30 days after treatment and complete response (CR) was defined as an absence of visible tumor on endoscopic evaluation and absence of malignant cells on cytology from instrumented urine sample from the renal pelvis or ureter. Atypical cytologies were categorized as negative, and suspicious cytologies were categorized as positive. Partial response was defined as an absence of the index tumor treated but evidence of recurrence outside the treatment area within the ipsilateral renal pelvis or ureter.

Analyses were conducted using R 4.1.0 utilizing the tidyverse (v1.3.1), gtsummary (v1.4.1), and CRM (v1.2.4) packages.[17–20]

RESULTS

A total of 22 patients were enrolled into the study. Three patients were removed after further screening per protocol, due to absence of visible tumor at the time of planned experimental treatment, leaving 19 patients who received the VTP treatment (Table 1). Of these 19 patients, all were eligible for the MTD assessment, and 18 were eligible for the secondary response endpoint. One patient was removed from the study 2 weeks after treatment for noncompliance (illicit drug use; Supplemental Figure 1, https://www.jurology.com).

One (5%) patient received a dose of 100 mW/cm, 4 (21%) patients received a dose of 150 mW/cm, and 14 (74%) patients received the highest dose of 200 mW/cm. No patients treated with 100 or 150 mW/cm experienced a DLT. Two patients treated with 200 mW/cm experienced a DLT (2/14; 14%). Both toxicities were pain-related and were graded 2 and 3 because they required additional intravenous medication for management and overnight hospital stay instead of outpatient discharge immediately after the procedure, respectively. These 2 DLTs were attributed to the procedure, likely due to the stent, and not the drug or device (Supplemental Table 1, https://www.jurology.com). The final recommended dose based on the mCRM study design was 200 mW/cm.

The rate of CR among patients eligible for the 30-day response assessment was 9/18 (50%; exact binomial 95% CI 26%, 74%; Table 2). Treatment efficacy stratified by tumor size yielded CR in 55% and 43% of tumors <15 and >15 mm, respectively. When stratified by tumor grade, the CR was 40% and 54% in high- and low-grade tumors, respectively. The rate of partial response was 8/18 (44%), after which all 8 patients underwent a second treatment, with a final 68% CR rate.

Serum creatinine and estimated glomerular filtration rate measures taken at days 2, 7, 14, and 30

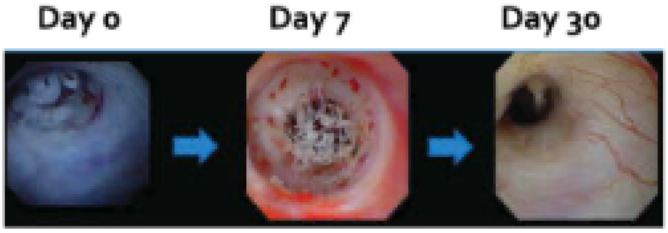

Figure 1. Endoscopic appearance of tumor before and after 1 vascular-targeted photodynamic therapy treatment.

Figure 2. Retrograde pyelogram before and after vascular-targeted photodynamic therapy.

following treatment did not show significant change from baseline (Table 3).

Of note, 1 patient treated early in the trial was incorrectly recorded as experiencing a Grade 3 treatment-related DLT (urinary tract infection), which was later investigated by a separate medical monitor and determined to be Grade 2 and resulting from follow-up endoscopy. The error was corrected after the final patient had received treatment. Because the mCRM algorithm uses all previously enrolled patients' information to inform the dose of each newly enrolled patient, the recording error modified the mCRM-recommended doses. However, this did not impact the final recommended MTD in this dose-finding study; if the recording error had not been made and patients' DLT statuses remained what was observed (Supplemental Figure 2, https://www.jurology.com), the final recommended dose would have remained 200 mW/cm.

DISCUSSION

This is the first study demonstrating the safety profile and treatment effects of WST-11 VTP in the endoscopic management of UTUC. According to the mCRM, the majority of patients received the MTD of 200 mW/cm, with no DLTs in the dose-escalation groups, and only 2 DLTs at the MTD. These 2 DLTs were pain-related and transient. No DLTs were related to the drug and no phototoxicity events were seen. There were no Grade 4 or 5 toxicities over the course of the study (Supplemental Tables 3-5, https://www.jurology.com). Typical for related types of procedures,[22] all patients

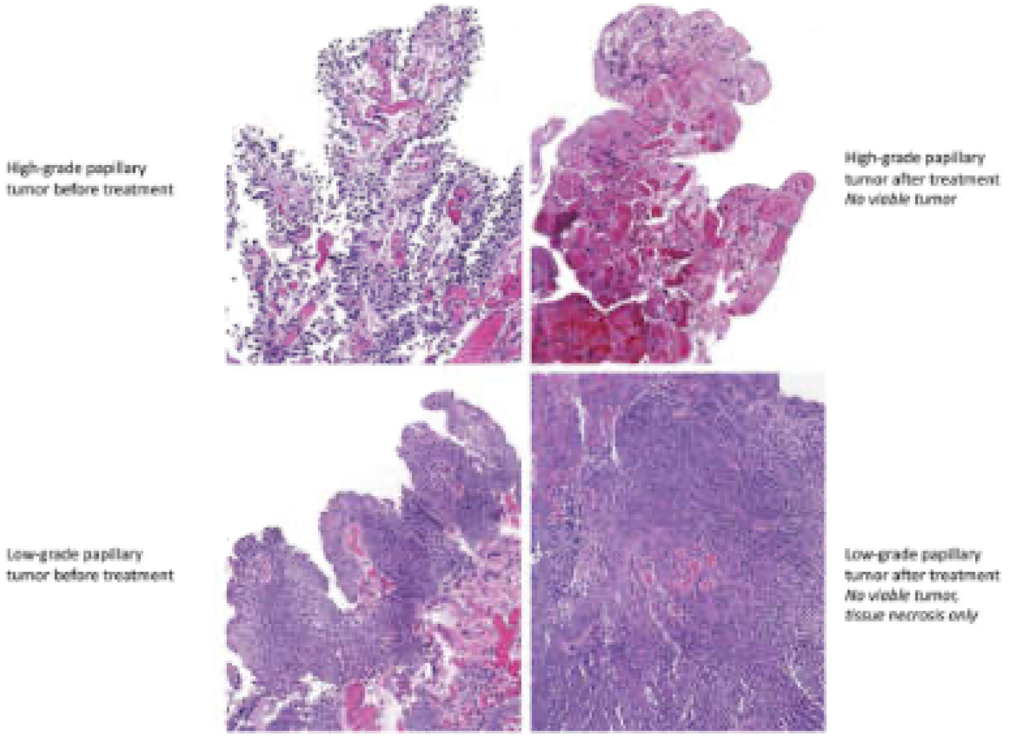

Figure 3. Histological appearance of tumor before and after 1 vascular-targeted photodynamic therapy treatment.

reported at least 1 adverse event, but the majority were minor (Grade 1-2), involving discomfort, hematuria, voiding symptoms, and fatigue. Severe adverse events were reported in 4 patients, with 2 related to the device and the remainder related to the procedure. Ureteral stenting was felt to be a contributor to several of the experienced events, including reports of flank pain, hematuria, and urinary frequency. These toxicities were minor and transient, and no adverse event led to study discontinuation. Renal function was essentially unchanged over the course of the study, and all treated kidneys were preserved at 6 months follow-up. Overall, VTP with WST-11 appears to be a safe endoscopic treatment option for UTUC.

In evaluating efficacy, VTP demonstrated tumor response in the majority (94%) of patients, with CR seen in half of patients after 1 treatment. CR was more often seen in tumors smaller than 15 mm but also achieved in tumors larger than 15 mm; however, case numbers are limited. Similarly, CR was more common in low-grade than high-grade tumors. An example of the endoscopic appearance of a UTUC tumor before and after therapy is presented in Figure 1, where a papillary lesion is clearly visualized on Day 0, collagenous fibers are present at Day 7, and absence of disease at Day 30. A retrograde pyelogram in a patient with multiple tumors prior to VTP, with complete resolution on follow-up retrograde pyelogram at 30 days, is presented in Figure 2. The histological appearances of both low- and high-grade UTUC tumors, before and after therapy, are presented in Figure 3. Cytology results (Supplemental Table 2, https://www.jurology.com) remained relatively unchanged over the course of the study, although the majority were negative at the onset, and the positive results at day 30 reflect tumors with a partial response. All 8 patients offered repeat treatment per protocol after their Day 30 evaluation elected a second VTP treatment, supporting the acceptability of VTP therapy. All second treatments were performed at the MTD, and an additional 4 patients (68% overall) achieved a CR within 30 days of the second treatment.

Regarding tolerability, treatment with WST-11 VTP in the upper urinary tract was not associated with off-target systemic, ureteral, and/or related collateral toxicities, as seen with other local ablative therapies. Endoscopic laser ablation treatments are associated with events such as perforation, stricture, and sepsis,[6] as well as major complications reported in over 5% of procedures.[21] Bacillus Calmette-Guérin instillation in the upper tract, either by cutaneous nephrostomy or retrograde ureteral catheterization, has been associated with rates of fever between 56% and 90%, as well as hematuria, hydronephrosis, and back pain. Severe sepsis and acute renal failure have been reported in 5.7% and 2.9% of patients, respectively.[22] With mitomycin thermal gel, which requires 6 weekly catheter-based instillations, events such as acute kidney injury (9%), myelosuppression (9%), ureteral stricture preventing further instillations (5%), and treatment discontinuation (27%) were described in the original report in which a 36% CR rate was seen.[23] In the Phase 3 trial of primary chemoablation with mitomycin thermal gel for low-grade UTUC (OLYMPUS), a 59% CR rate was seen, while 44% of patients developed ureteric stenosis.[24] Our study demonstrated similar efficacy, in both low- and high-grade tumors, with no cases of treatment-related ureteral stricture.

Based on this trial's results, the multicenter Phase 3 ENLIGHTED trial (NCT04620239) has been initiated for low-grade disease. The multicenter nature of the ENLIGHTED trial underscores the portability of this treatment option, which can be performed by any urologist trained in ureteroscopy, as additional equipment necessary only includes a laser fiber and light source.

Limitations of this Phase 1 dose-finding study include its small sample size; limited follow-up duration; and broad patient selection criteria, which did not limit tumor size or grade. Patients in the study were followed for 6 months to evaluate for late toxicities, but long-term treatment durability and recurrence assessment is limited. Further, the utility of continued maintenance treatment was not included in this trial design. Lastly, the majority of patients in the trial had previously failed other local ablative therapies and thus may represent a more treatment-resistant phenotype, including 1 patient who failed induction treatment on trial with mitomycin thermal gel but experienced a CR with VTP therapy.

CONCLUSIONS

The results of our Phase 1 trial demonstrate that WST-11 VTP for UTUC has an acceptable safety profile and promising therapeutic effect. The MTD of 200 mW/cm was reached, and only 2 DLTs were reported at the highest dose. Safety events were mainly local effects, with relatively negligible systemic toxicity. The procedure led to a 50% CR rate at 30 days and 68% CR rate after a second VTP treatment. Overall, VTP with WST-11 has the potential for use as a safe, efficacious, and kidney-sparing treatment option for UTUC. The recently initiated multicenter Phase 3 ENLIGHTED trial (NCT04620239) is expected to provide further evidence on this treatment option.

REFERENCES

1. Munoz JJ, Ellison LM. Upper tract urothelial neoplasms: incidence and survival during the last 2 decades. *J Urol*. 2000;164(5):1523-1525.
2. Roulow GP, Martin SF. Upper tract urothelial carcinoma: epidemiology, high risk populations and detection. *Minerva Urol Nefrol*. 2016;68(4):350-358.
3. Favaretto RL, Shariat SF, Chade DC. The effect of tumor location on prognosis in patients treated with radical nephroureterectomy at Memorial Sloan-Kettering Cancer Center. *Eur Urol*. 2010;58(4):574-580.
4. Lane BR, Smith AK, Larson BT. Chronic kidney disease after nephroureterectomy for upper tract urothelial carcinoma and implications for the administration of perioperative chemotherapy. *Cancer*. 2010;116(12):2967-2973.
5. Raman J, Shore ND. Management of low-grade upper tract urothelial carcinoma: an unmet need. *Rev Urol*. 2009;22(1):1-8.
6. Cutress ML, Stewart GD, Tudor EC. Endoscopic versus laparoscopic management of noninvasive upper tract urothelial carcinoma: 20-year single centre experience. *J Urol*. 2013;189(6):2054-2060.
7. Cutress ML, Stewart GD, Zakikhani P. Ureteroscopic and percutaneous management of upper tract urothelial carcinoma (UTUC): systematic review. *BJU Int*. 2012;110(5):614-628.
8. Brown SB, Brown EA, Walker I. The present and future role of photodynamic therapy in cancer treatment. *Lancet Oncol*. 2004;5(8):497-508.
9. Mazor O, Brandis A, Plaks V. WST11, a novel water-soluble bacteriochlorophyll derivative; cellular uptake, pharmacokinetics, biodistribution and vascular-targeted photodynamic activity using melanoma tumors as a model. *Photochem Photobiol*. 2005;81(2):342-351.
10. Eymerit-Morin C, Zidane M, Lebdai S. Histopathology of prostatic tissue after vascular-targeted photodynamic therapy for localized prostatic cancer. *Virchows Arch*. 2013;463(4):547-552.
11. Trachtenberg J, Bogaards A, Weersink RA, et al. Vascular targeted photodynamic therapy with palladium-bacteriopheophorbide photosensitizer for recurrent prostate cancer following definitive radiation therapy: assessment of safety, treatment planning and preliminary results. *J Urol*. 2007;178(3 Pt 1):770-777.
12. Trachtenberg J, Weersink RA, Davidson SR, et al. Vascular-targeted photodynamic therapy (padoporfin, WST09) for recurrent prostate cancer after failure of external beam radiotherapy: a study of escalating light dose and drug dose. *BJU Int*. 2008;101(11):1393-1399.
13. Azzouzi AR, Barret E, Moore CM, et al. TOOKAD Soluble vascular-targeted photodynamic (VTP) therapy: determination of optimal treatment conditions and assessment of effects in patients with localised adenocarcinoma of the prostate who have undergone unilateral prostatic ablation. *BJU Int*. 2013;112(6):766-774.
14. Azzouzi AR, Vincendeau S, Barret E, et al. Padeliporfin vascular-targeted photodynamic therapy versus active surveillance in men with low-risk localised prostate cancer (PCM301): an open-label, randomised, phase 3 trial. *Lancet Oncol*. 2017;18(2):181-191.
15. Azzouzi AR, Vincendeau S, Barret E, et al. Padeliporfin vascular-targeted photodynamic therapy versus active surveillance in men with low-risk localised prostate cancer (PCM301): an open-label, randomised, phase 3 trial. *Lancet Oncol*. 2017;18(2):181-191.
16. O'Quigley J, Pepe M, Fisher L. Continual reassessment method: a practical design for phase 1 clinical trials in cancer. *Biometrics*. 1990;46(1):33-48.
17. R Core Team. *R: A Language and Environment for Statistical Computing*. R Foundation for Statistical Computing; 2021.
18. Wickham H, Averick M, Bryan J. Welcome to the tidyverse. *J Open Source Softw*. 2019;4(43):1686.
19. Sjoberg DD, Whiting K, Curry M, Lavery J, Larmarange J. Reproducible summary tables with the gtsummary package. *R J*. 2021;13(1):570-580.
20. Mu Q. *CRM: Continual Reassessment Method (CRM) for Phase I Clinical Trials*; 2018.
21. Gudziak AJ, Roberts WW, Fentiker GJ. Long-term outcomes of nephroureterectomy versus endoscopic management for upper tract urothelial carcinoma. *J Urol*. 2010;183(6):2148-2153.
22. Linehan J, Schoenberg M, Schiller E. Complications associated with endoscopic management of upper tract urothelial carcinoma. *Urology*. 2021;147:87-95.
23. Kleinmann N, Wirth G, Lin JS. Thermo reversible hydrogel based delivery of mitomycin C (UGN-101) for treatment of upper tract urothelial carcinoma (UTUC). *Bladder Cancer*. 2015;5(1):21-29.
24. Kleinmann N, Matin SF, Pierorazio PM. Primary chemoablation of low-grade upper tract urothelial carcinoma using UGN-101, a mitomycin-containing reverse thermal gel (OLYMPUS): an open-label, single-arm, phase 3 trial. *Lancet Oncol*. 2020;21(6):776-785.

www.nature.com/scientificreports

scientific reports

OPEN

Neoadjuvant vascular-targeted photodynamic therapy improves survival and reduces recurrence and progression in a mouse model of urothelial cancer

Barak Rosenzweig[1,2✉], Renato B. Corradi[3], Sadna Budhu[4], Ricardo Alvim[3], Pedro Recabal[5], Stephen La Rosa[3], Alex Somma[3], Sebastien Monette[5,6], Avigdor Scherz[7], Kwanghee Kim[3] & Jonathan A. Coleman[1,6✉]

Locally advanced urothelial cancer has high recurrence and progression rates following surgical treatment. This highlights the need to develop neoadjuvant strategies that are both effective and well-tolerated. We hypothesized that neoadjuvant sub-ablative vascular-targeted photodynamic therapy (sbVTP), through its immunotherapeutic mechanism, would improve survival and reduce recurrence and progression in a murine model of urothelial cancer. After urothelial tumor implantation and 17 days before surgical resection, mice received neoadjuvant sbVTP (WST11; Tookad Soluble, Steba Biotech, France). Local and systemic response and survival served as measures of therapeutic efficacy, while immunohistochemistry and flow cytometry elucidated the immunotherapeutic mechanism. Data analysis included two-sided Kaplan–Meier, Mann–Whitney, and Fischer exact tests. Tumor volume was significantly smaller in sbVTP-treated animals than in controls (135 mm^3 vs. 1222 mm^3, $P < 0.0001$) on the day of surgery. Systemic progression was significantly lower in sbVTP-treated animals (17% vs. 30%, $P < 0.01$). Both median progression-free survival and overall survival were significantly greater among animals that received sbVTP and surgery than among animals that received surgery alone ($P < 0.05$). Neoadjuvant-treated animals also demonstrated significantly lower local recurrence. Neoadjuvant sbVTP was associated with increased early antigen-presenting cells, and subsequent improvements in long-term memory and increases in effector and active T-cells in the spleen, lungs, and blood. In summary, neoadjuvant sbVTP delayed local and systemic progression, prolonged progression-free and overall survival, and reduced local recurrence, thereby demonstrating therapeutic efficacy through an immune-mediated response. These findings strongly support its evaluation in clinical trials.

Abbreviations

sbVTP	Sub-ablative vascular-targeted photodynamic therapy
VTP	Vascular-targeted photodynamic therapy
UC	Urothelial carcinomas
UBC	Urothelial bladder cancer
NAC	Neoadjuvant chemotherapy
UTUC	Upper-tract urothelial carcinoma

[1]Department of Surgery, Urology Service, Memorial Sloan Kettering Cancer Center, 1275 York Ave., New York, NY 10065, USA. [2]Department of Urology, Urologic-Oncology Service, The Chaim Sheba Medical Center, Affiliated with the Sackler School of Medicine, 5262080 Ramat Gan, Israel. [3]Department of Surgery, Sloan-Kettering Institute, Memorial Sloan Kettering Cancer Center, New York, NY, USA. [4]Immunology Program, The Jedd Wolchok Lab, Memorial Sloan Kettering Cancer Center, New York, NY, USA. [5]Laboratory of Comparative Pathology, Memorial Sloan Kettering Cancer Center, New York, NY, USA. [6]Weill Cornell Medical College, New York, NY, USA. [7]Department of Plant Sciences, Weizmann Institute of Science, Rehovot, Israel. ✉email: Barak.rosenzweig@sheba.health.gov.il; colemanj@mskcc.org

BCG	Bacillus Calmette–Guerin
PDT	Photodynamic therapy
MB-49	Murine bladder 49
MB-49-luc	MB-49 luciferase-expressing
PBS	Phosphate-buffered saline
IHC	Immunohistochemistry
HIER	Heat-induced epitope retrieval
H&E	Hematoxylin and eosin
OS	Overall survival
MFS	Metastasis-free survival
PFS	Progression-free survival
VTPS	SbVTP and surgical resection
IFN	Intracellular interferon
APCs	Antigen-presenting cells

Urothelial carcinomas (UC) can involve the lower (bladder and urethra) or upper (renal pelvis and ureters) urinary tract. The vast majority (90–95%) occur in the bladder. Urothelial bladder cancer (UBC) is the ninth most common cancer in the world[1]. The estimated deaths in the United States for UBC were 17,980 for 2020[2].

Surgical treatment as sole modality can be curative, mainly for organ-confined, lymph-node negative disease. However, survival rates decrease dramatically for locally and regionally advanced disease[3], even with aggressive surgical and medical interventions. Platinum-based neoadjuvant chemotherapy (NAC) for invasive UBC produces significant survival as well as disease-free survival benefit[4] and is considered the most appropriate standard treatment for invasive UBC[5]. Although evidence supporting NAC in advanced upper-tract urothelial carcinoma (UTUC) is less well-developed, 45–60% of patients will progress following surgery, necessitating the use of chemotherapy[6]. Despite these data, NAC for UBC and UTUC has gained very limited clinical acceptance[7], probably reflecting concerns over the toxicity associated with it.

A strong need therefore exists for developing innovative, less toxic, and more clinically acceptable neoadjuvant therapies for invasive urothelial carcinoma.

The importance of immunotherapy in the treatment of UC was first reported in 1971, when bacillus Calmette-Guerin (BCG) was used as a localized immunotherapy[8]. In the past few years, promising evidence has indicated an expanding role for systemic immunotherapy in urologic cancers including bladder cancer[9]. Although robust evidence supporting immunomodulating drugs in the adjuvant setting exists, there is a gap in knowledge about their role in the neoadjuvant scenario. Furthermore, because response to immune checkpoint inhibitors tends to be individualized and adverse events, while rare, tend to be potentially serious, immunomodulating drugs may be less appealing as a first-line neoadjuvant approach[10].

Evidence supporting use of photodynamic therapy (PDT) for UC was introduced in the 1980s with long-term efficacy that suggested an immune-related response[11–13]. Later reports consistently supported the role of PDT in cancer treatment inducing an antitumor immune response[14–17]. Despite profound supporting evidence for PDT, limitations, such as prolonged phototoxicity, delayed clinical acceptance, prompting the development of better performing photosensitizing molecules[18].

One of these better performing molecules, WST11 (Tookad Soluble, Steba Biotech, France), is a water-soluble, near-infrared-activated Pd-bacteriochlorophyll derivative[19–21]. Following intravenous administration, WST11 noncovalently binds to albumin and is sequestered within the circulation. Upon illumination within tissues, WST11 vascular-targeted photodynamic therapy (VTP) produces localized, soft-tissue ablation mediated by cytotoxic-reactive oxygen species and destroys malignant cells[22,23]. In contrast to former photodynamic therapies, VTP is confined to the vasculature of the tumor, arresting the tumor's blood supply by rapid occlusion and causing profound tumor necrosis within 48 h[21]. WST11-VTP of tumor-bearing solid organs was found to be safe and effective in prostate cancer clinical trials[24–26]. In addition to its local effect, VTP has been shown to induce long-lasting systemic antitumor immunity including both cellular and humoral components[27,28].

As locally applied ablation effects may be variable in advanced UC cancers, we sought to investigate the role for VTP as a neoadjuvant rather than primary therapy. Therefore, we utilized less optimal treatment conditions, or sub-ablative settings, in which tumors would be damaged but not completely destroyed. We used the murine bladder 49 (MB-49) cell line, known to metastasize spontaneously to lymph, spleen, and lungs. We transfected it with a luciferase-expressing gene to generate MB-49 luciferase-expressing (MB-49-luc) cell line.

Results

Experiment 1: Standalone sbVTP. The goal of this experiment was to determine the influence of sbVTP on overall survival (OS), metastasis-free survival (MFS), and tumor progression as compared to control and surgical resection.

sbVTP treatment led to reductions in tumor progression. By 22 days after tumor implantation, the early (2 weeks) sbVTP group showed tumor and lung fluorescence signals significantly lower than control ($P<0.05$) but higher than the early surgery group ($P<0.0001$) (Fig. 1 and Supplementary Table). Tumor radiance for the late (3 weeks) sbVTP group also demonstrated signals lower than control ($P<0.05$).

Tumor size at day 21 similarly showed benefits for sbVTP treatment. The early and late sbVTP groups on this day had an average tumor size of 211 mm^3 (95% CI, 50–372 mm^3; $P<0.01$) and 422 mm^3 (95% CI, 163–682 mm^3; $P<0.05$) respectively, compared to with 769 mm^3 (95% CI, 588–950 mm^3) for control. Tumors could not be measured in surgically resected animals.

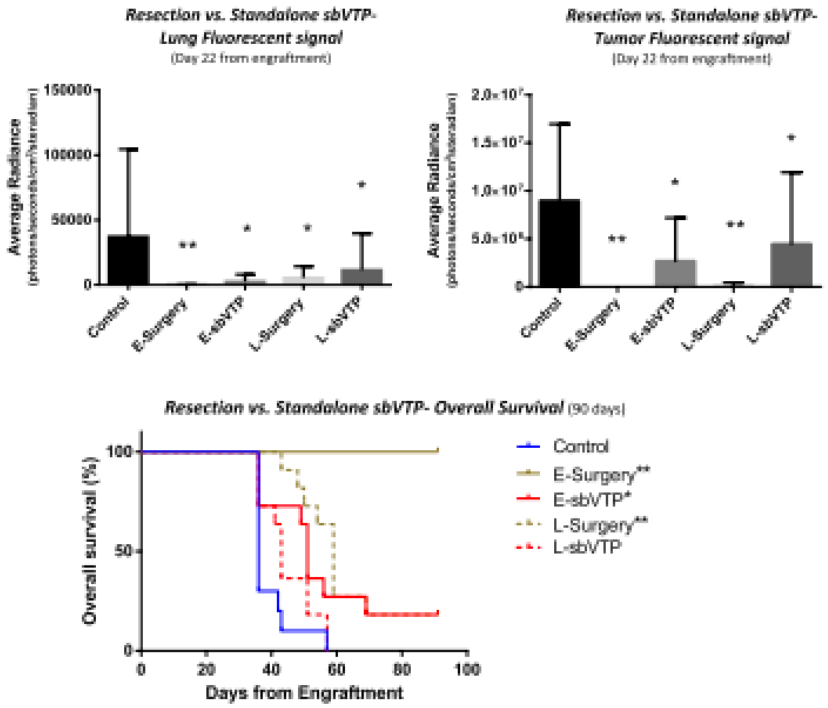

Figure 1. (Upper panel) Fluorescence signal from thorax and the primary tumor implant site in mice injected with MB-49 urothelial cancer cell line ($n=54$). (Lower panel) Kaplan–Meier curves showing overall survival. Animals were treated with surgery or sbVTP, 2 or 3 weeks (early or late, respectively) after tumor injection, compared to control group ($n=11$ per treated groups, $n=10$ per control). *E-sbVTP* early sub-ablative vascular-targeted-photodynamic therapy, *E-Surgery* early tumor surgical resection, *L-sbVTP* late sub-ablative vascular-targeted-photodynamic therapy, *L-Surgery* late tumor surgical resection. *$P<0.05$ as compared to control; **$P<0.0001$ as compared to control.

Early sbVTP demonstrated survival benefits compared to control but not to early surgery. OS and MFS were significantly longer in the early sbVTP group compared to control ($P<0.05$), but shorter than in the early surgery group ($P<0.001$). The late sbVTP group failed to show an advantage over control regarding these endpoints (Fig. 1). Median OS per group was as follows: control, 36 days; early surgery, undefined (did not reach below 50% survival for 90 days); early sbVTP, 51 days; late surgery, 59 days; and late sbVTP, 43 days. Median MFS per group was as follows: control, 22 days; early surgery, undefined (did not reach below 50% survival for 90 days); early sbVTP, 36 days; late surgery, 36 days; and late sbVTP, 29 days.

sbVTP possibly suggests long-term systemic immunity. When animals were rechallenged with tumor cells injection more than 100 days following treatment, no sbVTP (0/2) and only 1/13 of the surgically treated animals developed signs of local or systemic disease. In contrast, all control mice ($n=5$) developed local tumors and metastasis, eventually succumbing to their disease ($P<0.05$). A following experiment further describes additional group of long term sbVTP treated animals re-challenged with tumor cells (see ahead, flow cytometry—experiment 5).

Experiment 2: Surgery timing following neoadjuvant sbVTP. The goal of this experiment was to investigate how surgery at different times affects OS.

sbVTP treatment, alone or in combination with surgical resection, demonstrated superior OS compared to control ($P<0.05$). Surgical resection plus sbVTP was significantly superior to sbVTP alone if performed at days 17 and 24 from tumor engraftment (3 and 10 days following sbVTP, respectively; $P<0.001$ and $P<0.05$, respectively). However, for later time points representing advanced disease, i.e., 31 days from engraftment, the advantage of combining surgical resection with sbVTP over sbVTP alone was no longer significant ($P=0.1$). Median OS per group was as follows: control, 43 days; sbVTP, 56 days; sbVTP + surgery at day 17, undefined

Neoadjuvant treatment	Group	Tumor regression	Tumor regression (overall, %)	Death	Lung metastasis	Systemic progression (overall, %)
None	Control	0	0/29 (0)*	1	1	9/30 (30)*
	Surgery	0		0	7	
sbVTP	sbVTP	7	12/45 (27)*	0	2	3/45 (7)*
	VTPS	5		0	1	

Table 1. Tumor regression and systemic progression by treatment group prior to surgical resection. *sbVTP* sub-ablative vascular-targeted photodynamic therapy, *VTPS* sub-ablative vascular-targeted photodynamic therapy followed by surgical resection of tumor. One control animal was censored from the tumor regression analysis due to death prior to surgery day. *$P < 0.05$.

(did not reach below 50% survival for 121 days); sbVTP + surgery at day 24, 69 days; and sbVTP + surgery at day 31, 66.5 days.

Experiment 3: Systemic progression timeline–imaging validation. The goal of this experiment was to validate the time from engraftment with tumor cells to systemic progression.

The average day for positive lung fluorescence signal (that is, systemic progression) was 33.5 days (standard deviation, 5.5 days) from tumor engraftment, as calculated from the control groups of standalone sbVTP and surgery following neoadjuvant sbVTP (experiments 1 and 2). This timeline was confirmed by gross and microscopic analysis. Out of the 18 animals engrafted with tumors as part of Experiment 3, fourteen (78%) showed gross lung metastasis on day 33. Two additional animals were found to have lung metastases on microscopic analysis, bringing the total to 16 (89%).

Experiment 4: Neoadjuvant sbVTP. The goal of this experiment was to define the effects of neoadjuvant sbVTP on OS, progression-free survival (PFS), tumor volume at surgery, and local recurrence as compared to control. sbVTP and surgical resection were performed 14 and 31 days following implantation of tumor cells, respectively with the intent of treating micrometastatic disease. Neoadjuvant treatment with sbVTP produced improvements in OS and PFS, reduced tumor volume at surgery, and decreased local recurrence following it. Average tumor volume at the day of sbVTP was 70 mm^3 [standard error (SE), 4.1; 95% CI, 60–80 mm^3]. At day of surgery tumor volume for sbVTP-treated animals (i.e., sbVTP and sbVTP + surgery at day 31[VTPS]) was 135 mm^3 (SE, 35; 95% CI, 66–204 mm^3) and for non-sbVTP-treated animals (i.e., control and surgery only) was 1222 mm^3 (SE, 125; 95% CI, 976–1468 mm^3) ($P < 0.0001$). Animals treated with sbVTP had a higher rate of tumor regression and a lower rate of systemic progression on the day of surgery (Table 1).

OS and PFS were significantly longer for VTPS as compared to the control and surgery only groups (Fig. 2, upper panel). Median OS per group was as follows: control, 43 days; sbVTP, undefined (did not reach below 50% survival for 121 days); surgery only, 55 days; and VTPS, undefined (did not reach below 50% survival for 121 days). Median PFS per group was as follows: control, 38 days; sbVTP, undefined (did not reach below 50% survival for 121 days); surgery only, 45 days; and VTPS, undefined (did not reach below 50% survival for 121 days).

Survival curves analysis in the short term following surgery (day 52 from engraftment) showed PFS for the VTPS group to be significantly longer than that for the sbVTP and surgery-only groups ($P < 0.05$) (Fig. 2, lower right panel).

Time to local recurrence was significantly longer for VTPS as compared to control and surgery-only groups (Fig. 3). Median local recurrence per group was as follows: control, 31 days; sbVTP, undefined (did not reach above 50% recurrence for 121 days); surgery only, 59 days; and VTPS, undefined (did not reach above 50% recurrence for 121 days).

Experiment 5: Flow cytometry and IHC. The goal of this experiment was to elucidate the mechanism of sbVTP and its long-term effect. sbVTP induced a long-term immune-mediated response based on our analysis of resected tumors, lungs, spleens, and blood using IHC and flow cytometry.

Tumor and lung histology analysis showed an evolving immune reaction at tumor site following sbVTP (Fig. 4). Chronic-active inflammation of tumor and adjacent tissues at days 17, 24, and 31 was shown by hematoxylin and eosin (H&E) staining. The lowest daily average tumor CD3 + (T-cells) score was 1.67 three days following sbVTP (i.e., day 17 from engraftment). This nadir was followed by gradual increases on day 24 (2.67) and day 31 (2.83). Average lung CD3 + score at death was 2.63. The average tumor Mac2 (macrophages and dendritic cells) score showed an opposite trend, reaching 3, its highest point, 3 days following sbVTP and then decreasing to 2.67 on day 24 and day 31. The average lung Mac2 score reached its lowest point (2) at death (Fig. 4). Surgery-only samples of tumor (day 31) and lungs (at death) showed similar directional trends (i.e., tumor score rising and lung score falling) although to a lesser degree (not shown).

sbVTP was associated with an early increase in antigen-presenting cells (APCs) as well as long-lasting immune responses. When immune cells were analyzed using flow cytometry in spleen, lungs, and blood to assess systemic response (Fig. 5; supplementary Fig. 1), APCs were significantly higher 3 days following sbVTP throughout all three foci. Surviving animals showed increased CD8 + T-cells in the spleens and increased memory T-cells and effector T-cells in all foci. Blood analysis of surviving animals found that both CD4 + and CD8 + active T-cells

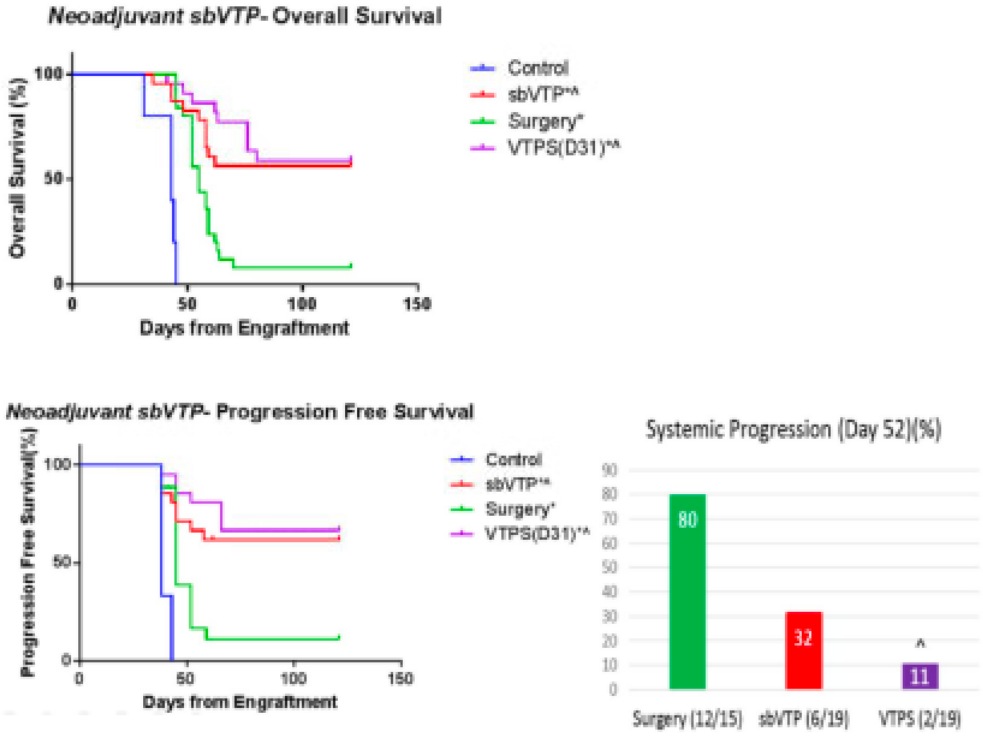

Figure 2. Kaplan–Meier analysis for overall survival and progression-free survival. Surgical resection was performed on day 31 for relevant groups (not illustrated). Control ($n=5$); *sbVTP* sub-ablative vascular targeted photodynamic therapy ($n=23$); Surgery ($n=25$); *VTPS(D31)* sub-ablative vascular-targeted photodynamic therapy followed by surgical resection of tumor 31 days from engraftment ($n=22$). Two and 3 animals were censored from the analysis in the sbVTP and VTPS groups, respectively, due to peri-procedure death. *$P<0.05$ versus control; ^$P<0.05$ versus Surgery group. *Note* The improved survival presented for sbVTP at 2 weeks as compared to Fig. 1 is attributed to the different sizes of the treated tumors (see "Discussion" section).

trended toward higher levels. Following tumor rechallenge to these animals, active CD4 + T-cells in blood were significantly higher.

Discussion

The five experiments in our study demonstrate that partial tumor ablation with sbVTP is an effective neoadjuvant treatment for urothelial cancer.

sbVTP reduces systemic progression and improves survival compared to control at early time points (Experiment 1). At late time points, representing advanced disease, sbVTP with or without surgery provided long-term benefit compared to surgical resection alone (Experiments 2 & 4). Although sbVTP advantage is shown in both experiments, we report differences in overall survival of animals treated by sbVTP only (Figs. 1, 2). We attribute this difference to tumor size which was larger in day of sbVTP treatment in experiments 1 and 2 (avg. ~ 200 cc) versus experiment 4 (avg. ~ 70 cc), and hence may have influenced sbVTP outcomes. The fact that sbVTP reduces systemic progression and improves survival suggests it to potentially reduce or eliminate seeding of micro-metastases and systemic progression while local tumor resection cannot (Fig. 2; Table 1).

These findings may help explain published data reporting a higher failure rate for surgical resection of UBC[3] and UTUC[4] in advanced disease, most probably caused by concealed systemic disease at the time of surgical resection. In our UC mouse model, we found day 33 to represent the onset of clinically evident metastatic disease. From this, we can infer that advanced disease characterized by concealed micro-metastases is highly probable at day 31. Indeed, our Experiment 4 showed that sbVTP treatment *before* surgery at day 31 was more effective than surgery alone at that day. This suggests that the cause of the higher failure rate for surgical treatment of advanced disease may be the existence of concealed micro-metastases. Therefore, in humans, we believe the optimal time for treating micro-metastases with sbVTP is *before* these metastases become clinically evident—that is, as neoadjuvant treatment. Supporting this recommendation, bladder cancer regression following neoadjuvant treatment has been correlated with improved recurrence-free survival[29] and OS[18]. Similarly, our model showed

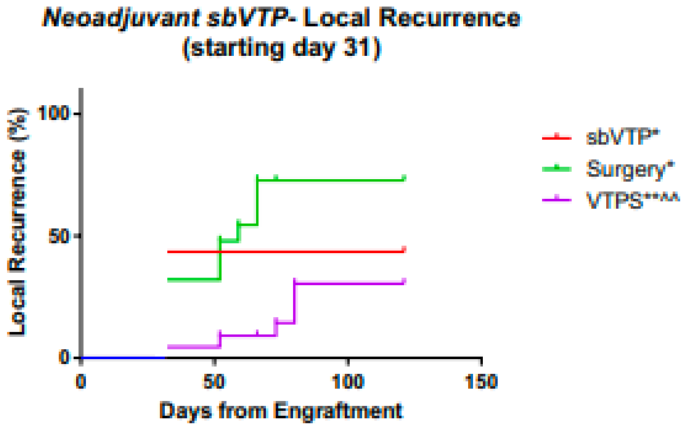

Figure 3. Kaplan–Meier analysis for local recurrence 121 days from tumor engraftment. Analysis started 31 days following tumor engraftment (day of tumor surgical resection for relevant groups). *sbVTP* sub-ablative vascular-targeted photodynamic therapy ($n=23$), *VTPS* sub-ablative vascular-targeted photodynamic therapy followed by surgical resection of tumor ($n=22$); Surgery ($n=25$). *$P<0.05$ versus control; **$P<0.01$ versus control; ^^$P<0.001$ versus Surgery group. Control ($n=5$) animals were omitted from figure as no "recurrence".

that animals treated with sbVTP prior to surgical resection have higher rates of tumor regression and lower rates of systemic progression prior surgery (Table 1) translated in to longer PFS and OS.

Our findings suggest that sbVTP produces a long-term systemic immune response. Tumor histology analysis (Experiment 5) showed chronic-active inflammation of tumor and adjacent tissues as abundant macrophages and T-cells infiltrated them (Fig. 4). Rechallenging mice more than 100 days after sbVTP resulted in no uptake of tumor grafts. Systemic progression was delayed following sbVTP (Table 1). These findings confirm published literature defining immune response as one of the main mechanisms by which PDT destroys tumor cells and initiates the long-term systemic immune response that follows[14,17,28,31,32].

In the long term, sbVTP produced superior PFS compared to all other treatments. In the early weeks, the VTPS group showed a significant advantage in PFS compared to the surgery-only group and the sbVTP-only group (Fig. 2). The VTPS group's advantage over the sbVTP-only group, however, later became non-significant, and in the long-term both groups receiving sbVTP (VTPS and sbVTP-only) demonstrated significantly longer PFS. A possible explanation for this phenomenon may be suggested by the immunoediting theory[33]. sbVTP may be sculpting the immunogenicity of the tumor cells, tilting the host-tumor immune balance toward an equilibrium state. Indeed, PDT may emit a powerful attracting signal for immune cells that can be engaged in additional eradication of disseminated and/or metastatic lesions of the same cancer[15,34]. VTP using WST11 also initiated a systemic immune response and established a prolonged immunity in animal cancer models in previous studies[27,28]. Our study found evidence of this immune-response mechanism by using Mac2, one marker of macrophage maturation in mice[35,36]. Using Mac2 tagging, we found an initial proliferation of dendritic cells and macrophages early after sbVTP and a subsequent reduction in their magnitude. Mac2 and CD3 + stained cells both demonstrated the ability to infiltrate tumor and peritumoral tissues (Fig. 4). Massive invasion of cancer tissue by activated myeloid cells following PDT enables tumor antigens to present and subsequently activate lymphoid cells, leading to tumor-specific immunity[14,17,34]. The combination of macrophages and T-cells is reportedly essential to maintaining long-term control of PDT-treated tumors[32]. This mechanism appears to explain why sbVTP leads to longer PFS and OS.

Our study provided further details about this important mechanism. Our flow analysis showed APCs increasing in the early phase after sbVTP throughout all three systemic foci (spleen, lungs, and peripheral blood) (Fig. 5 and supplementary Fig. 1). Correspondingly, surviving animals showed an increase in memory T-cells and effector T-cells at all foci. These data illustrate the proposed "crosstalk" between antigen presentation, T-cells, and tumor cells as suggested by the immunoediting theory[33]. This crosstalk initiates the adaptive immune response that takes place long after sbVTP is administered. Identification of active T-cells in all foci further supports that actual tumor elimination/equilibrium is occurring in surviving animals. Finding the populations of CD8 + T-cells to be significantly higher in surviving animals suggests their pivotal role in the antitumor, immune-mediated, sbVTP effect. Indeed, Murphy et al. suggested CD8 + T-cells and IFN-gamma promote antitumor responses in advanced metastatic cancer[37]. The higher levels of active CD4 + T-cells in spleen and lungs, which were harvested long after treatment, further suggests that active antitumor immune reaction continues well after sbVTP[38,39].

sbVTP can potentially reduce metachronous UBC following UBC and UTUC. Under current treatment regimens, some 15–50% of patients with a UTUC will subsequently develop a metachronous UBC. In most cases, UBC arises in the first 2 years after UTUC management. However, the post-UTUC risk of UBC is lifelong and repeated episodes are common, as reflected by the strict and frequent follow-up guidelines recommended by

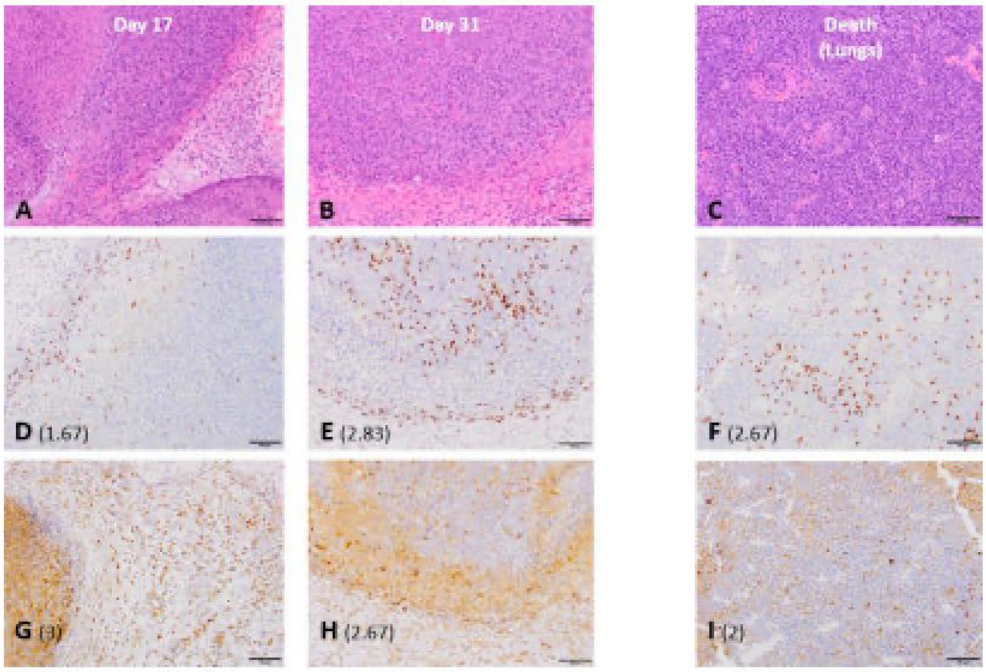

Figure 4. Tumor and lung histology analysis showing evolving immune reaction at tumor site following sub-ablative vascular-targeted photodynamic therapy. Semi-quantitative score (shown in parentheses) indicates the number of positive cells infiltrating tumor and peri-tumoral tissues, on a scale of 0 (no positive cells) to 4 (large number of positive cells). CD3 + is shown in (**D**–**F**), and Mac2 in (**G**–**I**), with both cell types observed in the same region. (**A**,**B**) Display results of hematoxylin and eosin (H&E) stain, showing skin, subcutis, and muscle with subcutaneous neoplasm. Note the chronic-active inflammation of tumor and adjacent tissues. (**D**,**E**) display results of CD3 + stain, illustrating time-dependent accumulation of T-cells. (**G**,**H**) display results of Mac2 (galectin 3) stain, illustrating initial accumulation of macrophages and dendritic cells followed by gradual decline. Lungs showed metastatic foci on H&E (**C**), aggregation of T-cells (CD3 + stain, **F**), and macrophages and dendritic aggregation (**I**).

the NCCN[5,40]. Immune-modulating drugs such as BCG have been shown to delay UC recurrence among other benefits[42–43], and intravesical PDT was reported to delay bladder recurrence[44]. On top of our findings that sbVTP improves survival and regression rates, our finding that sbVTP has a long-lasting systemic effect can potentially benefit UC patients by lowering recurrence rates.

Drug toxicity—in particular, renal impairment—is the major impediment to perioperative chemotherapy in patients with bladder cancer[29]. As many as 50% of patients have renal impairment, and approximately one third have other comorbidities that may preclude cisplatin-based treatment. VTP using WST11 appears to be an acceptable form of treatment for at least some and perhaps all of these patients, based on our knowledge to date. Although our experiments were not designed to assess the toxicity of sbVTP, we observed nothing that would suggest any toxicity issues, supporting recent studies. When sbVTP was tried on normal swine model tissue, as our group reported before, it preserved critical organ structures and bystander blood vessels within solid organs, as well as functionally preserving creatinine value within a normal physiological range[45,46]. Notably, VTP using WST11 is reported to be well-tolerated in men with prostate cancer[47]. VTP may enhance the neoadjuvant arsenal by offering a similar, if not superior, long-term effect at a considerably lower toxicity than existing treatments.

UTUC is oftentimes diagnosed using an endoluminal or percutaneous approach. Since a similar surgical approach can be used for VTP[48], we believe that VTP treatment is simple and convenient enough to use even at the time of biopsy. This approach could enable the urologist to locally apply potent systemic treatment at the time of diagnosis, proceeding to curative surgical resection without any delay. As mentioned above, in contrast to former photodynamic therapies, VTP is confined to the vasculature of the tumor, arresting the tumor's blood supply by rapid occlusion and causing profound tumor necrosis within 48 h, a reaction which is strongly immunogenic compared with the apoptotic cell death with the other reagents[21]. Considering the benefits of neoadjuvant photodynamic therapy, we suggest alternatives such as Visudyne and 5-aminolevulinic acid, previously described to effect urothelial cancer[48–51], to be tested in this setting as well.

Our study has limitations typical to the use of animal models to approximate the treatment conditions and outcomes that might be applicable in humans. Future usage of orthotopic bladder cancer mouse model

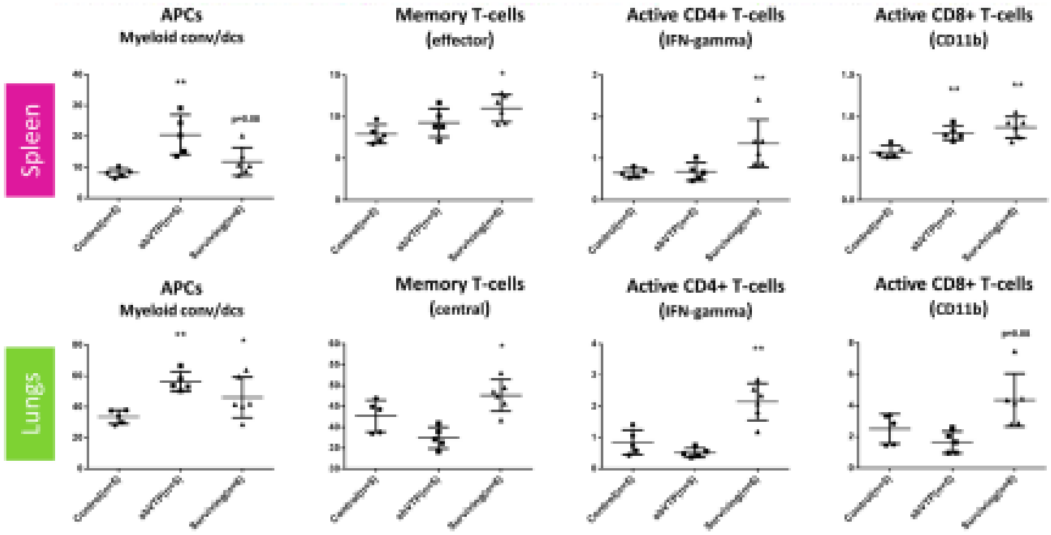

Figure 5. Flow data: cells' sub-population percentage by organ. Left to right: first column represents antigen-presenting cells (APCs), second column represents memory T-cells (central/effector), third column represents active CD4 + T-cells as indicated by IFN-gamma positivity, and fourth column represents active CD8 + T-cells as indicated by IFN-gamma and CD11B positivity. CD45 +, CD4 +, Foxp3-were used to evaluate CD4 T effector cells. CD62L + CD44 + were used to evaluate central memory T cells and CD62L-CD44 + to evaluate effector or effector memory T cells. *APCs* antigen-presenting cells, *conv* conventional, *dcs* dendritic cells, *IFN* interferon, *sbVTP* sub-ablative vascular-targeted photodynamic therapy, *surviving* surviving animals. $^{*}P \leq 0.05$; $^{**}P < 0.01$, compared to control.

may better simulate urothelial cancer pathophysiology and validate our findings. Engraftment of luciferase-expressing tumor cells via an intra-urethral approach, followed by spontaneous systemic metastasis of these tumor cells, will probably create a better model to investigate our results. However, we are currently unaware of such stable model to exist. In addition, our study has some limitations applicable to the particular design of it. We used treatment parameters that were below the level of complete ablation, which introduces variability in the treatment effects to the primary tumor. This is reflected in the range of responses at the local tumor site. Our focus, however, was primarily on the systemic effects associated with partial treatment as well as on the effects in the tumor microenvironment under these conditions. Although optimal conditions would be expected to improve VTP therapy outcomes locally, our technique may better simulate the clinical scenario in which, for example, complete endoscopic treatment to an upper urinary tract tumor might not be feasible. Furthermore, the immune-modulating effect of sbVTP as compared to VTP is yet to be elucidated. Another limitation is that in our testing for mechanism, we compared younger mice to surviving animals who were 3 months older (Experiment 5). Although protective immunity may decline with age, mice are not considered "old" until they are over 18 months[62], and we therefore believe that an age difference between 1 and 4 months, as in our study, is unlikely to confound our findings.

In summary, vascular-targeted photodynamic therapy, performed under sub-ablative parameters, demonstrates long-lasting therapeutic efficacy in a mouse model of urothelial cancer. Applying this treatment neoadjuvantly delays local and systemic progression prior to surgery, prolongs both PFS and OS, and reduces local recurrence. This therapy induces an early increase in antigen-presenting cells, followed by increases in long-term memory cells, effector cells, and active T-cells, establishing its immune-mediated mechanism. These findings provide a strong rationale for evaluating this therapy in clinical trials of locally advanced urothelial cancer.

Materials and methods

Our experiments applied a syngeneic non-orthotopic model. Cell culture, vascular targeted photodynamic therapy (VTP), imaging and tissue analysis were based on prior work by our group[53,54].

Cell culture. In brief, murine bladder 49 (MB-49) is a carcinogen-induced urothelial cell carcinoma derived from male C57BL/6 mice (Taconic Farms, New York, NY, USA). The MB-49 cells were cultured in Dulbecco's modified eagle medium supplemented with 10% fetal bovine serum, 1% penicillin/streptomycin, and 0.1% sodium pyruvate. Murine stem cell virus puromycin–luciferase–GFP was transfected into GP2-293 pantropic retroviral packaging cells (BD Biosciences, San Jose, CA, USA) using lipofectamin 2000 (Invitrogen, Grand Island, NY, USA), and the collected retrovirus was used to infect cells from the MB-49 mouse-bladder cancer cell line. Infected cells were selected with 0.5 μg/ml. puromycin (Invitrogen) and the surviving pool of cells was

designated as MB-49-luc. Infection was carried out in the presence of 6 µg/mL polybrene (Sigma, St. Louis, MO, USA). Prior to injection, MB-49-luc cells were washed and re-suspended in phosphate-buffered saline (PBS) pH 7.4 and viable cells were counted using Trypan blue exclusion and a hemocytometer. Tumor cells were subcutaneously injected in animals' right flank. For all experiments, the same number of MB-49-luc cells was injected (50 K).

Tumor measurement. The size of the primary tumor was assessed by caliper and validated by bioluminescence signals. The progression of lung metastases was monitored by luminescent imaging and validated by immunohistochemistry (see Experiment 3 below).

Animals. The study was performed using 7–8-week-old male C57BL/6 mice (Taconic Farms). Animals were housed in a light-controlled room with a 12:12-h light–dark cycle and allowed access to water and food ad libitum.

Sub-ablative vascular-targeted photodynamic therapy (sbVTP). Lyophilized WST11 was reconstituted with sterile 5% dextrose water under light-protected conditions and filtered through 0.22-µm disc filter. Infusion of weight-based WST11 at 9 mg/kg was administered via tail vein injection for 5 min. Two min after completing the drug injection, laser illumination was provided by a 753-nm medical diode laser (Biolitec, East Longmeadow, MA, USA) with front-face fiber optics. The light beam was adjusted to cover the same area regardless of fluency assuming an average tumor size for the different treated animals at 2 weeks post grafting. Light was delivered for 10 min at a fluency of ~ 122 mW/cm^2. Under these conditions an increased number of animals showed tumor relapse starting at the treated tumors margin. This observation reflects on the Gaussian shape of the laser beam and the threshold dependence of the VTP treatment efficacy. Due to the Gaussian shape of the applied beam the margin of illumination is the first to drop below that threshold when reducing the light fluency from 150 to 122 mW/cm^2 allowing for tumor relapse at the tumor margin. Complementary, slight increase of the tumor margin further decrease the cure rate. Accordingly, under the treatment conditions and the illuminated area size, we considered the amount of energy delivered to the tumor at 122 mW/cm^2 as sub-ablative compared to former studies by our group[53].

sbVTP and surgical resection. Adequate anesthesia with a ketamine–xylazine cocktail (150 mg/kg ketamine, 10 mg/kg xylazine) and isoflurane, was administered prior to sbVTP treatments. For surgical resection of tumor animals were anesthetized by volatile fluorocarbon isoflurane (2.5%) administered with a precision vaporizer in an induction chamber, followed by use of a nose cone. After a suitable anesthetic plane (no response to stimulation) was attained, the animal was placed in position for mass removal on a surgical tray with heat support provided by a SnuggleSafe (Pet Supply Imports, South Holland, IL, USA). An injection of 2 mg/kg of meloxicam was given for pre-emptive analgesia immediately after the animal was anesthetized. Skin was then shaved and prepped for surgery. Tumors were resected *en bloc* with overlying skin and surrounding tissues as required to achieve zero margins. Hemostasis was achieved by application of local pressure. Skin was re-approximated using 9 mm surgical clips (AutoClips, Braintree Scientific, Braintree, MA, USA). Animal care before and during the experimental procedures was conducted in accordance with the policies of the National Institutes of Health Guidelines for the Care and Use of Laboratory Animals. All protocols received prior approval by the Institutional Animal Care and Use Committee.

Luminescence imaging. Imaging was performed with a highly sensitive, cooled, charge-coupled device camera mounted in a light-tight specimen box (IVIS, Xenogen, Alameda, CA, USA). The acquisition and analysis software Living Image (Xenogen) were used for imaging and quantification of tumor progression. Following anesthesia with 1–2.5% isoflurane, mice were retro-orbitally injected with D-luciferin (PerkinElmer, Waltham, MA, USA) at a dose of 3 mg per mouse. Mice were then placed inside the light-tight camera box with continuous exposure to 1–2% isoflurane. Imaging time ranged from 1 s to 2 min. The level of light emitted from the tumors or metastatic foci was detected by the IVIS camera system, integrated, and displayed. Regions of interest from displayed images were designated around the tumor and lung sites and quantified using the software. Absolute signal measurement was corrected for background bioluminescence in vivo.

Tissue fixation and histological evaluation. Tumors and lungs were harvested, preserved, and analyzed. During lungs processing, the trachea was identified and injected with approximately 0.5 to 1 mL of India ink stain (Boston BioProducts, Ashland, MA, USA) and the lungs were inflated adequately. Lungs were then removed *en bloc*, excluding all other tissues, and placed in Fekete's solution for 24 h[53]. After collection, mice tumors and lungs were fixed in 10% neutral buffered formalin, processed in alcohol and xylene, paraffin embedded, sectioned at 5-µm thickness, and then stained with hematoxylin and eosin, CD3+, and Mac2; immunohistochemistry (IHC) for CD3 was performed on a Leica Bond RX automated staining platform (Leica Biosystems, Buffalo Grove, IL, USA). Following heat-induced epitope retrieval (HIER) at pH 9.0, the primary antibody (rabbit monoclonal, catalog #ab16669, Abcam, Cambridge, UK) was applied at a concentration of 1:100 and was followed by application of a polymer detection system (DS9800, Novocastra Bond Polymer Refine Detection, Leica Biosystems). For IHC for Mac2, the antibody CL8942B (Cedarlane, Burlington, NC, USA) applied at a concentration of 1:100 following HIER in a pH 6.0 buffer; Mac2 staining was performed manually with an avidin–biotin detection system (Vectastain ABC Elite Kit, Vector Laboratories, Burlingame, CA, USA). We used a semiquantitative score to indicate the number of positive CD3+ and Mac2 cells infiltrating tumor and peritu-

moral tissues, on a scale of 0 (no positive cells) to 4 (large number of positive cells). Analysis was performed by a board-certified veterinary pathologist.

Fluorescence-activated staining for surface antigens and intracellular proteins. Cell suspensions were incubated in Fc-block (CD16/32 antibodies, BD Biosciences) for 20 min on ice in PBS + 0.5% bovine serum albumin + 2 mm ethylenediaminetetraacetic acid [fluorescence-activated cell sorting (FACS) buffer] prior to surface staining. Samples were incubated with fluorophore conjugated CD4, CD8, CD25, CD62L, CD44, CD45, CD11c, Ly6G, Ly6C, MHC II, CD86, CD11b, and TGFβ for 20–30 min and then washed three times with FACS buffer. Foxp3 Staining Kit (eBioscience, San Diego, CA, USA) was used for intracellular staining of Foxp3, Ki67, and Granzyme B. Dead cell exclusion was done using the Fixable Viability Dye eFluor 506 (eBioscience). Samples were acquired on 12-color LSRII cytometer and analyzed using FlowJo software (Tree Star, Ashland, OR, USA).

Experiments. Using animals' survival, tumor measurements, luminescence imaging, immunohistochemistry, and flow cytometry, five experiments were conducted.

Experiment 1: Standalone sbVTP. The goal of this experiment was to determine the influence of sbVTP on OS, metastasis-free survival (MFS), and tumor progression as compared to control and surgical resection. Fifty-four animals were allocated into five groups based on tumor equivalent luciferase signal prior to treatment: control (no treatment, $n = 10$); early surgical resection ($n = 11$); early sbVTP ($n = 11$); late surgical resection ($n = 11$); and late sbVTP ($n = 11$). For sbVTP treatment, WST11 was administered intravenously as previously described. Surgery and sbVTP were performed at 2 weeks ("early") or 3 weeks ("late") after the implantation of tumor cells. Surgical margins were assessed by histology. All groups were examined with weekly luminescent imaging to determine MFS and the extent of progression. OS data was calculated.

A second phase of this experiment was designed to assess for development of systemic immunity following sbVTP and to measure time from engraftment to systemic progression using luminescent imaging. In this phase, all surviving animals (11 from early surgery, 2 from late surgery, and 2 from early sbVTP) were re-challenged 122 days after first tumor engraftment and over 100 days following any form of treatment. Animals were injected with MB-49-luc cells on the contralateral flank as previously described. Endpoints were the same clinical outcomes as before (OS, MFS, and local recurrence). Five treatment-naïve mice served as control.

Experiment 2: Surgery timing following neoadjuvant sbVTP. The goal of this experiment was to investigate how surgery at different times affects OS. In repeated sets of experiments, animals were allocated into five groups: control (no treatment; $n = 5$), sbVTP alone ($n = 26$), and three groups with the combination of sbVTP and surgery at different time points. The latter groups received sbVTP 14 days after the tumor cells were implanted, followed by surgical resection of the tumor at three time points: 17 days after implantation of tumor cells ($n = 25$), 24 days after implantation ($n = 22$), and 31 days after implantation ($n = 18$). All groups were examined with weekly luminescent imaging to determine time to progression (for Experiment 3) and the extent of progression (data not reported). OS data was calculated. Resected tumor tissue was preserved for further analysis, and sample animals' lungs were harvested and preserved after the animals had succumbed to their disease.

Experiment 3: Systemic progression timeline–imaging validation. The goal of this experiment was to validate the time from engraftment with tumor cells to systemic progression. The average day of positive lung luminescence (a marker for systemic progression) was calculated from the control groups of the two previous experiments. Eighteen treatment-naïve animals were engrafted with tumor cells. On the day that was calculated for positive lung fluorescence, animals were euthanized to permit physical validation of systemic progression. Gross metastases were assessed using India ink stain (Boston BioProducts, Ashland, MA, USA). Grossly negative or inconclusive lungs were assessed for micro-metastases using immunohistochemistry (IHC).

Experiment 4: Neoadjuvant sbVTP. The goal of this experiment was to define the effects of neoadjuvant sbVTP on OS, progression-free survival (PFS), tumor volume at surgery, and local recurrence as compared to control. Eighty animals were allocated into four groups: control (no treatment, $n = 5$); sbVTP ($n = 25$); surgical resection ($n = 25$); and the combination of sbVTP and surgical resection (VTPS, $n = 25$). sbVTP and surgical resection were performed 14 and 31 days following implantation of tumor cells, respectively. Progression was defined as positive lung signal determined by an in vivo imaging system or death. Resected tumor tissue was preserved for further analysis. Animal lungs were harvested and preserved at the time of necropsy after animals expired.

Experiment 5: Flow cytometry and immunohistochemistry. The goal of this experiment was to elucidate the mechanism of sbVTP and its long-term effect. Using immunohistochemistry, we analyzed tumor tissue collected on days 17 and 31 post-engraftment and lungs collected at time of death in experiments 2 and 4. In addition, we used naïve mice and surviving animals from Experiment 4. Animals were allocated into four groups: control (naïve mice, no treatment, $n = 5$); sbVTP (naïve mice treated with sbVTP, $n = 5$); long-term surviving animals ($n = 6$); and long-term surviving re-challenged animals ($n = 3$). Control, sbVTP, and long-term re-challenged animals were engrafted with tumor cells as previously described. sbVTP treatment took place on the fourteenth day after tumor engraftment for the sbVTP group. Mice were sacrificed 3 days after sbVTP (17 days after tumor engraftment for control and long-term re-challenged animals). Long-term surviving animals were sacrificed with no additional intervention; spleens, lungs, and blood were collected for flow analysis. We used intracellular

interferon (IFN)-gamma + and CD11b + as markers for T-cell activity as suggested by Cristensen et al.[36] and Fiorentini et al.[37].

Statistical analysis. Kaplan–Meier plots were used to analyze OS, PFS, and local recurrence. Comparative analysis of different groups was performed using the Mann–Whitney *U* test. Fisher's exact test was used for Table 1. Statistical evaluations were performed using the GraphPad Prism software (GraphPad Software, La Jolla, CA, USA).

Received: 26 July 2020; Accepted: 8 February 2021
Published online: 01 March 2021

References

1. Wong, M. C. S. *et al.* The global epidemiology of bladder cancer: a joinpoint regression analysis of its incidence and mortality trends and projection. *Sci. Rep.* **8**, 1129 (2018).
2. National Cancer Institute Surveillance, Epidemiology, and End Results Program. SEER stat fact sheets: bladder cancer. http://seer.cancer.gov/statfacts/html/urinb.html%3E. Accessed 26 July 2020.
3. Meeks, J. J. *et al.* A systematic review of neoadjuvant and adjuvant chemotherapy for muscle-invasive bladder cancer. *Eur. Urol.* **62**, 523–533 (2012).
4. Neoadjuvant chemotherapy in invasive bladder cancer: update of a systematic review and meta-analysis of individual patient data advanced bladder cancer (ABC) meta-analysis collaboration. *Eur. Urol.* **48**, 202–205 (2005) (**discussion 205–6**).
5. NCCN—MIBC Guidelines 6.2020. https://www.nccn.org/professionals/physician_gls/pdf/bladder.pdf. Accessed 26 July 2020.
6. Ozsahin, M. *et al.* Prognostic factors in urothelial renal pelvis and ureter tumours: a multicentre Rare Cancer Network study. *Eur. J. Cancer* **35**, 738–743 (1999).
7. Adibi, M. *et al.* Oncological outcomes after radical nephroureterectomy for upper tract urothelial carcinoma: comparison over the three decades. *Int. J. Urol.* **19**, 1060–1066 (2012).
8. Morales, A., Eidinger, D. & Bruce, A. W. Intracavitary Bacillus Calmette–Guerin in the treatment of superficial bladder tumors. *J. Urol.* **116**, 180–183 (1976).
9. Carosella, E. D., Ploussard, G., LeMaoult, J. & Desgrandchamps, F. A systematic review of immunotherapy in urologic cancer: evolving roles for targeting of CTLA-4, PD-1/PD-L1, and HLA-G. *Eur. Urol.* **68**, 267–279 (2015).
10. Topalian, S. L. *et al.* Safety, activity, and immune correlates of anti-PD-1 antibody in cancer. *N. Engl. J. Med.* **366**, 2443–2454 (2012).
11. Benson, R. C. Treatment of diffuse transitional cell carcinoma in situ by whole bladder hematoporphyrin derivative photodynamic therapy. *J. Urol.* **134**, 675–678 (1985).
12. Hisazumi, H., Misaki, T. & Miyoshi, N. Photoradiation therapy of bladder tumors. *J. Urol.* **130**, 685–687 (1983).
13. Shumaker, B. P. & Hetzel, F. W. Clinical laser photodynamic therapy in the treatment of bladder carcinoma. *Photochem. Photobiol.* **46**, 899–901 (1987).
14. Jalili, A. *et al.* Effective photoimmunotherapy of murine colon carcinoma induced by the combination of photodynamic therapy and dendritic cells. *Clin. Cancer Res.* **10**, 4498–4508 (2004).
15. Kabingu, E., Oseroff, A. R., Wilding, G. E. & Gollnick, S. O. Enhanced systemic immune reactivity to a Basal cell carcinoma associated antigen following photodynamic therapy. *Clin. Cancer Res.* **15**, 4460–4466 (2009).
16. Kousis, P. C., Henderson, B. W., Maier, P. G. & Gollnick, S. O. Photodynamic therapy enhancement of antitumor immunity is regulated by neutrophils. *Cancer Res.* **67**, 10501–10510 (2007).
17. Saji, H., Song, W., Furumoto, K., Kato, H. & Engleman, E. G. Systemic antitumor effect of intratumoral injection of dendritic cells in combination with local photodynamic therapy. *Clin. Cancer Res.* **12**, 2568–2574 (2006).
18. O'Connor, A. E., Gallagher, W. M. & Byrne, A. T. Porphyrin and nonporphyrin photosensitizers in oncology: preclinical and clinical advances in photodynamic therapy. *Photochem. Photobiol.* **85**, 1053–1074 (2009).
19. Brandis, A. *et al.* Novel water-soluble bacteriochlorophyll derivatives for vascular-targeted photodynamic therapy: synthesis, solubility, phototoxicity and the effect of serum proteins. *Photochem. Photobiol.* **81**, 983–993 (2005).
20. Fabre, M.-A., Fusseau, É. & Ficheux, H. Selection of dosing regimen with WST11 by Monte Carlo simulations, using PK data collected after single IV administration in healthy subjects and population PK modeling. *J. Pharm. Sci.* **96**, 3444–3456 (2007).
21. Madar-Balakirski, N. *et al.* Permanent occlusion of feeding arteries and draining veins in solid mouse tumors by vascular targeted photodynamic therapy (VTP) with Tookad. *PLoS ONE* **5**, e10282 (2010).
22. Gross, S., Gilead, A., Scherz, A., Neeman, M. & Salomon, Y. Monitoring photodynamic therapy of solid tumors online by BOLD-contrast MRI. *Nat. Med.* **9**, 1327–1331 (2003).
23. Manor, O. *et al.* WST11, a novel water-soluble bacteriochlorophyll derivative; cellular uptake, pharmacokinetics, biodistribution and vascular-targeted photodynamic activity using melanoma tumors as a model. *Photochem. Photobiol.* **81**, 342–351 (2005).
24. Azzouzi, A.-R. *et al.* TOOKAD(®) Soluble vascular-targeted photodynamic (VTP) therapy: determination of optimal treatment conditions and assessment of effects in patients with localised prostate cancer. *BJU Int.* **112**, 766–774 (2013).
25. Eymerit-Morin, C. *et al.* Histopathology of prostate tissue after vascular-targeted photodynamic therapy for localized prostate cancer. *Virchows Arch.* **463**, 547–552 (2013).
26. Nowecki, A. *et al.* Medium-term follow-up of vascular-targeted photodynamic therapy of localized prostate cancer using TOOKAD soluble WST-11 (Phase II Trials). *Eur. Urol. Focus* **5**, 1022–1028 (2019).
27. Preise, D. *et al.* Systemic antitumor protection by vascular-targeted photodynamic therapy involves cellular and humoral immunity. *Cancer Immunol. Immunother.* **58**, 71–84 (2009).
28. Preise, D., Scherz, A. & Salomon, Y. Antitumor immunity promoted by vascular occluding therapy: lessons from vascular-targeted photodynamic therapy (VTP). *Photochem. Photobiol. Sci.* **10**, 681 (2011).
29. Sternberg, C. N. & Apolo, A. B. Everything old is new again! Neoadjuvant chemotherapy in the treatment of muscle-invasive bladder cancer. *J. Clin. Oncol.* **32**, 1868–1870 (2014).
30. Petrelli, F. *et al.* Correlation of pathologic complete response with survival after neoadjuvant chemotherapy in bladder cancer treated with cystectomy: a meta-analysis. *Eur. Urol.* **65**, 350–357 (2014).
31. Juarranz, A., Jaén, P., Sanz-Rodríguez, F., Cuevas, J. & González, S. Photodynamic therapy of cancer. Basic principles and applications. *Clin. Transl. Oncol.* **10**, 148–154 (2008).
32. Korbelik, M. & Cecic, I. Contribution of myeloid and lymphoid host cells to the curative outcome of mouse sarcoma treatment by photodynamic therapy. *Cancer Lett.* **137**, 91–98 (1999).
33. Schreiber, R. D., Old, L. J. & Smyth, M. J. Cancer immunoediting: integrating immunity's roles in cancer suppression and promotion. *Science* **331**, 1565–1570 (2011).

34. Korbelik, M. Induction of tumor immunity by photodynamic therapy. *J. Clin. Laser Med. Surg.* **14**, 329–334 (1996).
35. Leenen, P. J., de Bruijn, M. F., Voerman, J. S., Campbell, P. A. & van Ewijk, W. Markers of mouse macrophage development detected by monoclonal antibodies. *J. Immunol. Methods* **174**, 5–19 (1994).
36. Rehg, J. E., Bush, D. & Ward, J. M. The utility of immunohistochemistry for the identification of hematopoietic and lymphoid cells in normal tissues and interpretation of proliferative and inflammatory lesions of mice and rats. *Toxicol. Pathol.* **40**, 345–374 (2012).
37. Murphy, W. J. *et al.* Synergistic anti-tumor responses after administration of agonistic antibodies to CD40 and IL-2: coordination of dendritic and CD8+ cell responses. *J. Immunol.* **170**, 2727–2733 (2003).
38. Briones, J., Timmerman, J. M., Panicalli, D. L. & Levy, R. Antitumor immunity after vaccination with B lymphoma cells overexpressing a triad of costimulatory molecules. *J. Natl. Cancer Inst.* **95**, 548–555 (2003).
39. Knutson, K. L. & Disis, M. L. Tumor antigen-specific T helper cells in cancer immunity and immunotherapy. *Cancer Immunol. Immunother.* **54**, 721–728 (2005).
40. Azémar, M.-D., Comperat, E., Richard, F., Cussenot, O. & Roupret, M. Bladder recurrence after surgery for upper urinary tract urothelial cell carcinoma: frequency, risk factors, and surveillance. *Urol. Oncol.* **29**, 130–136 (2011).
41. Katz, M. H., Lee, M. W. & Gupta, M. Setting a new standard for topical therapy of upper-tract transitional-cell carcinoma: BCG and interferon-alpha2B. *J. Endourol.* **21**, 374–377 (2007) (**discussion 377**).
42. Sarosdy, M. F. A review of clinical studies of bropirimine immunotherapy of carcinoma in situ of the bladder and upper urinary tract. *Eur. Urol.* **31**(Suppl 1), 20–26 (1997).
43. Thalmann, G. N., Markwalder, R., Walter, B. & Studer, U. E. Long-term experience with bacillus Calmette–Guerin therapy of upper urinary tract transitional cell carcinoma in patients not eligible for surgery. *J. Urol.* **168**, 1381–1385 (2002).
44. Manyak, M. J. & Ogan, K. Photodynamic therapy for refractory superficial bladder cancer: long-term clinical outcomes of single treatment using intravesical diffusion medium. *J. Endourol.* **17**, 633–639 (2003).
45. Kimm, S. Y. *et al.* Nonthermal ablation by using intravascular oxygen radical generation with WST11: dynamic tissue effects and implications for focal therapy. *Radiology*. https://doi.org/10.1148/radiol.2016141571 (2016).
46. Murray, K. S. *et al.* Treatment effects of WST11 vascular targeted photodynamic therapy for urothelial cell carcinoma in swine. *J. Urol.* https://doi.org/10.1016/j.juro.2016.01.107 (2016).
47. Azzouzi, A.-R. *et al.* Padeliporfin vascular-targeted photodynamic therapy versus active surveillance in men with low-risk prostate cancer (CLIN1001 PCM301): an open-label, phase 3, randomised controlled trial. *Lancet Oncol.* **18**, 181–191 (2017).
48. Dong, L., Lin, F., Wu, W., Liu, Y. & Huang, W. Verteporfin inhibits YAP-induced bladder cancer cell growth and invasion via hippo signaling pathway. *Int. J. Med. Sci.* **15**, 645–652 (2018).
49. Celli, J. P., Solban, N., Liang, A., Pereira, S. P. & Hasan, T. Verteporfin-based photodynamic therapy overcomes gemcitabine insensitivity in a panel of pancreatic cancer cell lines. *Lasers Surg. Med.* **43**, 565–574 (2011).
50. Hu, Z., Rao, B., Chen, S. & Duanmu, J. Targeting tissue factor on tumour cells and angiogenic vascular endothelial cells by factor VII-targeted verteporfin photodynamic therapy for breast cancer in vitro and in vivo in mice. *BMC Cancer* **10**, 1–13 (2010).
51. Inoue, K. 5-Aminolevulinic acid-mediated photodynamic therapy for bladder cancer. *Int. J. Urol.* **24**, 97–101 (2017).
52. Flurkey K, Currer JM, H. D. Normative biology, husbandry, and models. in *The Mouse in Biomedical Research* (ed. Fox JG, Davisson MT, Quimby FW, Barthold SW, Newcomer CE, S. AL) 637–672 (Elsevier, Amsterdam, 2007).
53. Corradi, R. B. *et al.* Effectiveness of the combination of vascular targeted photodynamic therapy and anti-cytotoxic T-lymphocyte-associated antigen 4 in a preclinical mouse model of urothelial carcinoma. *Int. J. Urol.* **26**, 414–422 (2019).
54. O'Shaughnessy, M. J. *et al.* Systemic antitumor immunity by PD-1/PD-L1 inhibition is potentiated by vascular-targeted photodynamic therapy of primary tumors. *Clin. Cancer Res.* **24**, 592–599 (2018).
55. Ya, Z., Hailemichael, Y., Overwijk, W. & Restifo, N. P. Mouse model for pre-clinical study of human cancer immunotherapy. *Curr. Protoc. Immunol.* **2015**, 20.1.1–20.1.43 (2015).
56. Christensen, J. E., Andreasen, S. O., Christensen, J. P. & Thomsen, A. R. CD11b expression as a marker to distinguish between recently activated effector CD8(+) T cells and memory cells. *Int. Immunol.* **13**, 593–600 (2001).
57. Fiorentini, S. *et al.* CD11b expression identifies CD8+CD28+ T lymphocytes with phenotype and function of both naive/memory and effector cells. *J. Immunol.* **166**, 900–907 (2001).

Acknowledgements

This research was carried out in compliance with the Animal Research: Reporting of In Vivo Experiments (ARRIVE) guidelines and approved by Memorial Sloan Kettering (MSK) Cancer Center Institutional Review Board.

Author contributions

B.R., S.L.R., K.K., A.S., J.A.C. conception and study design B.R., R.B.C., R.A., P.R., S.L.R. and A.S. animals' experiments S.B., S.M., S.L.R, A.S. histology analysis B.R., K.K., A.S., J.A.C. interpretation of data B.R., P.R., R.A., R.B.C manuscript drafting A.S., J.A.C. manuscript revision.

Funding

This study received support from the following grants or institutions to the following authors: 1. NIH Grant P30-CA008748 (cancer center support grant) for all authors except A. Scherz; 2. Sidney Kimmel Center for Prostate and Urologic Cancers for all authors except A. Scherz; 3. The Wade Thompson Foundation.

Competing interests

A. Scherz has ownership interest (including patents) as the inventor of WST11. No potential conflicts of interest were disclosed by the other authors.

Additional information

Supplementary Information The online version contains supplementary material available at https://doi.org/10.1038/s41598-021-84184-y.

Correspondence and requests for materials should be addressed to B.R. or J.A.C.

Reprints and permissions information is available at www.nature.com/reprints.

Publisher's note Springer Nature remains neutral with regard to jurisdictional claims in published maps and institutional affiliations.

molecules

MDPI

Review

Developments in Vascular-Targeted Photodynamic Therapy for Urologic Malignancies

Lucas Nogueira [1], Andrew T. Tracey [1], Ricardo Alvim [1], Peter Reisz [1], Avigdor Scherz [2], Jonathan A. Coleman [1] and Kwanghee Kim [3,*]

1 Urology Service, Department of Surgery, Memorial Sloan Kettering Cancer Center, New York, NY 10065, USA; nogueirl@mskcc.org (L.N.); traceya@mskcc.org (A.T.T.); ricardoalvim1103@gmail.com (R.A.); reiszp@mskcc.org (P.R.); colemanj@mskcc.org (J.A.C.)
2 Department of Plant and Environmental Sciences, The Weizmann Institute of Science, Rehovot 7610001, Israel; avigdor.scherz@weizmann.ac.il
3 Department of Surgery, Memorial Sloan Kettering Cancer Center, New York, NY 10065, USA
* Correspondence: kimk1@mskcc.org; Tel.: +1-646-422-4432; Fax: +1-212-452-3323

Academic Editors: M. Amparo F. Faustino, Carlos J. P. Monteiro and Catarina I. V. Ramos
Received: 12 October 2020; Accepted: 12 November 2020; Published: 19 November 2020

Abstract: With improved understanding of cancer biology and technical advancements in non-invasive management of urological malignancies, there is renewed interest in photodynamic therapy (PDT) as a means of focal cancer treatment. The application of PDT has also broadened as a result of development of better-tolerated and more effective photosensitizers. Vascular-targeted PDT (VTP) using padeliporfin, which is a water-soluble chlorophyll derivative, allows for tumor-specific cytotoxicity and has demonstrated efficacy in the management of urologic malignancies. Herein, we describe the evolution of photodynamic therapy in urologic oncology and the role of VTP in emerging treatment paradigms.

Keywords: vascular-targeted photodynamic therapy; prostate cancer; urothelial cancer

1. Introduction

With more than two million new cases of prostate, bladder, and kidney cancer diagnosed worldwide annually, malignancy of the urinary tract has a significant impact on global health [1]. Furthermore, the increasing age of populations in developed nations has increased disease burden. While extirpative surgery and traditional radiation therapy have been the mainstay of treatment for control of these diseases at the clinically localized stage, the growing effort to reduce treatment-related morbidity has led researchers to seek less invasive therapeutic options that do not sacrifice oncologic efficacy.

Photodynamic therapy (PDT) has seen renewed interest among urologic oncologists as a cancer treatment modality, attributable, in part, to more powerful and safer photosensitizing agents and more convenient light delivery systems. A growing body of preclinical and clinical evidence suggests that PDT may be an effective treatment for cancers of the prostate, bladder, and kidney, particularly when vascular-targeted photosensitizing agents are utilized. The following narrative review discusses the history of photodynamic therapy in urologic cancers as well as the evidence supporting current and future clinical applications of vascular-targeted photodynamic therapy (VTP).

2. PDT and Urological Cancer

Photodynamic therapy is a minimally invasive tissue ablation modality in which a photosensitizing substance is activated through exposure to laser light radiation delivered at a specific wavelength.

In the presence of oxygen, this triggers a photochemical reaction that generates oxidant species (radicals, singlet oxygen, triplet species), leading to targeted tissue destruction through direct cytotoxicity, vascular shutdown, and activation of an immune response [2].

Initially described in 1903 for the treatment of skin cancer [3], several agents have been tested and used for PDT in the ablation of various tumors. Most PDT techniques are based on cellular-targeted photochemotherapy (CTP) in which the photosensitizer preferentially accumulates in parenchymal cells, causing local damage through light radiation. Although many agents have been evaluated, only a few have been approved for clinical use. Photosensitizing agents that are currently approved or being tested in clinical trials are listed in Table 1.

Table 1. Photosensitizers that have been approved or are under investigation for cancer treatment.

Agent	Cancer Types	Administration
Porfimer sodium [4]	Lung, esophagus, bile duct, bladder, brain, ovarian, breast, skin metastases	Intravenous injection
5-aminolevulinic acid (5-ALA) [5]	Skin, bladder, brain, esophagus	Topical, oral, or intravenous injection
Methyl-aminolevulinate (MAL) [6]	Skin	Topical
Hexyl aminolevulinate (h-ALA) [7]	Skin	Topical
Verteporfin/ benzoporphyrin derivative (BDP) [4]	Pancreas, breast	Intravenous injection
Padeliporfin/ WST-11 [8,9]	Prostate, esophagus, pancreas, urothelial	Intravenous injection
Temoporfin [10]	Head and neck, lung, brain, bile duct, pancreas skin, breast	Intravenous injection
Talaporfin [4]	Liver, colon, brain, lung, breast skin metastases	Intravenous injection
HPPH [11]	Head and neck, esophagus, lung	Intravenous injection
Rostaporfin [4]	Skin, breast	Intravenous injection
Fimaporfin [12]	Skin, bile duct	Intra-tumoral or intravenous injection
Motexafin lutetium [13]	Breast	Intravenous injection

There has been growing interest in PDT as a treatment modality for prostate cancer over the past two decades, driven in part by earlier detection due to increased use of prostate imaging. In addition, the functional damage, such as urinary and sexual dysfunction, caused by radical treatments for prostate cancer, including radical prostatectomy and radiation therapy, have favored development of less invasive therapeutic modalities [14]. Addressing this concern, PDT offers comparable oncological efficacy in treating the index lesion, while theoretically sparing the urethra and the neurovascular bundles from debilitating damage. Early studies of PDT for prostate cancer used trans-urethral or trans-perineal irradiation with photosensitizers such as hematoporphyrin derivative meso-tetra-(m-hydroxyphenyl)chlorin, 5-aminolevulinic acid, motexafin lutetium, or temoporfin [15]. Unfortunately, these initial studies were limited by an inability to correctly localize the lesions of interest as well as poor selectivity for tumor tissue, leading to significant side effects. This poor selectivity resulted from the fact that these studies tested CTP strategies, which do not safely preserve sensitive surrounding structures including the neurovascular bundles, rectum, and urethral sphincter. Furthermore, the long half-life of early photosensitizing agents led to prolonged phototoxicity [16].

More recently, critical developments in understanding the disease dynamics, along with image and devices improvements, helped to consolidate the role of PDT in prostate cancer. In this scenario, the consolidation of the index lesion concept and tumor behavior patterns were paramount. The development and wider use of other types of focal therapy as high-intensity focused ultrasound (HIFU) and electroporation contributed to improve PDT techniques. Moreover, the advances in imaging methods including multiparametric magnetic resonance imaging have improved the accuracy of prostatic lesion localization, particularly clinically significant disease [17]. These advances made greater accuracy in the insertion of lighting fibers possible, increasing the effectiveness of PDT-based therapies. Furthermore, the development of photosensitizers such as padoporfin and padeliporfin that accumulate in endothelial cells, called vascular-targeted photodynamic therapy (VTP), causing damage in the vascular environment after light activation, have allowed the development of new focal treatments for prostate cancers, which preserve adjacent structures and yield better functional results.

Upper tract urothelial cancer encompasses neoplasia involving the renal pelvis or the ureter. The natural access throughout the urethra and the well-developed ureteroscopy technics provide the possibility of accessing the tumors without needing insertion with minor aggressiveness. The use of the photosensitizer has helped to improve tumor detection in this setting [17–20].

3. VTP Mechanism of Action

As mentioned above, vascular-targeted photodynamic therapy (VTP) is the latest form of PDT and distinct from CTP. The photosensitizers employed in this treatment, the first generation padoporfin (WTS-09), and the second generation padeliporfin (WST-11), spontaneously and noncovalently forms a complex with serum albumin, which circulates in the blood until cleared, with minimal or no extravasation to adjacent tissues. They generate an intense local release of cytotoxic reactive oxygen species (ROS) upon illumination with the 753-nm laser light. ROS-induced damage to the tumor vasculature results in complete tumor collapse, while preserving organ collagen structure. VTP photosensitizers remain confined within the circulation even at high doses, with minimal, or even no, extravasation to other tissues, and are rapidly cleared by the hepatic and renal systems [21]. Therefore, ROS generated upon laser activation, mostly superoxide and hydroxyl radicals, are similarly contained in the vasculature and do not directly kill tumor cells.

A preclinical study of VTP by Madar-Balakirski et al. revealed that a single illumination led to tumor necrosis with 24–48 h, and eradication and healing several weeks after that [22]. This study also showed the immediate ROS impact is within the tumor circulation and not in vascular endothelial cells via clots in the tumor-feeding arteries, which is followed by the vein system, leading to irreversible vascular collapse and blood stasis. These clots formed on the inner artery walls, particularly at precapillary bifurcation points, a few seconds after initiation of laser illumination, and mobilized toward the interface of the tumor microcirculation, leading to vessel occlusion. This occlusion is thought to result from the unusual fragility and absence of contractile smooth muscle elements in tumor vessels, which makes them selectively susceptible to VTP-induced collapse. In this study, the adjacent healthy tissue remained functional with intact vessels, despite exposure to the same ablative procedure.

Importantly, VTP's effects are nonthermal. Kimm et al. demonstrated that the biochemical reaction in VTP does not induce heat or thermal injury [23]. At 208 mW/cm^2 laser energy, VTP did not generate a clinically significant temperature change, defined as $\Delta T \geq 8$ °C because coagulation effects would be expected with extended animal tissue heating to >45 °C. Together, these studies show that VTP leads to nonthermal, complete tissue ablation characterized by uniform coagulation necrosis, while preserving tissue collagen scaffolding, blood vessels ≥40 µm in diameter, and surrounding stroma. These effects preserve normal organ function and allow fast recovery after treatment.

The Kimm et al. study, performed in non-tumor-bearing swine, also showed that this approach spares vessels ≥40 µm in diameter, confirming its safety in proximity to important large vessels, such as in the ureter and renal pelvis [23]. Finally, the authors determined optimal laser fiber distribution, specifically spaced 1 cm apart, and the relationship between laser fluence and the radius of tissue ablation. A companion study similarly confirmed the safety of endoluminal ablation in the ureter and renal pelvis and the intensity dependence of the depth of tissue necrosis [24]. This investigation further showed that tissue in the irradiated area, in this case, the urothelium, regenerates within 4 weeks with no functional changes.

4. New Imaging Methods to Evaluate a VTP Response in Urologic Cancers

The only imaging method that has been clinically assessed for the monitoring of the VTP response is magnetic resonance imaging (MRI) [25], but studies, so far, have been small series without comprehensive tissue-based correlation [26,27]. The accuracy of post-treatment MRI is inconsistent possibly due to low-volume disease, anatomic distortion, and fibrosis, which can influence sampling accuracy and radiographic interpretation [25]. Toward the development of more accurate methods,

a variety of noninvasive imaging modalities have been assessed preclinically for monitoring of VTP-induced changes, which have all proven feasible, even though none has yet advanced to the clinic.

Among the sound-based technologies, Cornelis et al. evaluated the accuracy of contrast-enhanced ultrasound (CEUS) in predicting tumor necrosis after VTP in a murine renal cancer tumor model through radiologic-pathologic comparison [28]. CEUS employs gas-filled microbubbles with high compressibility and resonance that make them useful intravascular contrast agents. The size and shape of the necrotic tumor on CEUS images performed at 24 h post-VTP correlated with those determined by pathology with good inter-observer concordance. While CEUS underestimated the necrotic area on pathology by approximately 5%, the difference was not statistically significant. While the study supports the feasibility of CEUS for VTP response monitoring, its accuracy at earlier time points and in non-hyper-vascular tumors remains to be studied. Another acoustic imaging method used for this purpose is multispectral optoacoustic tomography (MSOT), which offers a view of the entire tumor. Neuschmelting et al. assessed whether MSOT-measured changes in oxygen saturation (SO_2) indicated VTP-induced necrosis [29]. Not only did areas of decreased SO_2 correlate with pathology findings, but MSOT allowed monitoring of the progressive decreases in SO_2 over time, from 60% at 1 h to >70% at 48 h post-treatment. The study also showed that MSOT illumination can be used to activate WST11. Building on this work, Haedicke et al. tested the ability of a higher-resolution acoustic imaging method, known as raster-scanning optoacoustic mesoscopy (RSOM), which measures oxygenation of hemoglobin, to evaluate the short-term and long-term anti-vascular therapeutic effects of VTP [30]. RSOM provided a detailed view of the distinct responses of two xenograft models of bladder cancer, employing the UMUC3 and patient-derived 5637 cell lines. At three days post-VTP, while vasculature in 5637 tumors, known to respond well to VTP, was completely collapsed, UMUC tumors presented with a necrotic center but vasculature regrowth at the periphery. These differences suggest that RSOM measurement of a vascular response may be useful for predicting VTP efficacy.

Two studies have also evaluated cancer-targeted radiotracer-based strategies for VTP-related imaging in prostate cancer. Since positron emission tomography/computed tomography using ^{68}Ga-labeled prostate-specific membrane antigen (^{68}Ga-PSMA PET/CT) is widely used to localize prostate tumors, Alvim et al. assessed its accuracy in detecting tumor recurrence after VTP in a xenograft model [31]. This approach detected all recurrent tumors and had negative results in all others, supporting its use for follow-up in patients after VTP to detect tumor recurrence early (Figure 1). While not strictly a response assessment, Cerenkov luminescence imaging (CLI) has been used to measure retention of the radiotracer/radiotherapeutic ^{90}Y-DOTA-AR and a bombesin/ gastrin-releasing peptide receptor (GRPr) antagonist peptide [32] in combination with VTP. VTP was shown to improve retention of this agent, leading to better tumor control in prostate cancer cell-xenografted mice [33].

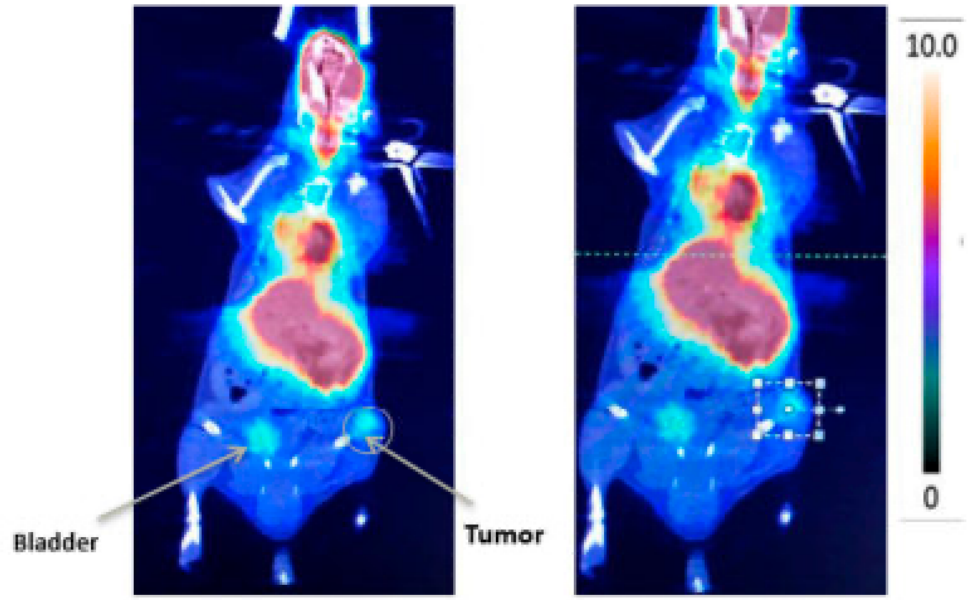

Figure 1. 68Ga-PSMA PET/CT images showing tumor recurrence.

5. Immune Modulation by VTP and Adjunct Immunotherapy

Since VTP-induced hypoxia and cell death initiates an acute local inflammatory cascade within the target tissue, its effects may also be immune-mediated, and it may enhance the efficacy of immunotherapies. Preise et al. were the first to describe the host immune response after VTP [34]. In mice bearing tumors from xenografted colon and mammary carcinoma cells, they demonstrated that a functional immune system is necessary for an effective treatment response and VTP induces long-lasting systemic antitumor immunity, involving both cellular and humoral components.

Given VTP's enhancement of antitumor immune responses, O'Shaughnessy et al. evaluated whether VTP could potentiate the efficacy of the programmed cell death protein-1 (PD-1) and the programmed death protein ligand-1 (PD-L1) pathway inhibition using an orthotopic murine model of renal cell carcinoma that develops lung metastases [35]. Combined VTP with PD-1/PD-L1 inhibition, but neither treatment alone, resulted in regression of the tumors, prevention of lung metastases, and prolonged survival. Combination therapy led to increases in the ratios of CD8+ and CD4+ cells relative to regulatory T cells in primary renal tumors and increased T cell infiltration in sites of lung metastasis, suggesting a role for both cytotoxic and memory T cells in the enhanced immune response. Similarly, supporting the clinical investigation of combining immune checkpoint inhibitors with VTP, Corradi et al. showed that the combination of VTP and anti-cytotoxic T-lymphocyte-associated protein 4 (CTLA-4) effectively treated the primary tumors, prevented lung metastasis, and extended survival in a urothelial carcinoma syngeneic mouse model [36]. Moreover, in mice previously treated with VTP or with VTP and anti-CTLA-4, cancer cells injected later did not grow into tumors. These studies provide rationale for clinical trials of combination VTP and immune checkpoint inhibitor therapy in both bladder and upper tract tumors.

Since immunosuppressive myeloid cells have also been implicated in limiting the anti-tumor immune response and, thus, promoting tumor growth, and are recruited to sites of wound healing. Lebdai et al. assessed the effect of VTP on infiltration of these cells [37]. Using a cell line-based prostate cancer xenograft model, the authors demonstrated that VTP induces the recruitment of myeloid-derived suppressor cells (MDSCs) to treated tumors as well as their expression of colony-stimulating factor 1 receptor (CSF1R), which is required for myeloid differentiation, proliferation, and tumor migration.

They also showed that the combination of VTP with CSF1R blockade inhibited myeloid infiltration and increased CD8+ T cell infiltration, leading to reduced tumor growth and increased survival. This study, thus, supports clinical investigation of this alternative VTP/immunotherapy combination and suggests that VTP may synergize with a range of immunotherapies.

6. VTP and Phosphatidylinositol 3-Kinase (Pi3k) Signaling Pathway

The PI3K cell signaling pathway is frequently altered in most cancer and may play an important role in endothelial cell survival and tumor recurrence after VTP. Kraus et al. performed an in vitro study to evaluate the association of three PI3K inhibitors (BYL719, BKM120, and BEZ235) and Verteporfin-VTP in SV40 endothelial and PC-3 prostate cancer cell. An enhanced VTP response were observed with all the three agents, and BEZ235 was presented as the best combination. These preliminary results support the combination of VTP and PI3K pathway inhibitors [38].

7. Clinical Trials in Urologic Cancers

7.1. Phase I

The first-in-human study of VTP, using padoporfin/WST-09 [39], specifically focused on its potential side effect of photosensitivity because of its residual uptake and longer clearance rate from the skin [40]. No cutaneous phototoxic effects were observed upon light exposure up to 128 J/cm^2 1–3 h after treatment with doses of 2 mg/kg, suggesting that photosensitivity after padoporfin-mediated VTP is negligible after a brief waiting period. The phase I study results reported by Trachtenberg et al. included safety, pharmacokinetics, and hypovascular lesion formation, as detected by contrast enhanced magnetic resonance imaging and transrectal ultrasound guided biopsies [41]. In 24 patients with recurrent prostate cancer after external beam radiation therapy (EBRT), escalating doses of both padoporfin and light, delivered using two 763-nm diode laser fibers, were evaluated. No skin photosensitivity was observed up to 48 h post-VTP, and no residual padoporfin in serum was detected 2 h post-treatment. Hypovascular lesion size was drug dose-dependent and light fluence-dependent with the best results observed at 2 mg/kg and 360 J/cm^2, respectively, and thresholds for detectable hypovascular lesions were defined as 2 mg/kg VTP dose and 100 J/cm^2 light fluence. No serious adverse events were observed, and sexual, urinary, and bowel function returned to baseline six months after VTP. Contrast-enhanced MRI at one-week post-VTP was considered a reliable early indicator of response as confirmed by a six-month biopsy.

7.2. Phase I/II

A phase I/II trial reported by Gertner et al. evaluated the safety, pharmacokinetics, and efficacy of padoporfin-mediated VTP in 15 patients with recurrent prostate cancer after EBRT [42]. In this trial, doses of padoporfin were escalated from 0.1 to 2 mg/kg at a fixed 100 J/cm^2 light fluence. VTP treatment was technically feasible and well-tolerated in all patients. Plasma concentration of padoporfin was linearly related to dose, and none was detectable in plasma 2 h after irradiation. Padoporfin was not detected in urine at any time point. Hypovascular lesion formation was detected by MRI in patients receiving 1.0 and 2.0 mg/kg doses. Average radiation penetration was 5.5 mm in the lesions and 3.2 mm in VTP-exposed tissue regions in which lesions were not detectable. The authors postulated that the decrease of radiation penetration in the unresponsive areas was caused by fibrosis and calcification in recurrent tumors.

Azzouzi et al. performed a pooled analysis of data from one phase I/II [43] and two-phase II clinical trials [44] involving 117 men with localized, ISUP grade ≤2 prostate cancer [45]. Patients received a 10-min intravenous infusion of a single dose of 4 mg/kg padeliporfin, activated by a 753 nm light at 200 J/cm^2. Hemi-ablation was performed in unilateral disease while conservative subtotal ablation techniques were used in the bilateral cases.

VTP treatment was technically feasible in all patients. The 6-month negative biopsy rate was 68.4% in the overall cohort and 80.6% for patients treated by hemi-ablation with light density index (LDI) ≥1 (n = 67), and the proportion of patients with MRI-detectable necrosis at seven days was 76.5% and 86.3%, respectively. Adverse events occurred in 82.9% of patients. Most of them were mild or moderate, and were related to the drug in 52.1% of patients, the device in 45.3% of patients, and the technical procedure in 76.9% of patients. The most common adverse events were dysuria, urinary retention, erectile dysfunction, and voiding urgency. At six months' follow-up, there was a slight improvement in urinary function and a slight deterioration of sexual quality. The authors recently published updated data from the two Phase II trials. After 3.5 years of follow-up time, the tumor free rate in the treated lobe was 75%. Side effect rates remained stable with longer follow-up with most of that had a lower grade (5% and 0% grade III and IV, respectively) [46].

7.3. *Phase II*

Trachtenberg et al. evaluated VTP for whole prostate ablation in 18 patients with recurrent prostate cancer after EBRT [47]. Patients were treated with a fixed dose of 2 mg/kg of padoporfin using up to six 763-nm diode laser fibers for light delivery. Patient-specific escalating light doses and fiber positioning were determined by planning software based on pre-treatment MRI. VTP treatment was technically feasible in all patients. Stronger light doses were associated with better treatment response, encompassing up to 80% of the prostate volume. Complete pathological responses at 6-month biopsy required ≥23 J/cm^2 light dose in 90% of the prostate and was seen in 8 of 13 patients who received such treatment. MRI changes were observed in all patients, and >60% of image responses were associated with a complete pathological response. Sexual, urinary, and bowel function returned to baseline 6 months after VTP. Rectal wall devascularization was observed in 10 patients, while recto-urethral fistula was diagnosed in two. These results support VTP's utility for the treatment of prostate cancer recurrence after EBRT.

VTP was first evaluated for the treatment of localized prostate cancer by Azzouzi et al. [48], who investigated the optimal padeliporfin concentration and light dose parameters to achieve prostate cancer ablation in patients who met active surveillance criteria. Patients (n = 86) were divided into two groups with one receiving a fixed light dose of 200 J/cm^2, and the other light doses varying from 200–300 J/cm^2. Drug concentration was defined by prostate size in both groups: 4 mg/kg if <60 mL, and 6 mg/kg for prostates ≥60 mL. VTP treatment was technically feasible in all but one patient. Optimal treatment parameters were defined as a padeliporfin concentration of 4 mg/kg and 200 J/cm^2 light, which led to an 83% negative biopsy rate at 6 months and 88% necrosis at 7-day MRI. Adverse events occurred in 87% of patients in which most of them are mild or moderate. At 6 months' follow-up, urinary function generally improved and sexual quality slightly deteriorated.

One year later, Moore et al. published a similar study, aiming to determine the optimal light and drug doses for VTP using padeliporfin in men with localized low-risk prostate cancer [49]. A total of 42 patients were treated with a fixed light dose of 200 J/cm^2 using two 753-nm diode laser fibers for delivery following infusion of padeliporfin over 10 min at escalating doses of 2, 4, and 6 mg/kg. VTP treatment was technically feasible in all but two patients. Treatment with the 4 mg/kg drug dose activated by a 753-nm light at 200 J/cm^2 and an LDI of >1 led to the best outcomes with a treatment effect in 95% of the planned treatment volume and a negative biopsy rate at 6 months of 83%. Adverse events occurred in 81% of patients, which were mostly mild or moderate. At 6 months' follow-up, there was no significant change in urinary or sexual function relative to baseline.

Another trial evaluated the efficacy of VTP hemiablation using 4 mg/kg padeliporfin in men with low-risk and intermediate-risk prostate cancer, including those with bilateral ISUP group 1 and 2, yielding similar results to earlier phase II studies [50]. At 12 months, 60 of 81 (74%) men had negative biopsies. Of the eight patients with ISUP group 2 prostate cancer who had biopsies at 6 and 12 months, all had negative biopsies at 12 months, and none underwent subsequent prostate cancer treatment during the study period.

Taken together, these studies demonstrate a strong correlation between total light energy delivered and efficacy, and defined the optimal VTP treatment parameters for subsequent phase III studies: 4 mg/kg padeliporfin, 200 J/cm^2, and LDI ≥1.

7.4. Phase III

In 2016, Azzouzi et al. published the only prospective randomized phase III study comparing VTP using padeliporfin versus active surveillance in 413 patients with low-risk prostate cancer. After an average follow-up of two years, patients undergoing VTP had a lower rate of disease progression (28% vs. 58%, hazard ratio(HR): 0.34, 95% confidence interval (CI) 0.24–0.46, $p < 0.0001$), higher rate of negative biopsies (49% vs. 14%, HR: 3.67, 95% CI 2.53–5.33, $p < 0.0001$) and less need for radiotherapy or surgery (6% vs. 29%, $p < 0.0001$) [51]. In the group treated with VTP, patient reports on the IIEF-15 and IPSS questionnaires showed a deterioration of erectile and voiding functions in the first 6 months, but, after two years' follow-up, these outcomes did not significantly differ when compared with active surveillance ($p = 0.64$). As expected, both the frequency and severity of adverse effects were higher among patients treated with VTP, but most patients had mild or moderate complications (Grade 1 or 2) that occurred in the first few days after the procedure, and fully recovered without sequelae. Perineal pain (15%) and urinary infection (10%) were the most common complications. This study led to the approval of VTP for the treatment of low-risk localized prostate cancer in Europe.

8. Current Studies in Prostate and Urothelial Upper Tract Cancers

A single-center single-arm phase IIb study is currently investigating VTP's efficacy, safety, and effects on quality of life in 50 patients with intermediate-risk prostate cancer [9]. The research includes men with a histologic diagnosis ISUP group 2 disease on one half of the prostate in ≤2 sextants of the prostate gland and not present in >50% of any one core, cT2a disease, prostate volume between 25–70 mL, and serum prostate-specific antigen (PSA) ≤10 ng/mL. Patients will be followed for 5 years by clinical evaluation, PSA, and prostate biopsies at 3, 12, 24, 36, 48, and 60 months. According to an early report, 40 of 49 patients (82%) had no ISUP group 2 or more significant cancer in the index lobe at 3 months [9]. Eleven (22%) underwent per-protocol second hemi-ablation treatment for the ISUP group 2 tumor at 3 months: nine for residual cancer and three for newly identified tumors. Fifteen of the 16 men (94%) who had undergone 12-month biopsy had no Gleason grade 4 or 5 cancer, including 6 of 7 (86%) receiving two treatments. Final results are expected in the near future.

A single-center single-arm phase I dose-finding study (NCT03617003) is currently evaluating 16 patients with recurrent UTUC treated with up to two sessions of endoscopic padeliporfin VTP. Eligibility included residual or recurrent urothelial carcinoma of the ureter or renal pelvis failing prior endoscopic treatment, who are unable or unwilling to undergo surgical management by resection of the involved ureter or kidney. Padeliporfin (4 mg/kg) was infused over 10 min and activated using a diode laser at 753 nm via a flexible ureteroscope. Light dose escalated from 100 mW/cm^2 up to a maximally tolerated dose of 200 mW/cm^2. The primary endpoint is the determination of maximally tolerated laser light fluence rate with secondary objectives of treatment efficacy and biomarker identification.

9. Conclusions

Vascular-targeted photodynamic therapy using padeliporfin/WST-11 is a safe and well-tolerated treatment for urological malignancies, as demonstrated in a large number of preclinical and clinical studies. It delivers focal tumor damage secondary to destruction of small vascular vessels, triggered by the release of cytotoxic reactive oxygen species upon specific light illumination. Due to its nonthermal mechanism of action, minimal effects on functional outcomes, and support by level 1 evidence from the only randomized controlled trial yet reported for any focal therapy. VTP holds significant promise as the focal therapy of choice over other modalities for patients with urological cancer. Further studies evaluating oncologic efficacy are warranted, given these promising results.

Author Contributions: Conception and design, L.N., A.T.T. and K.K.; manuscript writing, L.N., A.T.T., R.A., P.R., J.A.C., A.S., and K.K. All authors have read and agreed to the published version of the manuscript.

Funding: This work was supported by the Sidney Kimmel Center for Prostate and Urologic Cancers and a National Institutes of Health/National Cancer Institute Cancer Center Support Grant [P30CA008748].

Conflicts of Interest: A. Scherz is the inventor of WST11, which has been licensed by the Weizmann Institute to Steba Biotech. A. Scherz, K. Kim, and J.A. Coleman are listed as co-inventors on a provisional patent application on VTP and combination therapy that is owned by Memorial Sloan Kettering Cancer Center and the Weizmann Institute of Science.

References

1. Koob, T.J.; Lim, J.J.; Massee, M.; Zabek, N.; Denozière, G. Properties of dehydrated human amnion/chorion composite grafts: Implications for wound repair and soft tissue regeneration. *J. Biomed. Mater. Res. Part B Appl. Biomater.* **2014**, *102*, 1353–1362. [CrossRef] [PubMed]
2. dos Santos, A.F.; De Almeida DR, Q.; Terra, L.F.; Baptista, M.S.; Labriola, L. Photodynamic therapy in cancer treatment—An update review. *J. Cancer Metastasis Treat.* **2019**, *5*, 25. [CrossRef]
3. Von Tappeiner, H. Therapeutische Versuche mit fluoreszierenden Stoffen. *Munch. Med. Wochenschr.* **1903**, *1*, 2042–2044.
4. Hamblin, M.R. Photodynamic Therapy for Cancer: What's Past is Prologue. *Photochem. Photobiol.* **2020**, *96*, 506–516. [CrossRef]
5. Casas, A. Clinical uses of 5-aminolaevulinic acid in photodynamic treatment and photodetection of cancer: A review. *Cancer Lett.* **2020**, *490*, 165–173. [CrossRef]
6. Tampa, M.; Sarbu, M.-I.; Matei, C.; Mitran, C.-I.; Mitran, M.-I.; Caruntu, C.; Constantin, C.; Neagu, M.; Georgescu, S.-R. Photodynamic therapy: A hot topic in dermato-oncology. *Oncol. Lett.* **2019**, *17*, 4085–4093. [CrossRef]
7. De Rosa, F.S.; Bentley, M.V.L.B. Photodynamic Therapy of Skin Cancers: Sensitizers, Clinical Studies and Future Directives. *Pharm. Res.* **2000**, *17*, 1447–1455. [CrossRef]
8. Azzouzi, A.-R.; Emberton, M. Padeliporfin vascular-targeted photodynamic therapy versus active surveillance in men with low-risk prostate cancer—Authors' reply. *Lancet Oncol.* **2017**, *18*, e188. [CrossRef]
9. Tracey, A.; Noguiera, L.; Alvim, R.; Wong, N.; Demac, Q.; McGill, M.; Sjoberg, D.; Estes, C.; ODea, C.; Benfante, N.; et al. LBA02-04 Interim Results: A Phase 2B Trial of Padeliporfin (WST11) Vascular-Targeted Photodynamic Therapy as Partial-Gland Ablation for Men with Intermediate-Risk Prostate Cancer. *J. Urol.* **2020**, *203* (Suppl. S4), e1116. [CrossRef]
10. Yanovsky, R.L.; Bartenstein, D.W.; Rogers, G.S.; Isakoff, S.J.; Chen, S.T. Photodynamic therapy for solid tumors: A review of the literature. *Photodermatol. Photoimmunol. Photomed.* **2019**, *35*, 295–303. [CrossRef]
11. Zheng, X.; Morgan, J.; Pandey, S.K.; Chen, Y.; Tracy, E.; Baumann, H.; Missert, R.G.; Batt, C.; Jackson, J.; Bellnier, D.A.; et al. Conjugation of 2-(1'-hexyloxyethyl)-2-devinylpyropheophorbide-a (HPPH) to carbohydrates changes its subcellular distribution and enhances photodynamic activity in vivo. *J. Med. Chem.* **2009**, *52*, 4306–4318. [CrossRef] [PubMed]
12. Hu, J.-J.; Lei, Q.; Zhang, X.-Z. Recent advances in photonanomedicines for enhanced cancer photodynamic therapy. *Prog. Mater. Sci.* **2020**, *114*, 100685. [CrossRef]
13. Chen, Z.; Woodburn, K.W.; Shi, C.; Adelman, D.C.; Rogers, C.; Simon, D.I. Photodynamic therapy with motexafin lutetium induces redox-sensitive apoptosis of vascular cells. *Arter. Thromb. Vasc. Biol.* **2001**, *21*, 759–764. [CrossRef] [PubMed]
14. Davidson, S.R.H.; Weersink, R.; Haider, M.A.; Gertner, M.R.; Bogaards, A.; Giewercer, D.; Scherz, A.; Sherar, M.D.; Elhilali, M.; Chin, J.L.; et al. Treatment planning and dose analysis for interstitial photodynamic therapy of prostate cancer. *Phys. Med. Biol.* **2009**, *54*, 2293–2313. [CrossRef]
15. Bugaj, A.M. Vascular targeted photochemotherapy using padoporfin and padeliporfin as a method of the focal treatment of localised prostate cancer—Clinician's insight. *World J. Methodol.* **2016**, *6*, 65–76. [CrossRef]
16. Nogueira, L.; Wang, L.; Fine, S.W.; Pinochet, R.; Kurta, J.M.; Katz, D.; Savage, C.J.; Cronin, A.M.; Hricak, H.; Scardino, P.T.; et al. Focal treatment or observation of prostate cancer: Pretreatment accuracy of transrectal ultrasound biopsy and T2-weighted MRI. *Urology* **2010**, *75*, 472–477. [CrossRef]
17. Bedi, N.; Reddy, D.; Ahmed, H.U. Targeting the cancer lesion, not the whole prostate. *Transl. Androl. Urol.* **2020**, *9*, 1518–1525. [CrossRef]

18. Ahmad, S.; Aboumarzouk, O.; Somani, B.; Nabi, G.; Kata, S.G. Oral 5-aminolevulinic acid in simultaneous photodynamic diagnosis of upper and lower urinary tract transitional cell carcinoma—A prospective audit. *BJU Int.* **2012**, *110*, E596–E600. [CrossRef]
19. Fukuhara, H.; Kurabayashi, A.; Furihata, M.; Setuda, S.; Takahashi, K.; Murakami, K.; Tanakac, T.; Inouea, K. 5-aminolevulinic acid-mediated photodynamic diagnosis using fluorescence ureterorenoscopy for urinary upper tract urothelial carcinoma approximately Preliminary prospective single centre trial approximately. *Photodiagnosis Photodyn. Ther.* **2020**, *29*, 101617. [CrossRef]
20. Fukuhara, H.; Yamamoto, S.; Karashima, T.; Inoue, K. Photodynamic diagnosis and therapy for urothelial carcinoma and prostate cancer: New imaging technology and therapy. *Int. J. Clin. Oncol.* **2020**, 1–8. [CrossRef]
21. Eymerit-Morin, C.; Zidane, M.; Lebdai, S.; Triau, S.; Azzouzi, A.R.; Rousselet, M.-C. Histopathology of prostate tissue after vascular-targeted photodynamic therapy for localized prostate cancer. *Virchows Archiv.* **2013**, *463*, 547–552. [CrossRef] [PubMed]
22. Madar-Balakirski, N.; Tempel-Brami, C.; Kalchenko, V.; Brenner, O.; Varon, D.; Scherz, A.; Salomon, Y. Permanent occlusion of feeding arteries and draining veins in solid mouse tumors by vascular targeted photodynamic therapy (VTP) with Tookad. *PLoS ONE* **2010**, *5*, e10282. [CrossRef] [PubMed]
23. Kimm, S.Y.; Tarin, T.V.; Monette, S.; Srimathveeravalli, G.; Gerber, D.; Durack, J.C.; Solomon, S.B.; Scardino, P.T.; Scherz, A.; Coleman, J. Nonthermal Ablation by Using Intravascular Oxygen Radical Generation with WST11: Dynamic Tissue Effects and Implications for Focal Therapy. *Radiology* **2016**, *281*, 109–118. [CrossRef] [PubMed]
24. Murray, K.S.; Winter, A.G.; Corradi, R.B.; LaRosa, S.; Jebiwott, S.; Somma, A.; Takaki, H.; Srimathveeravalli, G.; Lepherd, M.; Monette, S.; et al. Treatment Effects of WST11 Vascular Targeted Photodynamic Therapy for Urothelial Cell Carcinoma in Swine. *J. Urol.* **2016**, *196*, 236–243. [CrossRef]
25. Muller, B.G.; Fütterer, J.J.; Gupta, R.T.; Katz, A.; Kirkham, A.; Kurhanewicz, J.; Moul, J.W.; Pinto, P.A.; Rastinehad, A.R.; Robertson, C.; et al. The role of magnetic resonance imaging (MRI) in focal therapy for prostate cancer: Recommendations from a consensus panel. *BJU Int.* **2014**, *113*, 218–227. [CrossRef]
26. Haider, M.A.; Davidson, S.R.H.; Kale, A.V.; Weersink, R.; Evans, A.J.; Toi, A.; Gertner, M.R.; Bogaards, A.; Wilson, B.; Chin, J.L.; et al. Prostate gland: MR imaging appearance after vascular targeted photodynamic therapy with palladium-bacteriopheophorbide. *Radiology* **2007**, *244*, 196–204. [CrossRef]
27. Vargas, H.A.; Wassberg, C.; Akin, O.; Hricak, H. MR imaging of treated prostate cancer. *Radiology* **2012**, *262*, 26–42. [CrossRef]
28. Cornelis, F.H.; Kim, K.; Durack, J.; Jebiwott, S.; Scherz, A.; Srimathveeravalli, G.; Coleman, J. Contrast enhanced ultrasound imaging can predict vascular-targeted photodynamic therapy induced tumor necrosis in small animals. *Photodiagnosis Photodyn. Ther.* **2017**, *20*, 165–168. [CrossRef]
29. Neuschmelting, V.; Kim, K.; Malekzadeh-Najafabadi, J.; Jebiwott, S.; Prakash, J.; Scherz, A.; Coleman, J.A.; Kircher, M.F.; Ntziachristos, V. WST11 Vascular Targeted Photodynamic Therapy Effect Monitoring by Multispectral Optoacoustic Tomography (MSOT) in Mice. *Theranostics* **2018**, *8*, 723–734. [CrossRef]
30. Haedicke, K.; Agemy, L.; Omar, M.; Berezhnoi, A.; Roberts, S.; Longo-Machado, C.; Skubal, M.; Nagar, K.; Hsu, H.-T.; Kim, K.; et al. High-resolution optoacoustic imaging of tissue responses to vascular-targeted therapies. *Nat. Biomed. Eng.* **2020**, *4*, 286–297. [CrossRef]
31. Alvim, R.; Nagar, K.; Das, S.; Lebdai, S.; Wong, N.; Somma, A.; Hughes, C.; Thomas, J.; Monette, S.; Scherz, A.; et al. Positron Emission Tomography/Computed Tomography with Gallium-68-labeled Prostate-specific Membrane Antigen Detects Relapse After Vascular-targeted Photodynamic Therapy in a Prostate Cancer Model. *Eur. Urol. Focus* **2019**. [CrossRef] [PubMed]
32. Lohrmann, C.; Zhang, H.; Thorek, D.L.; Desai, P.; Zanzonico, P.B.; O'Donoghue, J.A.; Irwin, C.P.; Reiner, T.; Grimm, J.; Weber, W.A. Cerenkov Luminescence Imaging for Radiation Dose Calculation of a ^{90}Y-Labeled Gastrin-Releasing Peptide Receptor Antagonist. *J. Nucl. Med.* **2015**, *56*, 805–811. [CrossRef] [PubMed]
33. Kim, K.; Zhang, H.; La Rosa, S.; Jebiwott, S.; Desai, P.; Kimm, S.; Scherz, A.; O'Donoghue, J.A.; Weber, W.A.; Coleman, J. Bombesin Antagonist-Based Radiotherapy of Prostate Cancer Combined with WST-11 Vascular Targeted Photodynamic Therapy. *Clin. Cancer Res.* **2017**, *23*, 3343–3351. [CrossRef] [PubMed]
34. Preise, D.; Oren, R.; Glinert, I.; Kalchenko, V.; Jung, S.; Scherz, A.; Salomon, Y. Systemic antitumor protection by vascular-targeted photodynamic therapy involves cellular and humoral immunity. *Cancer Immunol. Immunother.* **2008**, *58*, 71–84. [CrossRef] [PubMed]

35. O'Shaughnessy, M.J.; Murray, K.S.; La Rosa, S.P.; Budhu, S.; Merghoub, T.; Somma, A.; Monette, S.; Kim, K.; Corradi, R.B.; Scherz, A.; et al. Systemic Antitumor Immunity by PD-1/PD-L1 Inhibition Is Potentiated by Vascular-Targeted Photodynamic Therapy of Primary Tumors. *Clin. Cancer Res.* **2018**, *24*, 592–599. [CrossRef] [PubMed]
36. Corradi, R.B.; LaRosa, S.; Jebiwott, S.; Murray, K.S.; Rosenzweig, B.; Somma, A.J.; Gomez, R.S.; Scherz, A.; Kim, K.; Coleman, J.A. Effectiveness of the combination of vascular targeted photodynamic therapy and anti-cytotoxic T-lymphocyte-associated antigen 4 in a preclinical mouse model of urothelial carcinoma. *Int. J. Urol.* **2019**, *26*, 414–422. [CrossRef]
37. Lebdai, S.; Gigoux, M.; Alvim, R.; Somma, A.; Nagar, K.; Azzouzi, A.R.; Cussenot, O.; Merghoub, T.; Wolchok, J.D.; Scherz, A.; et al. Potentiating vascular-targeted photodynamic therapy through CSF-1R modulation of myeloid cells in a preclinical model of prostate cancer. *Oncoimmunology* **2019**, *8*, e1581528. [CrossRef]
38. Kraus, D.; Palasuberniam, P.; Chen, B. Targeting Phosphatidylinositol 3-Kinase Signaling Pathway for Therapeutic Enhancement of Vascular-Targeted Photodynamic Therapy. *Mol. Cancer Ther.* **2017**, *16*, 2422–2431. [CrossRef]
39. Weersink, R.A.; Forbes, J.; Bisland, S.; Trachtenberg, J.; Elhilali, M.; Brún, P.H.; Wilson, B.C. Assessment of cutaneous photosensitivity of TOOKAD (WST09) in preclinical animal models and in patients. *Photochem. Photobiol.* **2005**, *81*, 106. [CrossRef]
40. Weersink, R.; Wilson, B.C.; Patterson, M.S. Determination of the peak absorption wavelength and disaggregation kinetics of TOOKAD in vivo using dynamic, spatially resolved diffuse reflectance spectroscopy in a rabbit model. *Int. Symp. Biomed. Opt.* **2002**, *4613*, 135–143. [CrossRef]
41. Trachtenberg, J.; Bogaards, A.; Weersink, R.; Haider, M.; Evans, A.; McCluskey, S.; Scherz, A.; Gertner, M.; Yue, C.; Appu, S.; et al. Vascular Targeted Photodynamic Therapy With Palladium-Bacteriopheophorbide Photosensitizer for Recurrent Prostate Cancer Following Definitive Radiation Therapy: Assessment of Safety and Treatment Response. *J. Urol.* **2007**, *178*, 1974–1979. [CrossRef] [PubMed]
42. Gertner, M.R.; Bogaards, A.; Weersink, R.A.; McCluskey, S.A.; Haider, M.A.; Yue, C.K.K.; Savard, J.; Simpson, S.; Brun, P.H.; Cohen, P. 839 Initial results of a phase I II trial of WST09-mediated photodynamic therapy (WST09-PDT) for recurrent prostate cancer following failed external beam radiation therapy (EBRT). *Eur. Urol. Suppl.* **2004**, *3*, 212. [CrossRef]
43. Steba Biotech, S. *Safety and Tolerability Study Using WST11 in Patients with Localized Prostate Cancer*; ClinicalTrials; National Library of Medicine (US): Bethesda, MD, USA, 2009.
44. Azzouzi, A.R.; Lebdai, S.; Benzaghou, F.; Stief, C. Vascular-targeted photodynamic therapy with TOOKAD(R) Soluble in localized prostate cancer: Standardization of the procedure. *World J. Urol.* **2015**, *33*, 937–944. [CrossRef] [PubMed]
45. Azzouzi, A.R.; Barret, E.; Bennet, J.; Moore, C.M.; Taneja, S.S.; Muir, G.H.; Villers, A.; Coleman, J.; Allen, C.; Scherz, A.; et al. TOOKAD® Soluble focal therapy: Pooled analysis of three phase II studies assessing the minimally invasive ablation of localized prostate cancer. *World J. Urol.* **2015**, *33*, 945–953. [CrossRef] [PubMed]
46. Noweski, A.; Roosen, A.; Lebdai, S.; Barret, E.; Emberton, M.; Benzaghou, F.; Apfelbeck, M.; Gaillac, B.; Gratzke, C.; Stief, C.; et al. Medium-term Follow-up of Vascular-targeted Photodynamic Therapy of Localized Prostate Cancer Using TOOKAD Soluble WST-11 (Phase II Trials). *Eur. Urol. Focus* **2019**, *5*, 1022–1028. [CrossRef]
47. Trachtenberg, J.; Weersink, R.; Davidson, S.R.; Haider, M.A.; Bogaards, A.; Gertner, M.R.; Evans, A.; Scherz, A.; Savard, J.; Chin, J.L.; et al. Vascular-targeted photodynamic therapy (padoporfin, WST09) for recurrent prostate cancer after failure of external beam radiotherapy: A study of escalating light doses. *BJU Int.* **2008**, *102*, 556–562. [CrossRef]
48. Azzouzi, A.R.; Barret, E.; Moore, C.M.; Villers, A.; Allen, C.; Scherz, A.; Muir, G.H.; De Wildt, M.J.; Barber, N.J.; Lebdai, S.; et al. TOOKAD®Soluble vascular-targeted photodynamic (VTP) therapy: Determination of optimal treatment conditions and assessment of effects in patients with localised prostate cancer. *BJU Int.* **2013**, *112*, 766–774. [CrossRef]

49. Moore, C.M.; Azzouzi, A.-R.; Barret, E.; Villers, A.; Muir, G.H.; Barber, N.J.; Bott, S.; Trachtenberg, J.; Arumainayagam, N.; Gaillac, B.; et al. Determination of optimal drug dose and light dose index to achieve minimally invasive focal ablation of localised prostate cancer using WST11-vascular-targeted photodynamic (VTP) therapy. *BJU Int.* **2015**, *116*, 888–896. [CrossRef]
50. Rodriguez-Rivera, J.; Rodriguez-Lay, R.; Zegarra-Montes, L.; Benzaghou, F.; Gaillac, B.; Azzouzi, A.; Reis, L.O.; Palma, P. Expanding indication of padeliporfin (WST11) vascular-targeted photodynamic therapy: Results of prostate cancer Latin-American multicenter study. *Actas Urol. Esp.* **2018**, *42*, 632–638. [CrossRef]
51. Azzouzi, A.-R.; Vincendeau, S.; Barret, E.; Cicco, A.; Kleinclauss, F.; Van Der Poel, H.G.; Stief, C.G.; Rassweiler, J.; Salomon, G.; Solsona, E.; et al. Padeliporfin vascular-targeted photodynamic therapy versus active surveillance in men with low-risk prostate cancer (CLIN1001 PCM301): An open-label, phase 3, randomised controlled trial. *Lancet Oncol.* **2017**, *18*, 181–191. [CrossRef]

nature COMMUNICATIONS

ARTICLE

https://doi.org/10.1038/s41467-020-15885-7 OPEN

Modeling biological and genetic diversity in upper tract urothelial carcinoma with patient derived xenografts

Kwanghee Kim[1,12], Wenhuo Hu[2,12], François Audenet[3], Nima Almassi[3], Aphrothiti J. Hanrahan[2], Katie Murray[3], Aditya Bagrodia[3], Nathan Wong[3], Timothy N. Clinton[3], Shawn Dason[3], Vishnu Mohan[4], Sylvia Jebiwott[1], Karan Nagar[1], Jianjiong Gao[5], Alex Penson[2], Chris Hughes[1], Benjamin Gordon[1], Ziyu Chen[2], Yiyu Dong[2], Philip A. Watson[2], Ricardo Alvim[1], Arijh Elzein[2], Sizhi P. Gao[2], Emiliano Cocco[2], Alessandro D. Santin[6], Irina Ostrovnaya[7], James J. Hsieh[8], Irit Sagi[4], Eugene J. Pietzak[3], A. Ari Hakimi[3], Jonathan E. Rosenberg[9], Gopa Iyer[9], Herbert A. Vargas[10], Maurizio Scaltriti[2], Hikmat Al-Ahmadie[11], David B. Solit[2,5,9✉] & Jonathan A. Coleman[3✉]

Treatment paradigms for patients with upper tract urothelial carcinoma (UTUC) are typically extrapolated from studies of bladder cancer despite their distinct clinical and molecular characteristics. The advancement of UTUC research is hampered by the lack of disease-specific models. Here, we report the establishment of patient derived xenograft (PDX) and cell line models that reflect the genomic and biological heterogeneity of the human disease. Models demonstrate high genomic concordance with the corresponding patient tumors, with invasive tumors more likely to successfully engraft. Treatment of PDX models with chemotherapy recapitulates responses observed in patients. Analysis of a HER2 S310F-mutant PDX suggests that an antibody drug conjugate targeting HER2 would have superior efficacy versus selective HER2 kinase inhibitors. In sum, the biological and phenotypic concordance between patient and PDXs suggest that these models could facilitate studies of intrinsic and acquired resistance and the development of personalized medicine strategies for UTUC patients.

[1] Department of Surgery, Memorial Sloan Kettering Cancer Center, New York, NY 10065, USA. [2] Human Oncology and Pathogenesis Program, Memorial Sloan Kettering Cancer Center, New York, NY 10065, USA. [3] Urology Service, Department of Surgery, Memorial Sloan Kettering Cancer Center, New York, NY 10065, USA. [4] Department of Biological Regulation, Weizmann Institute of Science, Rehovot 7610001, Israel. [5] Marie-Josée and Henry R. Kravis Center for Molecular Oncology, Memorial Sloan Kettering Cancer Center, New York, NY 10065, USA. [6] Gynecology & Reproductive Sciences, Department of Obstetrics, Yale University School of Medicine, New Haven, CT 06510, USA. [7] Department of Epidemiology-Biostatistics, Memorial Sloan Kettering Cancer Center, New York, NY 10017, USA. [8] Molecular Oncology, Department of Medicine, Siteman Cancer Center, Washington University, St. Louis, MO 63110, USA. [9] Genitourinary Oncology Service, Department of Medicine, Memorial Sloan Kettering Cancer Center, New York, NY 10065, USA. [10] Body Imaging Service, Department of Radiology, Memorial Sloan Kettering Cancer Center, New York, NY 10065, USA. [11] Department of Pathology, Memorial Sloan Kettering Cancer Center, New York, NY 10065, USA. [12] These authors contributed equally: Kwanghee Kim, Wenhuo Hu. ✉email: solitd@mskcc.org; colemanj@mskcc.org

Upper tract urothelial carcinoma (UTUC) is a rare malignancy of the renal pelvis or ureter. Although it arises from the same urothelium and shares similarities to urothelial carcinoma of the bladder (UCB), UTUC has distinct molecular characteristics that are of clinical significance. Unlike UCB, UTUC is a Lynch Syndrome-associated malignancy, with the most recent study demonstrating 8.7% of UTUC patients having a pathogenic germline mutation in a Lynch Syndrome-associated gene[1]. Given the relative rarity of this cancer type, treatment guidelines such as the recommendation for the use of neoadjuvant chemotherapy are often extrapolated from UCB studies.

Recent genomic analyses of UTUC[2–5] have identified a high incidence of potentially actionable genomic alterations including recurrent activating mutations in receptor tyrosine kinases (*FGFR3*, *ERBB2*), *HRAS*, *PIK3CA* and *TSC1*. These molecular profiling studies have also, however, identified significant genetic diversity among UTUC patients and a large number of genomic variants of unknown significance[6,7]. Patient-derived UTUC models would facilitate the biological characterization of these variants of unknown significance and could also be used as preclinical models to test novel precision therapy approaches. Although PDX models have been developed from patients with UCB[8–10], the development of UTUC PDX models has yet to be reported. Similarly, although there are several dozen bladder cancer cell lines in widespread use[11,12], few are of upper tract origin. The lack of UTUC-specific cell line and animal models is thus a major hurdle to the development of more effective treatment strategies for this disease.

Here, we report on the successful development of UTUC models that reflect the genetic and biological heterogeneity of the human disease. In a subset of PDX models, chemotherapy sensitivity mirrors the drug sensitivity observed in the patients from which they were derived. Although HER2 alterations are common in patients with urothelial cancer, HER2-targeted therapies have had only modest clinical impact in this disease. We thus used a HER2-mutant PDX/PDC model to explore the biological basis for the limited clinical activity observed to date with HER2-directed therapies in patients with urothelial carcinoma.

Results

Integrated genomic and transcriptomic analysis of UTUC. With the goal of facilitating the development of personalized therapeutic approaches for patients with UTUC, we began in 2014 offering prospective clinical tumor sequencing using the MSK-IMPACT assay to patients with UTUC[13]. MSK-IMPACT is a targeted capture-based next-generation sequencing (NGS) assay that can detect mutations, copy number alterations and select gene fusions in up to 468 cancer-associated genes[6]. To define the frequency of potentially actionable genomic alterations in UTUC, we analyzed 37 UTUC patients from this prospectively generated cohort and 82 UTUC patients previously analyzed retrospectively[2]. In total, tumor samples from 119 UTUC patients (118 nephroureterectomy and 1 resection of metastasis) were analyzed (Supplementary Fig. 1). Consistent with prior studies in UTUC[2,3], we observed frequent mutations in potentially actionable genes including *FGFR3* (47%), *ERBB2* (9%), *HRAS* (12%), *PIK3CA* (16%) and *TSC1* (14%).

Gene expression profiling analyses of muscle-invasive bladder cancers have identified basal and luminal subtypes with the basal sub-type associated with a more aggressive disease course[14,15]. To determine whether UTUC tumors can be similarly stratified, we performed whole-transcriptome RNA sequencing (RNA-seq) (Fig. 1a, b) on 80 of the 119 UTUC tumors for which MSK-IMPACT data was available. Patient demographic and clinical information for the RNA-seq cohort are reported in Supplementary Table 1. Clustering analysis based on the BASE47 gene classifiers[15] found that 70 tumors (87.5%) had a luminal phenotype and 10 (12.5%) a basal phenotype (Fig. 1b). In addition, application of a consensus classifier developed by the Bladder Cancer Molecular Taxonomy Group[16] revealed that the majority of UTUC in the cohort were luminal–papillary (LumP, 66 tumors, 82.5%) sub-type including all 14 of the low-grade tumors. The remainder were classified as luminal unstable (LumU, 7 tumors, 8.75%), luminal non-specific (LumNS, 1 tumor, 1.25%), Stroma-rich (1 tumor, 1.25%) and basal/squamous type (Ba/Sq, 5 tumors, 6.25%). The latter had high expression of tumor basal markers including *CDH3* (Cadherin-3), *CD44* (CD44 antigen), *KRT5* (Keratin, type II cytoskeletal 5), *EGFR* and *KRT6* (Keratin, type II cytoskeletal 6) present in 4 of 5 of the Ba/Sq-type tumors. There was no significant sub-type difference between high- and low-grade tumors ($P = 0.5389$, chi-square test).

Next, we explored differences in the frequency of common driver mutations in UTUC tumors with basal or luminal phenotypes as defined by the BASE47 classifier[15]. The median tumor mutation burden was 4.21 (1.7–853.2) for the luminal and 4.56 (3.1–16.4) for the basal phenotype tumors (Fig. 1a, $P = 0.89$). Somatic *FGFR3* mutations, which have previously been associated with a favorable prognostic outcome in UTUC[17], were only present in luminal subtype. Conversely, there were no significant differences among the two subtypes in the percentage of patients with mutations in *TP53* or other driver genes commonly present in UTUC. Finally, using a curated knowledge base of the known biological effects of individual mutant alleles[18], we observed that 39.3% of all somatic mutations identified were variants of unknown functional significance (Fig. 1c).

Establishment and characterization of UTUC PDX and PDC. With the goal of exploring the biological and clinical significance of individual mutational events identified in the UTUC cohort, we leveraged our prospective clinical sequencing initiative to develop models of UTUC that reflect the genomic and biological diversity of the human disease. Surgical specimens primarily obtained following radical nephroureterectomy (RNU) were grafted into immunocompromised NOD *scid* gamma (NSG) mice to generate patient-derived xenograft (PDX) models with a subset also cultured in vitro to develop patient-derived cell line (PDC) models. In total, we successfully established 17 PDX models from 34 UTUC tumors (50% take rate). The tumor fragments at early passages of 16 among 17 PDX models were successfully preserved as frozen stocks for future implantation (Supplementary Table 2) to avoid late passage failure in tumorigenicity. Six PDC models among 24 tumors (6/24: take rate 25%) also survived beyond 10 passages (Supplementary Fig. 2). Although not statistically significantly different, we did observe a trend towards PDX growth in tumors that were muscle-invasive (≥pT2 tumor stage, $P = 0.166$) (Table 1). All three tumors collected from distant (UCC3 [abdominal wall] and UCC11 [liver]) or lymph node (UCC32) metastatic sites successfully engrafted. The only tumor collected at endoscopic biopsy (UCC27) did not engraft.

To determine whether the PDX models reflected the histological characteristics of the patient tumors from which they were derived, hematoxylin and eosin (H&E) stained sections from each were evaluated by a board-certified pathologist with expertise in GU pathology (H.A-A.) based on the current WHO classification for urinary tract tumors[19]. This analysis demonstrated histological concordance for 16/17 tumors and their corresponding patient-matched PDX models, as well as xenografts subsequently derived from the PDC models (Fig. 2a and Supplementary

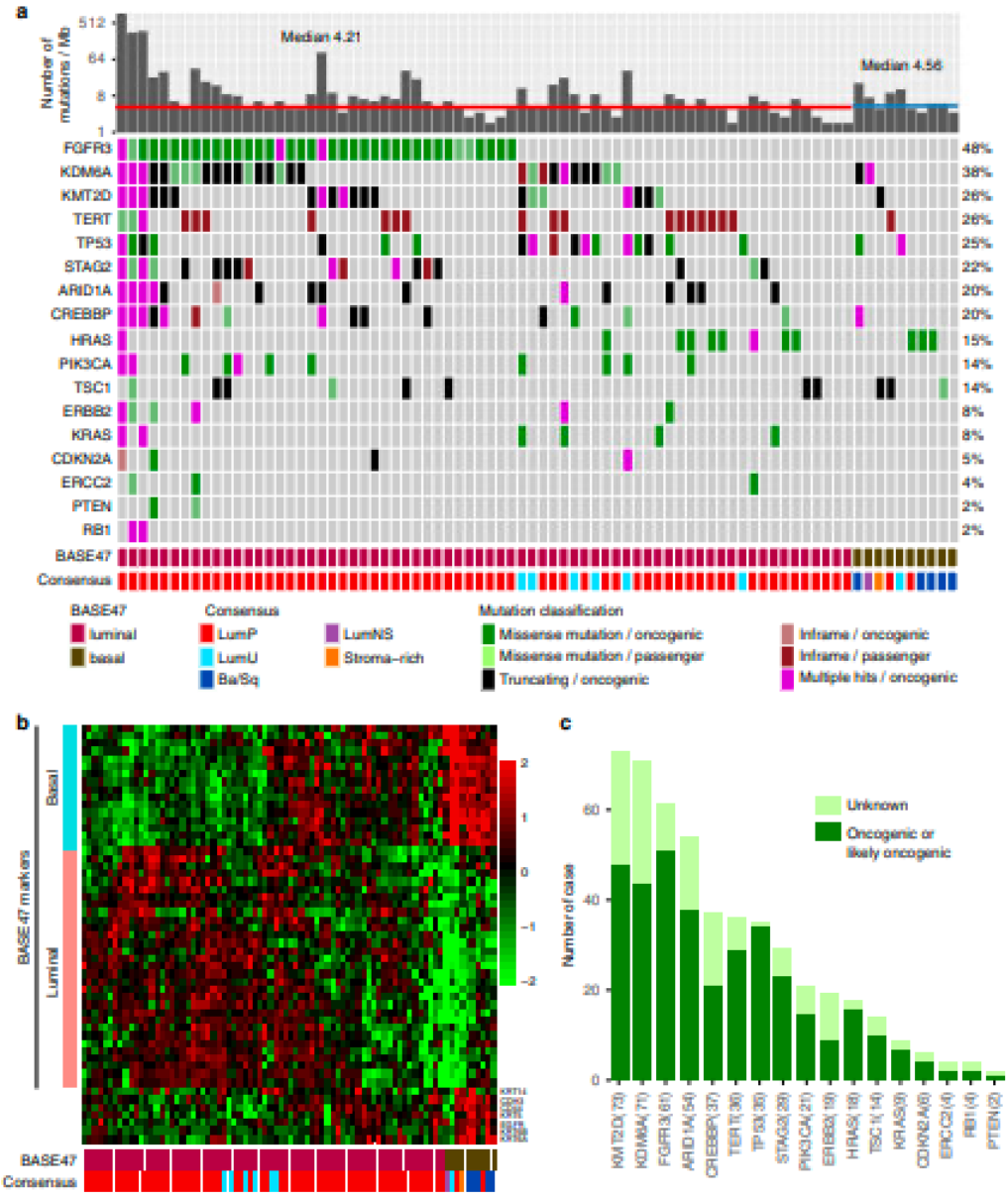

Fig. 1 Integrated genomic and transcriptomic analysis of UTUC cancers. a Somatic genomic landscape of 80 UTUC tumors analyzed by MSK-IMPACT sequencing stratified by RNA sequencing analysis into luminal-like and basal-like subtypes defined using the BASE47 classifier ($K = 2$)[15], and 5 subtypes based on a consensus molecular classification of muscle-invasive bladder cancer[16]. Tumor mutation burden per megabase (Mb) is indicated in log2 scale for each sample. **b** Clustering analysis of RNA-seq data from 80 UTUC tumor samples based on the BASE47 classifier (basal marks shown as a turquoise vertical bar; luminal marks shown as a salmon vertical bar). Analysis of genes expressed in cancer cells of a basal-like phenotype (*KRT14*, *CDH3*, *CD44*, *KRT5*, *EGFR*, *KRT6A/B*) is also shown (color key on the top of **b**). **c** The number of tumors with oncogenic/likely oncogenic and variants of unknown significance in 17 genes frequently mutated in UTUC. Source data for **a** and **b** are provided as a Source Data file.

Table 1 Clinico-pathological characteristics of the samples used for UTUC PDX.

Variable	PDX growth (N = 17)	No PDX growth (N = 17)	P-value
Median age at surgery, years (IQR)	69.6 (65.7–75.7)	65.6 (60.0–75.3)	0.390
Gender			1.000
Male	11 (64.7)	11 (64.7)	
Female	6 (35.3)	6 (35.3)	
Lynch syndrome/MSI-H			0.166
Yes	4 (23.5)	1 (5.9)	
No	12 (70.6)	16 (94.1)	
Not tested	1 (5.9)	0 (0)	
Smoking status			0.039
Current/former	10 (58.8)	16 (94.1)	
Never	7 (41.2)	1 (5.9)	
Prior history of urothelial cancer			1.000
Yes	5 (29.4)	6 (35.3)	
No	12 (70.6)	11 (64.7)	
Location of primary tumor			1.000
Renal pelvis	15 (88.2)	14 (82.4)	
Ureter	2 (11.8)	3 (17.6)	
Specimen type			0.6[a]
Primary	14 (82.4)	16 (94.1)	
Lymph node	1 (5.9)	0 (0)	
Distant metastasis	2 (11.8)	0 (0)	
Endoscopic biopsy	0 (0)	1 (5.9)	
Grade			0.480
Low	2 (11.8)	0 (0)	
High	15 (88.2)	17 (100)	
pT stage			0.166
<pT2 (non-invasive)	5 (29.4)	10 (58.8)	
≥pT2 (invasive)	12 (70.6)	7 (41.2)	
pN stage			0.460
pN0	10 (58.8)	13 (70.5)	
pN+	5 (29.4)	2 (11.8)	
pNx	2 (11.8)	2 (11.8)	
Prior chemotherapy			0.688
Yes	3 (17.6)	5 (29.4)	
No	14 (82.4)	12 (70.6)	

Two-sided P-values were obtained using Wilcoxon-rank sum for continuous and Fisher's exact test for categorical variables.
[a]Specimen type was dichotomized as primary vs all others for this comparison.

Table 3). For example, squamous differentiation observed in patient tumor UCC15 was retained in the corresponding PDX model.

As the properties and composition of extracellular matrix (ECM) can influence cancer cell behavior[20] and as optimal preclinical models would be enriched with ECM similar to the original cancer tissue, we performed histological staining with Picro Sirius red followed by two-photon microscopy-second harmonics generation imaging[21,22] on UCC36 and Masson's trichrome staining[23], which highlights the fibrous collagenous tracts in blue on UCC36, 17 and 19. Comparison of the collagen distribution in the tumor microenvironment of patient tumors and the corresponding patient-matched PDX models showed that both PDX and xenografts derived from PDC retained collagen structure although the percentage area covered by collagen matrix in PDX models was reduced as compared to that of the corresponding patient tumors (Supplementary Fig. 3a, b). All three PDX models and two PDC xenografts also retained the structure of matching patient tumors based on the presence of a fibrotic capsule and the presence of collagen fibers within the body of the tumor as assessed by Masson's trichrome staining (Supplementary Fig. 3c).

To confirm that the PDX and PDC models mirrored the genomic alterations present in the tumors from which they were derived, we performed targeted sequencing using the MSK-IMPACT assay for all 17 tumor/PDX pairs that successfully engrafted. Overall, the somatic mutational profiles of the patient tumors and resulting PDX models were highly concordant (72.7% concordance of known and likely oncogenic mutations). The top recurring mutated genes found in the PDX models were *TERT* (53%), *FGFR3* (59%), *KDM6A* (24%) and *TP53* (29%) (Fig. 2b). In 29% of the PDX, we observed PDX-specific deep deletions in *CDKN2A/CDKN2B*, consistent with selection for loss of these tumor suppressor genes during the process of PDX engraftment[24].

Four of the 17 tumors that engrafted were derived from patients with microsatellite instability high (MSI-H, MSIsensor scores ≥10) tumors including three from patients with Lynch Syndrome (germline mutations were present in *MLH1* in UCC15 and *MSH2* in UCC36, UCC34). UCC17 had loss of MSH2 and MSH6 expression by immunohistochemistry in the absence of germline mutations in either gene. One additional Lynch case failed to engraft. As would be expected, all four MSI-H tumors had a high tumor mutational burden (range: 20.3–157.2 mutation per Mb, Fig. 2c). Mutation signature decomposition analysis[25] for all four MSI-H tumor/PDX pairs revealed stable mutational signatures across passages with the MMR/MSI and aging signatures being most predominant (Supplementary Fig. 4). Finally, the *FGFR3* R248C hotspot mutation, which has previously been shown to be enriched in Lynch Syndrome-associated UTUC as compared to sporadic UTUC tumors[26], was present in 3 of the 4 MSI-H tumor/patient-matched PDX pairs (UCC17, UCC36 and UCC34). In sum, there was a high level of genomic concordance between radical nephroureterectomy-derived tumor samples and the corresponding PDX models (Fig. 2c) with only one PDX model, the hypermutated UCC34 PDX, displaying <50% concordance of known or likely pathogenic mutations.

To assess the extent of genomic drift resulting from establishment of the PDX and PDC models, we performed whole-exome sequencing (WES) on two cases (UCC03 and UCC30). Phylogenetic analysis of the WES data provided evidence of both linear and branched evolution in the tumors and PDX/patient-derived cell lines, as demonstrated by the presence of both private and shared mutations among samples derived from the same patient (Fig. 2d and Supplementary Fig. 5a). Analysis of the UCC03 samples, which were derived from resection of an abdominal wall metastasis, demonstrated that both the cell line (CL) and PDX (X1, X2) were more genomically related to the metastasis than to the primary tumors (P1, P2). Mutational signature decomposition analysis[26] of the UCC03 samples identified a predominant AID/APOBEC gene editing signature (Signatures 2 and 13), a common finding in bladder UC[27,28], in both the tumors and the PDX models. A similar AID/APOBEC gene editing signature (Signatures 2 and 13) was identified in the tumor of patient UCC30, however, the AID/APOBEC(2) signature was lost in the corresponding PDX (Fig. 2e and Supplementary Fig. 5b).

Genomic and transcriptomic predictors of engraftment. As only 50% of the UTUC tumors successfully propagated as PDX models, we sought to determine whether successful engraftment was associated with specific mutational or transcriptomic signatures. Among the top 15 most frequently altered genes in our PDX cohort, *STAG2* and *ERBB2* mutations were positively and

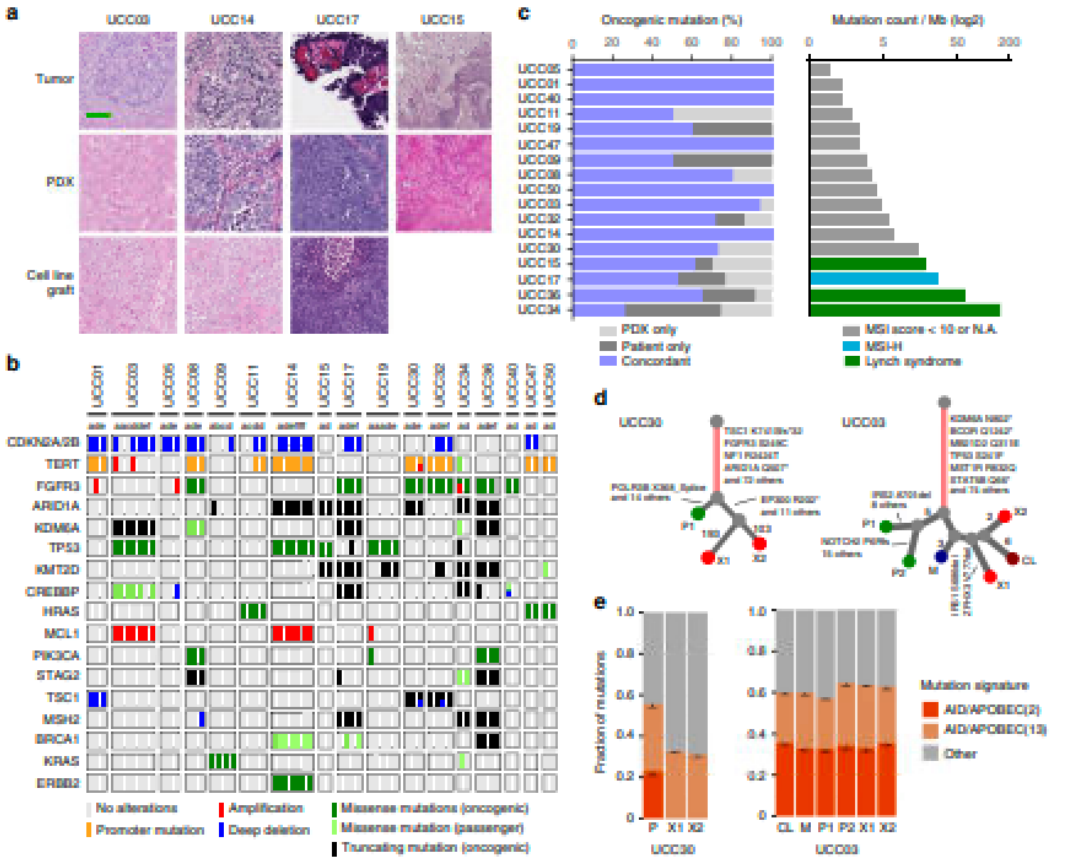

Fig. 2 Histological and genomic comparison of patient tumors and paired patient-derived models. a UTUC tumors and corresponding PDX models demonstrated similar histological features as assessed by H&E staining. Scale bar corresponds to 200 µm. H&E slides of a section of each patient tumor (UCC03, $n = 3$; UCC14, $n = 1$; UCC17, $n = 1$; UCC15, $n = 1$), matching PDX (UCC03, $n = 3$; UCC14, $n = 2$; UCC17, $n = 2$; UCC15, $n = 1$) and matching cell line/cell line-derived xenograft (UCC03, $n = 1$; UCC14, $n = 1$; UCC17, $n = 1$) were reviewed by a board-certified pathologist (H.A-A.) and representative pictures are shown. **b** Concordance of selected cancer-associated genes for the 17 tumors and paired PDX models that successfully engrafted in mice [a: primary tumor, b: lymph node metastasis, c: distal metastasis, d: PDX at early passage (P1-P3), e: PDX at late passage (P4-P6), f: cell line/cell line-derived xenograft]. The UCC03 and UCC11 PDX models were established from abdominal wall and liver resections, respectively, whereas UCC32 was from a lymph node. The UCC11 PDX was generated from the frozen cell pellet of a patient specimen. All others were established from primary tumors. **c** Concordance of somatic oncogenic mutations of the patient tumor and corresponding PDX models and tumor mutational burden (TMB) of the patient tumors. Four PDX models were derived from MSI-H tumors (right panel, green and blue). **d** Phylogenetic analysis of whole-exome sequencing data for two patients (UCC30 and UCC03) revealed evidence of linear and branched tumor evolution [P: primary, M: metastasis, PDX: X1 (early passage) and X2 (late passage) which represent replicates of different passage numbers, CL: PDC]. The number of mutations is shown between branch points. **e** AID/APOBEC mutational signatures (Signatures 2 and 13) were predominant in UCC30 and UCC03 patient tumors while AID/APOBEC(2) was lost in UCC30 PDX. The mutation signatures with FDR < 0.05 are shown. Data are presented as mean values ± SD. Source data for **b**–**e** are provided as a Source Data file.

negatively associated with successful engraftment respectively, although the differences were not statistically significant, possibly due to the small sample size (Fig. 3a).

We next compared the transcriptomic profiles of the patient tumors that successfully engrafted to those that did not. In total, RNA-seq data was available for 17 of the UTUC patient tumors for which we attempted to establish PDX models, 8 of which engrafted and 9 of which failed to grow as PDX. There was a distinct gene expression pattern with 749 genes differentially expressed (FDR < 0.05 and Log FC > 1.5) between UTUC tumors that engrafted vs those that did not (Fig. 3b). Clustering of the patient tumors that engrafted (PDX group) vs those that failed to engraft (No PDX group) did not strongly correlate with luminal or basal classification (Fig. 1a, b) based on the BASE47 classifier[15]. More specifically, while the PDX group had higher expression of the basal gene set as compared to the No PDX group (Fig. 3c), this difference was not statistically significant. There was also no difference in ssGSEA scores for luminal genes between the PDX and No PDX groups. However, there was correlation between successful engraftment and the basal/squamous signature ($P = 0.04$) based on the consensus clustering classification[16]. In addition, GSEA revealed that genes in cell cycle and DNA replication pathways including *SMC1* (Structural maintenance of chromosomes protein 1 A), *MCM5* (DNA

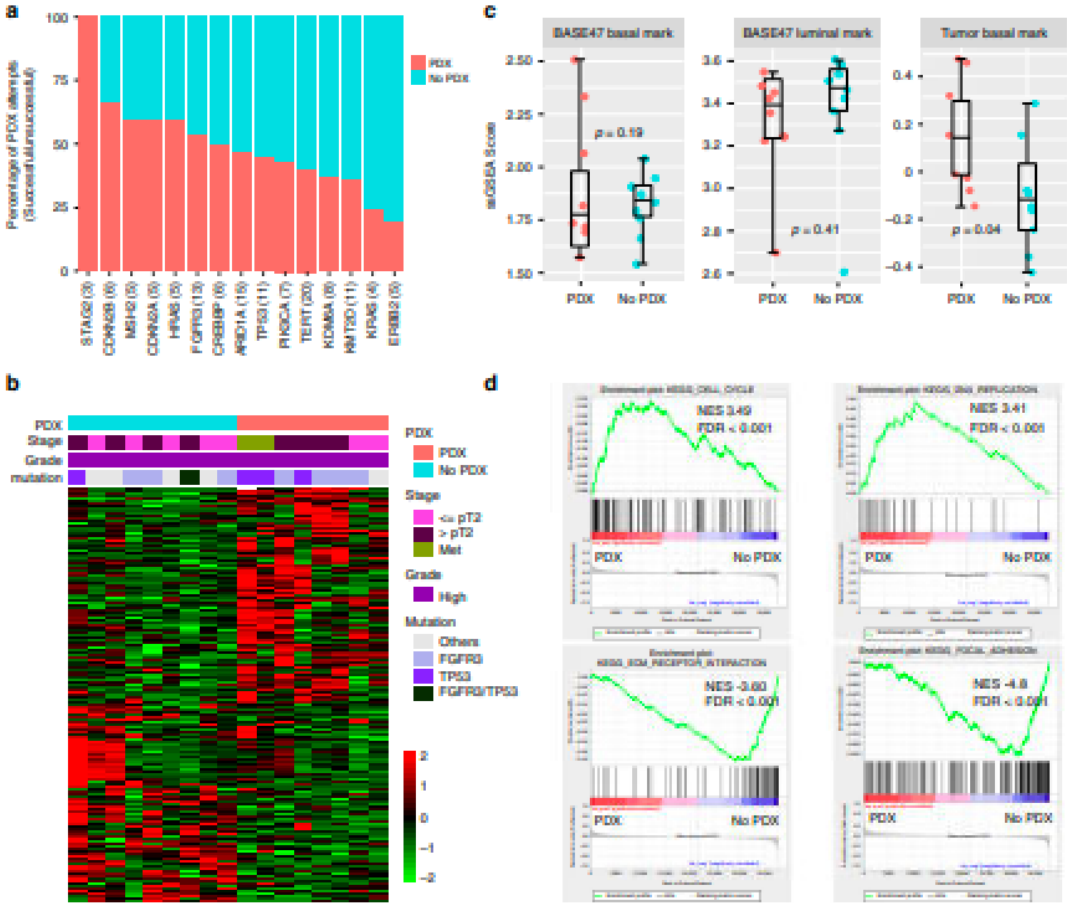

Fig. 3 Comparison of mutation frequencies and RNA expression profiles. Patient specimens that resulted in successful engraftment (PDX) vs those that did not (No PDX) were compared. **a** The rates of successful engraftment differed among tumors with putative driver mutations. The number of patient cases with mutation in the gene is shown in parenthesis. **b** Comparison of RNA-seq data from patient specimens that successfully engrafted (PDX, $n = 8$, salmon) vs those that did not (No PDX, $n = 9$, turquoise). 749 genes (428 upregulated and 321 downregulated) were differentially expressed between UTUC tumors that did and did not engraft based on the *z*-score of normalized gene reads from RNA-seq. **c** Single Sample Gene Set Enrichment Analysis (ssGSEA) scores of basal ($P = 0.19$) and luminal gene sets ($P = 0.41$) based on the BASE47 classifier and ssGSEA scores of tumor basal genes (expressed in cancer cells of a basal-like phenotype, indicated at the bottom of Fig. 1b, $P = 0.04$) plotted for the patient tumors resulting in PDX ($n = 8$) vs No PDX ($n = 9$). Error bars are mean standard error from bootstrap. The center line in the boxplots indicates the mean, the lower and upper hinges correspond to the first and third quartiles, the upper whisker is the maxima and the lower whisker the minima. *P*-value indicates two-sided two group *t*-test without adjustment. **d** GSEA plots comparing specimen that did and did not yield PDX. Enrichment of cell cycle/DNA replication pathways was observed in the PDX group, whereas extracellular matrix receptor interaction and focal-adhesion pathways were enriched in the No PDX group. Source data for **b**–**d** are provided as a Source Data file.

replication licensing factor MCM5) and *MCM7* (DNA replication licensing factor MCM7) were positively enriched in the patient tumors that successfully engrafted, suggesting that the rate of cell proliferation is an important factor for successful PDX establishment. Extracellular Matrix (ECM) receptor interaction and focal-adhesion pathways including *FN1* (Fibronectin), *THBS2* (Thrombospondin-2) and *COMP* (Cartilage oligomeric matrix protein) were also positively enriched in primary tumors that failed to produce PDX tumors, suggesting that greater dependence of tumors on microenvironmental factors may have impeded successful engraftment in a subset of patients (Fig. 3d).

Chemosensitivity of patients and corresponding PDX. To evaluate whether the sensitivity of the PDX models to cytotoxic chemotherapy mirrored that of the UTUC tumors from which they were derived, mice bearing established PDX tumors from three patients were treated with chemotherapy regimens and dosing schedules similar to that of the corresponding patients. As an example, patient UCC03 developed abdominal wall, bone and pelvic metastases 11 months after RNU for pT3bN0 disease. The patient was treated with palliative excision of the left abdominal wall metastasis and radiotherapy followed by gemcitabine/carboplatin (Gem/Carbo) chemotherapy. A PET-CT at 3-months follow-

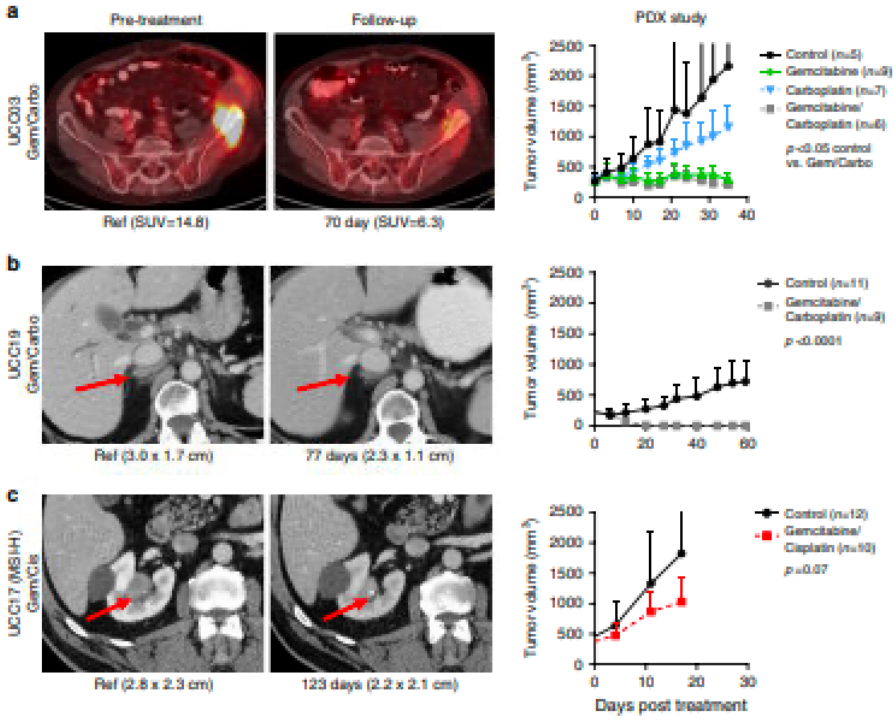

Fig. 4 Chemosensitivity of patients and corresponding PDX. Imaging of target lesions in patients before chemotherapy (pre-treatment) and at the time specified post treatment. Tumor volumes for the corresponding PDX models were graphed as a function of days post-start of drug treatment. **a** UCC03: FDG PET/CT scan after two cycles of gemcitabine/carboplatin (Gem/Carbo) chemotherapy demonstrated decreased radiopharmaceutical accumulation in left iliac metastasis (partial response according to RECIST). Mice bearing the UCC03 PDX were randomized and treated with Gem/Carbo, gemcitabine, carboplatin or vehicle ($P = 0.0177$, vehicle vs Gem/Carbo combination; $P = 0.0065$, vehicle vs gemcitabine; $P = 0.138$, vehicle vs carboplatin). **b** UCC19 received a combination of Gem/Carbo at recurrence followed by gemcitabine alone and demonstrates stable disease by RECIST criteria off treatment for 15 months. The corresponding PDX model was highly sensitive to Gem/Carbo ($P < 0.0001$). **c** UCC17 (MSI-H) received 4 cycles of neoadjuvant gemcitabine/cisplatin. The patient's radiographic response was minimal (stable disease by RECIST criteria) and there was no pathological response (pT3 disease at RNU). Minimal tumor growth inhibition was observed with Gemcitabine/Cisplatin in the corresponding PDX ($P = 0.07$). Two-way ANOVA test (Prism) was used for statistical analysis without adjustment. Data are presented as mean values ± SD (standard deviation). Source data for preclinical studies are provided as a Source Data file.

up demonstrated a partial response by RECIST criteria as well as decreased ^{18}F-fluorodeoxyglucose (FDG) avidity within the dominant pelvic osseous metastasis. A PDX derived from the abdominal metastasis was similarly responsive to Gem/Carbo (Fig. 4a).

Patient UCC19 underwent RNU for pT3 disease and relapsed 16 months later with retroperitoneal lymphadenopathy. The patient responded to Gem/Carbo followed by gemcitabine maintenance and has been off therapy with RECIST stable disease for the past 15 months. Consistent with the patient's durable response to chemotherapy, a PDX generated at the time of RNU (UCC19) demonstrated exquisite sensitivity to Gem/Carbo (Fig. 4b). As DNA damage response (DDR) gene alterations have been associated with sensitivity to platinum-based chemotherapy and improved survival in patients with advanced UC patients[29,30], we assessed whether there was evidence of a likely pathogenic DDR gene alteration. Indeed, both the primary tumor and corresponding PDX harbored a truncating mutation in *RECQL4* (F987*), a gene which has a role in DNA repair by homologous recombination[31].

Patient UCC17, who had an MSI-H tumor, received gemcitabine/cisplatin neoadjuvant chemotherapy (NAC) to which he demonstrated minimal decrease in size on CT from 2.8 to 2.2 cm (stable disease by RECIST criteria) (Fig. 4c) and no pathologic response (pT3N0 at RNU). The PDX generated from the primary tumor was also unresponsive to gemcitabine/cisplatin ($P = 0.07$). Similarly, UCC36 which was derived from a patient with an MSI-H Lynch syndrome-associated UTUC was also resistant to gemcitabine/cisplatin (Supplementary Fig. 6). As chemoresistance has been reported in colorectal cancer patients with MSI-H tumors[32,33] and as the MSI-H UCC17 and UCC36 models were relatively resistant to gemcitabine/cisplatin chemotherapy, we assessed MSI status and chemotherapy responsiveness in a surgical cohort of UTUC patients treated with NAC. Of the 20 patients with UTUC who received NAC before RNU, two were MSI-H (one of which was UCC17), one was MSI-indeterminant (MSIsensor scores 3–10), and 17 were microsatellite stable (MSS, MSIsensor scores <3). Defining pathologic response as ≤pT1N0[34,35], we observed pathologic response in 10 of 17 MSS patients (59%) and in neither of the two MSI-H patients.

HER2-targeted therapy in HER2-mutant UTUC. Consistent with retrospective studies, prospective genomic profiling of 44,183

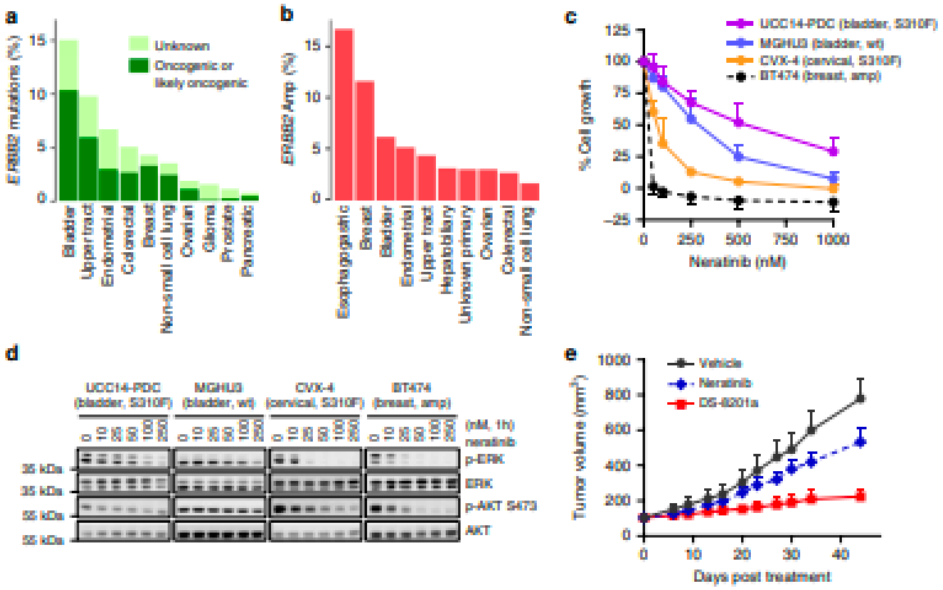

Fig. 5 Assessment of HER2-targeted strategies. a, **b** Fraction of patients with *ERBB2* mutation or amplification, respectively, in bladder, UTUC and other common solid tumors in a prospectively sequenced cohort of 44,183 tumors. **c** Neratinib sensitivity of the UCC14-PDC (HER2 S310F-mutant UTUC), MGHU3 [*ERBB2* wildtype (wt) bladder cancer], CVX-4 (HER2 S310F-mutant cervical cancer) and BT-474 (*ERBB2* amplified breast cancer) was determined 5 days post-neratinib treatment. The average values from three separate experiments ($n = 3$) for UCC14-PDC, MGHU3, and CVX-4 and 5 separate experiments ($n = 5$) for BT-474 are shown. IC50s for neratinib were 508.3, 245.9, 56.8 and 0.1 nM for UCC14, MGHU3, CVX-4 and BT-474, respectively. **d** Inhibition of ERK and AKT, downstream HER2 effectors by neratinib. Western blot was performed (repeated three times) on samples treated with neratinib or vehicle for 1h at the indicated concentrations. The samples were derived from the same experiment and the gels/blots were processed in parallel. **e** Mice with established UCC14 tumors were treated with neratinib 20 mg/kg PO daily (5 days a week), DS-8201a 10 mg/kg i.v. once every 3 weeks or vehicle only as control. Mice bearing the PDX were randomly assigned to 3 cohorts ($n = 8$ per each group) and monitored twice a week [$P = 0.0034$, vehicle vs neratinib; $P < 0.0001$, vehicle vs DS-8201a; $P < 0.0001$, neratinib vs DS-8201a]. Two-way ANOVA test (Prism) was used for statistical analysis. Data are presented as mean values ± SD. Source data for **c**–**e** are provided as a Source Data file.

tumors including 1032 bladder and 204 UTUC at our institution using MSK-IMPACT revealed that mutations in *ERBB2* (oncogenic/likely oncogenic) were more common in urothelial cancer (UC) than in other common solid tumors (10.3% in bladder and 5.9 % in UTUC as compared to 3.2% in breast, 2.9% in endometrial, 2.6% in colorectal, and 2.4% in NSCLC) (Fig. 5a). *ERBB2* amplification was also common in bladder cancer and UTUC (6.2%: 64 of 1032 bladder tumors and 4.4% of UTUC: 9 of 204 tumors, Fig. 5b). As HER2 is a validated drug target in breast and esophagogastric cancers, there has been enthusiasm for targeting HER2 in patients with UC. However, only limited efficacy has been observed to date with HER2 kinase inhibitors, such as an irreversible EGFR/HER2 kinase inhibitor, neratinib[36].

Efforts to define the dependence of HER2-mutant urothelial carcinoma cells on HER2 signaling have been hampered by the lack of available preclinical models of HER2-mutant UC. As genomic analysis revealed that the UCC14 patient tumor and paired PDX harbored a hotspot mutation in *ERBB2* (HER2 S310F), we sought to leverage this model to explore the biological basis for the limited anti-tumor activity of HER2-targeted therapies in patients with UC. We thus generated a cell line from an early passage UCC14-PDX (UCC14-PDC) and assessed its sensitivity to neratinib, a HER2 kinase inhibitor. Both UCC14-PDC (IC50 508.3 nM) and MGHU3 (an *ERBB2* wildtype bladder cancer line, IC50 245.9 nM) were significantly less sensitive to neratinib as compared to CVX-4[37] (a HER2 S310F-mutant cervical cancer line, IC50 56.8 nM) and BT-474 (an *ERBB2* amplified breast cancer cell line, IC50 0.1 nM)(Fig. 5c). The greater concentration of neratinib required to inhibit UCC14-PDC cell growth as compared to other HER2 altered lines was consistent with the higher concentration of drug needed to inhibit activation of ERK, a downstream effector of HER2 (Fig. 5d). Expression of phosphorylated AKT was also potently down-regulated by neratinib in BT-474 and CVX-4 cells, but was unchanged in UCC14-PDC, suggesting that AKT pathway activation was not HER2 dependent in this UC model. Finally, the limited sensitivity of the HER2 S310F-mutant UCC14-PDC to HER kinase inhibition in culture was consistent with the relative insensitivity of the UCC14-PDX to neratinib therapy in vivo (Fig. 5e). In contrast to the lack of efficacy of neratinib, DS-8201a, a humanized HER2 antibody topoisomerase I inhibitor drug conjugate (trastuzumab deruxtecan, Daiichi-Sankyo) recently approved by the FDA for unresectable or metastatic HER2-positive breast cancer (NCT03248492)[38], significantly inhibited UCC14-PDX growth. These data suggest that antibody drug conjugates targeting HER2 may be more effective than selective HER kinase inhibitors in patients with HER2-mutant UC.

Discussion

A major hurdle to the development of personalized treatment approaches for UTUC has been the lack of laboratory models for biological and preclinical studies. Here, we report the development and biological and genomic characterization of PDX and

PDC models from patients with UTUC. We find that the PDX and PDC models recapitulated the diverse landscape of genomic alterations in UTUC. Furthermore, in the select cases tested, the PDX models mirrored the sensitivity/resistance to standard cytotoxic agents of the patients from which the PDX models were derived.

Transcriptomic-based clustering analysis of 80 UTUC tumors using the BASE47 gene classifier[15] found that the majority (70/80, 87.5%) of tumors had a luminal phenotype. Further, application of the recently reported Bladder Cancer Molecular Taxonomy Group consensus classifier resulted in 66 of 80 tumors being classified as luminal–papillary sub-type, including all 14 tumors with low-grade histology (Fig. 1b)[16]. These data are consistent with those of Robinson et al.[5] and suggest that the luminal–papillary sub-type is enriched in UTUC as compared to bladder cancer where only 24% of tumors were luminal–papillary sub-type[16].

Another notable difference between urothelial carcinomas arising in the upper tract and the bladder is the significantly higher incidence of microsatellite instability in renal pelvis and ureteral tumors. It has been reported that patients with Lynch syndrome-associated colorectal cancer have diminished response to chemotherapy relative to patients with sporadic colorectal cancer[32]. Our data suggest that a similar association between chemotherapy sensitivity and MSI status might exist in patients with UTUC. More specifically, we evaluated the sensitivity of two UTUC PDX models (UCC17 and UCC36) derived from patients with MSI-H tumors to platinum chemotherapies and gemcitabine and found that both were relatively resistant to these cytotoxic chemotherapies. Given recent studies suggesting that MSI may be a predictive biomarker of response to immune checkpoint blockade in multiple cancers[39,40], these results suggest that MSI status may be useful in assessing whether UTUC patients should receive neoadjuvant cytotoxic chemotherapy, or, instead be directed to immunotherapy-based clinical trials.

Despite the recent FDA-approval of erdafitinib for *FGFR3*-mutated metastatic bladder cancers[41], the clinical impact of targeted therapies in UC has been limited to date. *ERBB2* is altered by amplification and/or overexpression in various cancer types, and antibodies that bind to the extracellular domain of HER2 are now standard-of-care in *ERBB2* amplified breast and esophagogastric cancers[42,43]. Our prospective clinical sequencing experience of over 44,000 patient tumors indicates that activating *ERBB2* mutations are more prevalent in both bladder and UTUC than in other common solid tumor types (Fig. 5a). However, the lack of *ERBB2* mutant models of UTUC has been a major impediment to the preclinical assessment of HER2-targeted therapies for UTUC patients.

As the UCC14-PDX and patient tumor from which it was derived harbored an activating hotspot mutation in the extracellular domain of HER2 (S310F), we leveraged this model to explore the biological basis for the limited clinical activity of HER kinase inhibitors observed to date in HER2-mutant UC patients. Consistent with the poor response of HER2-mutant UC patients to the HER kinase inhibitor neratinib as compared to HER2-mutant breast and cervical cancer patients[36], the HER2 S310F-mutant cell line UCC14-PDC was significantly less sensitive to neratinib than the HER2-amplified BT-474 breast cancer and HER2 S310F-mutant CVX-4 cervical cancer cell lines. The relative lack of neratinib sensitivity of the UCC14 cell line was consistent with the higher doses of neratinib required to inhibit downstream ERK signaling in this cell line model as compared to BT-474 and CVX-4 cells[37]. This result suggests that the variable sensitivity of different tumor lineages to HER2-directed therapies as reported in a recent basket trial[36], is likely due, at least in part, to differences among cancers in their dependence on HER2 signaling for tumor growth and survival.

Li et al.[44] recently reported that the HER2 antibody drug conjugate ado-trastuzumab emtansine (T-DM1) has significant clinical activity in HER2-mutant lung cancer, even in tumors with low HER2 expression. One hypothesis as to why HER2-mutant tumors with low HER2 expression are sensitive to T-DM1 is that mutation of HER2 may increase the efficiency of receptor internalization following antibody binding[45]. Consistent with this finding, the UCC14-PDX was highly sensitive to DS-8201a, a HER2 antibody drug conjugate, which was recently approved by the FDA for unresectable or metastatic HER2-positive breast cancer[38]. In sum, the data highlight the potential ability of PDX models to guide the development of clinical trials for UTUC patients and suggest that antibody drug conjugates targeting HER2 may be more effective in UTUC patients than selective HER2 kinase inhibitors.

A limitation of the current study is that detailed biological characterization of the large number of variants of unknown significance identified in the PDX models is beyond the capability of any single laboratory. Thus, to facilitate biological discovery and the development of novel therapies for UTUC, all genomic data from the current work is available through cBioPortal [https://www.cbioportal.org/study/summary?id=utuc_msk_2019; https://www.cbioportal.org/study/summary?id=utuc_pdx_msk_2019] and all models reported here will be provided as a resource to the broader scientific community. In addition, the current collection of PDX models was mostly derived from large surgical specimens. Generating PDX models from ureteroscopic biopsies in the pre-radical nephroureterectomy setting would be of particular interest to assess the potential benefits of neoadjuvant chemotherapy for patients with UTUC. This will be the focus of future work seeking to leverage PDX models to inform clinical decision-making.

Methods

Specimen acquisition. From March 2014 to April 2017, tumors and matched normal tissue from 34 patients with UTUC (31 radical nephroureterectomy [RNU] specimens, 2 samples from distant metastasis and 1 UTUC biopsy) were collected under protocols (NCT01779072, MSKCC IRB #89-076 and IRB #06-107) approved by the Memorial Sloan Kettering Cancer Center (MSKCC) Institutional Review Board. We have obtained informed consent from all participants of this study. RNU specimens were dissected robotically in a usual manner with the hilum stapled as late as feasible to limit ischemia time. Extraction of the specimen was performed immediately to ensure no more than 20–30 min of surgical ischemia time before specimen removal. The specimens were then transported directly to pathology, tumor(s) was identified grossly by a pathologist and a fresh sample for PDX generation was collected under sterile condition. Surgical samples were then transported to a research laboratory in RPMI medium or PBS on ice. Time from surgical removal of tissue in the OR to placement in medium in pathology and time from pathology to the research laboratory was ~20–40 min and 10 min, respectively. For all specimens, representative hematoxylin and eosin (H&E) slides from frozen tissue and formalin-fixed paraffin-embedded (FFPE) sections were reviewed by a board-certified genitourinary pathologist (H.A-A.) to confirm histology, grade and stage. Clinical and demographic information was obtained from a prospectively maintained institutional database.

Establishment of xenografts from surgical specimen. All animal work was approved by the MSKCC Institutional Animal Care and Use Committee (IACUC). We have complied with all relevant ethical regulations. All surgical specimens were transported in RPMI medium or PBS on ice, washed with cold PBS, cut into small pieces (2 × 2 to 3 × 3 mm^3) and then implanted subcutaneously into one or two sides of the flank of 6–8-week-old male immunocompromised NOD-SCID $IL2Rg^{-/-}$ (NSG) mice (Jackson Laboratory) via a 4–5 mm skin incision over the mid-lumbar spine[46,47]. PDX from UCC11 was generated from a frozen cell pellet after a collagen-based digestion process. PDX were serially transplanted for expansion when the tumor volume reached 0.5–1 cm^3. Harvested xenograft tumors were cut into small fragments as earlier and either stored in freezing media (Recovery™ Cell Culture Freezing Medium, Thermo Fisher Scientific) in liquid nitrogen for future implantation and/or flash frozen for molecular studies including RNA-seq and/or western blot analysis.

Primary culture and xenograft implantation. Tumor tissues were minced to small pieces, processed using 225 U/ml Collagenase type III at 37 °C for 15–30 min before plating into collagen-coated plates in advanced DMEM/F12 medium, supplemented with 10% FBS, 2 mM Glutamax, 1 mM sodium pyruvate, 1× non-essential amino acid, 10 mM HEPES, 100 µg/ml primocin (InVivoGen), 50 ng/ml EGF (MilliporeSigma) and 10 µM Y-27632 (Selleck Chemicals). All cell culture components were from Thermo Fisher Scientific unless otherwise stated. When the plates became confluent, cells were trypsinized using 0.25% TrypLE for expansion. For generation of the UCC14 patient-derived cell line (UCC14-PDC), a PDX piece at passage 3 was processed using 225 U/ml Collagenase type III, mixed with Matrigel (growth factor reduced; Corning Life Sciences) at 1:1 and plated as multiple 50 µl drops in 6-well plates to establish a 3D culture and then converted to a cell line for growth in 2D for in vitro assays. For in vivo tumorigenesis studies of the patient-derived cell lines shown in Supplementary Fig. 2, 3–5 million cells of PDC in media mixed with Matrigel at 1:1 were subcutaneously injected into the flank of NSG mice and tumor growth was measured weekly by calipers.

Targeted (MSK-IMPACT) and whole-exome sequencing. Targeted sequencing was performed using the MSK-IMPACT (Memorial Sloan Kettering Integrated Mutation Profiling of Actionable Cancer Targets) assay using FFPE tumors and matched FFPE normal tissue or frozen blood. Matched normal tissue samples were obtained from renal parenchyma or lymph nodes that were confirmed to be histologically benign. MSK-IMPACT is a hybridization capture-based assay for deep sequencing of cancer-associated genes. A 300 gene version was used for the UTUC samples analyzed retrospectively, whereas 341, 410 or 468 versions were used for the prospectively sequenced tumors and PDX and PDC models. Briefly, following DNA extraction, an equimolar pool of barcoded libraries was subjected to exon capture using custom oligonucleotides, sequenced on an Illumina HiSeq 2500 instrument (Illumina Inc), and analyzed using a customized pipeline for somatic mutation calling, copy number alterations and structural rearrangements[6].

DNA samples for whole-exome sequencing were barcoded and then processed using SureSelect Human All Exon V4 (Agilent Technologies) according to the manufacturer's instructions followed by sequencing on a HiSeq 2500 instrument in 100-bp paired-end mode. The average aligned reads per samples were 95 million, with 235-fold coverage on targeted regions, and an average duplication rate of 17.6%. For phylogenetic analysis, sample distances between pairs of samples were calculated based on non-shared mutations, followed by hierarchical clustering using the average agglomeration method. We used the Stringlist package in R software to count the non-shared mutations and the Analysis of Phylogenetics and Evolution package to plot the tree. The resulting phylogenetic trees were then denoted with notable oncogenic mutations.

RNA sequencing and transcriptome analyses. Total RNA from frozen tissue was isolated using Trizol (Thermo Fisher Scientific) and the quantity and quality of the resulting RNA was measured using an Agilent 2100 Bioanalyzer. The TruSeq RNA Library Prep Kit v2 (Illumina) was used for library preparation, followed by sequencing (60 million paired-end reads) on an Illumina HiSeq 2500. Read numbers for genes were extracted by RSEM (using the STAR alignment program)[48]. Mean aligned reads per sample was 25 million. The consensusMIBC package (https://github.com/cit-bioinfo/consensusMIBC, Bladder Cancer Molecular Taxonomy Group)[16] was used for a consensus clustering analysis. Differentially expressed genes between the tumors that led to PDX (PDX group) vs those that failed to produce PDX (No PDX group) were identified by DESeq2[49]. Gene Set Enrichment Analysis was applied to identify pathways significantly different in the PDX vs No PDX groups[50].

Two-photon microscopy and second harmonics generation. Unstained patient, PDX and PDC-derived FFPE tumors were cut into 15-µm-thick sections, de-paraffinized, hydrated and visualized using a two-photon microscope (2PM: Zeiss LSM 880 upright Laser Scanning Microscope) with non-linear optics, coupled with a Chameleon MPX (Coherent Inc.) femtosecond pulsed, tunable Ti: Sapphire laser for two-photon excitation with Plan Apochromat ×20/0.8 (Carl Zeiss, Germany). For collagen second harmonic imaging, a wavelength of 880 nm was used. Both reflected and transmitted signals were collected for image analysis and processed using Zeiss Zen imaging software.

Picro Sirius red staining. The patient, PDX and PDC-derived tumor FFPE sections were stained with Picro Sirius red[51] to quantitate changes in deposition or architecture of extracellular matrix structures, specifically collagen fibers. De-waxed and hydrated paraffin sections were stained for 1 h and washed in two changes of acidified water. Slides were dehydrated in three changes of 100% ethanol, cleared in xylene and mounted in a resinous medium. Slides were scanned using Pannoramic scanner (3D Histech Ltd.) and analyzed using Pannoramic viewer (3D Histech Ltd.) and FIJI (ImageJ) software.

Masson's trichrome staining. For direct visualization of collagen fibers and histological assessment of collagen deposition, patient, PDX and PDC-derived tumor FFPE sections were de-waxed, hydrated and a trichrome staining[21] was performed using the Masson Trichrome Staining Kit (Sigma-Aldrich, St Louis, MO, USA). Slides were dehydrated quickly in 95% and absolute ethanol, cleared in xylene and mounted. Slides were scanned using Pannoramic scanner (3D Histech Ltd.) and analyzed using Pannoramic viewer (3D Histech Ltd.).

Treatment of PDX-bearing mice with chemotherapy. Chemotherapy was administered intraperitoneally when tumor volumes reached 100–300 mm^3. For drug studies, mice were randomly assigned into vehicle control (saline for gemcitabine and platin drugs) and treatment groups (6–12 mice per each group). Mice were treated with the combination of weekly 50 mg/kg of gemcitabine and 5 mg/kg cisplatin (4-week cycle; weekly gemcitabine with 4th week off and cisplatin at every 4 weeks) or the combination of weekly 50 mg/kg of gemcitabine and 50 mg/kg carboplatin (4-week cycle). Tumor growth was quantitated weekly using calipers and growth curves were generated using GraphPad Prism software. Following guidelines set forth by the IACUC, mice were killed when tumor volume reached 1 cm^3. All drugs were purchased from Selleck Chemicals.

Neratinib and DS-8201a sensitivity assays. UCC14-PDC (*ERBB2* S310F mutated bladder cancer), BT-474 (*ERBB2* amplified breast cancer), MGHU3 (*ERBB2* wildtype bladder cancer, kindly provided by Dr. Margaret Knowles) and CVX-4 (*ERBB2* S310F mutated cervical cancer) cells were treated with neratinib (Puma Biotechnology) at concentrations ranging from 0 to 1000 nM. For growth assays, cells were seeded into 6-well plates. After allowing 24 h for adherence, cells were then counted at Day 0 time point, or at Day 5 post treatment with neratinib or DMSO using the Vi-CELL XR 2.03 (Beckman Coulter). Growth curves were generated from the averages of at least 3 experiments in duplicate (±SE) by plotting percent growth [(mean cell number at drug dose D5 − mean cell number of control D0)/(mean cell number of DMSO D5 − mean cell number of control D0) × 100)] against drug concentration. For in vivo drug studies, a UCC14-PDX tumor was mechanically dissociated, resuspended in Matrigel at 1:1 and subcutaneously injected into the flanks of male NSG mice (Jackson Laboratories). Once tumors reached an average volume of 100 mm^3, mice were randomized to receive either vehicle control (0.5% methylcellulose/0.2% Tween 80 for neratinib, PBS for DS-8201a), neratinib, or DS-8201a (Daiichi-Sankyo). The dosing schedules were as follows: neratinib at 20 mg/kg p.o. daily 5 days/week, DS-8201a at 10 mg/kg i.v. once every 3 weeks. Tumors were measured twice a week using calipers. Interested parties should contact Dr. Alessandro Santin for CVX-4 and Dr. Margaret Knowles for MGHU3 cell lines.

For western blot studies, cells were seeded into 60 mm dishes. At 75% confluence in log phase growth, cells were treated with neratinib at 0–250 nM for 1 h and then lysed in 1% NP-40 lysis buffer or RIPA buffer and processed for immunoblotting[37,52]. For primary antibodies, phospho-antibodies were used at 1:500 in TBST/5%BSA and totals were used at 1:1000 TBST/5% BSA with incubation overnight at 4 °C. Secondary antibodies were used at 1:2000 TBST/5% BSA for 1 hr at room temperature. ERK (#9102), p-ERK (T202/Y204) (#9101), AKT (#9272) and p-AKT (Ser473) (#9271) antibodies were from Cell Signaling Technology. Proteins were visualized using the Fuji LAS-4000 (GE LifeSciences).

Statistical analysis. A xenograft was deemed to have successfully engrafted when the tumor volume reached 1 cm^3 or the maximum tumor diameter reached 1.5 cm, and urothelial carcinoma was confirmed by histopathology of the grafted tumors. Clinical variables of patients and differences in engraftment rates were analyzed using Fisher's exact testing for categorical variables and Wilcoxon rank sum for continuous variables. Treatment effects on tumor growth were evaluated by two-way analysis of variance (two-way ANOVA, GraphPad Prism software Version 8). R/Bioconductor packages[53] were used to analyze RNA-Seq data (DESeq2 package) and DNA mutations (maftools package). In addition, gene set variation analysis was performed using single sample GSEA (within GSVA package).

Reporting summary. Further information on research design is available in the Nature Research Reporting Summary linked to this article.

Data availability

All genomic data are accessible on cBioPortal at the following two links; Upper Tract Urothelial Carcinoma (MSK, 2019) [https://www.cbioportal.org/study/summary?id=utuc_msk_2019] or Upper Tract Urothelial Carcinoma PDX (MSK, 2019) [https://www.cbioportal.org/study/summary?id=utuc_pdx_msk_2019]. The raw and normalized RNA sequencing data are available in the database of Gene Expression Omnibus (GEO) associated with series entry number GSE134292. The source data underlying Figs. 1a, b, 2b–e, 3b–d, 4a–c, 5c–e and Supplementary Figs. 2, 4, 6 are provided as a Source Data File.

Received: 11 September 2019; Accepted: 24 March 2020;
Published online: 24 April 2020

References

1. Carlo, M. I. et al. Cancer susceptibility mutations in patients with urothelial malignancies. *J. Clin. Oncol.* **38**, 404–414 (2020).
2. Sfakianos, J. P. et al. Genomic characterization of upper tract urothelial carcinoma. *Eur. Urol.* **68**, 970–977 (2015).
3. Moss, T. J. et al. Comprehensive genomic characterization of upper tract urothelial carcinoma. *Eur. Urol.* **72**, 641–649 (2017).
4. Audenet, F. et al. Clonal relatedness and mutational differences between upper tract and bladder urothelial carcinoma. *Clin. Cancer Res* **25**, 967–976 (2019).
5. Robinson, B. D. et al. Upper tract urothelial carcinoma has a luminal-papillary T-cell depleted contexture and activated FGFR3 signaling. *Nat. Commun.* **10**, 2977 (2019).
6. Cheng, D. T. et al. Memorial Sloan Kettering-Integrated Mutation Profiling of Actionable Cancer Targets (MSK-IMPACT): a hybridization capture-based next-generation sequencing clinical assay for solid tumor molecular oncology. *J. Mol. Diagn.* **17**, 251–264 (2015).
7. Van Allen, E. M. et al. Whole-exome sequencing and clinical interpretation of formalin-fixed, paraffin-embedded tumor samples to guide precision cancer medicine. *Nat. Med.* **20**, 682–688 (2014).
8. Park, B. et al. Development and characterization of a bladder cancer xenograft model using patient-derived tumor tissue. *Cancer Sci.* **104**, 631–638 (2013).
9. Jäger, W. et al. Patient-derived bladder cancer xenografts in the preclinical development of novel targeted therapies. *Oncotarget* **6**, 21522–21532 (2015).
10. Abe, T. et al. Establishment and characterization of human urothelial cancer xenografts in severe combined immunodeficient mice. *Int J. Urol.* **13**, 47–57 (2006).
11. Barretina, J. et al. The cancer cell line encyclopedia enables predictive modelling of anticancer drug sensitivity. *Nature* **483**, 603–607 (2012).
12. DeGraff, D. J. et al. Current preclinical models for the advancement of translational bladder cancer research. *Mol. Cancer Ther.* **12**, 121–130 (2013).
13. Zehir, A. et al. Mutational landscape of metastatic cancer revealed from prospective clinical sequencing of 10,000 patients. *Nat. Med.* **23**, 703–713 (2017).
14. Choi, W. et al. Identification of distinct basal and luminal subtypes of muscle-invasive bladder cancer with different sensitivities to frontline chemotherapy. *Cancer Cell* **25**, 152–165 (2014).
15. Damrauer, J. S. et al. Intrinsic subtypes of high-grade bladder cancer reflect the hallmarks of breast cancer biology. *Proc. Natl Acad. Sci. USA* **111**, 3110–3115 (2014).
16. Kamoun, A. et al. A Consensus molecular classification of muscle-invasive bladder cancer. *Eur. Urol.* https://doi.org/10.1016/j.eururo.2019.09.006 (2019).
17. Bagrodia, A. et al. Genomic biomarkers for the prediction of stage and prognosis of upper tract urothelial carcinoma. *J. Urol.* **195**, 1684–1689 (2016).
18. Chakravarty, D. et al. OncoKB: a precision oncology knowledge base. *JCO Precis. Oncol.* https://doi.org/10.1200/PO.17.00011 (2017).
19. Moch, H. *WHO Classification of Tumours of the Urinary System and Male Genital Organs*. (International Agency for Research on Cancer, 2016).
20. Pickup, M. W., Mouw, J. K. & Weaver, V. M. The extracellular matrix modulates the hallmarks of cancer. *EMBO Rep.* **15**, 1243–1253 (2014).
21. Chen, X., Nadiarynkh, O., Plotnikov, S. & Campagnola, P. J. Second harmonic generation microscopy for quantitative analysis of collagen fibrillar structure. *Nat. Protoc.* **7**, 654–669 (2012).
22. Lattouf, R. et al. Picrosirius red staining: a useful tool to appraise collagen networks in normal and pathological tissues. *J. Histochem Cytochem.* **62**, 751–758 (2014).
23. Gomori, G. A rapid one-step trichrome stain. *Am. J. Clin. Pathol.* **20**, 661–664 (1950).
24. Kuramboulas, C. & Aitken, L. Patient-derived xenografts: a promising resource for preclinical cancer research. *Mol. Cell Oncol.* **6**, 1558684 (2019).
25. Alexandrov, L. B., Nik-Zainal, S., Wedge, D. C., Campbell, P. J. & Stratton, M. R. Deciphering signatures of mutational processes operative in human cancer. *Cell Rep.* **3**, 246–259 (2013).
26. Donahue, T. F. et al. Genomic characterization of upper-tract urothelial carcinoma in patients with lynch syndrome. *JCO Precis. Oncol.* https://doi.org/10.1200/PO.17.00143 (2018).
27. Faltas, B. M. et al. Clonal evolution of chemotherapy-resistant urothelial carcinoma. *Nat. Genet.* **48**, 1490–1499 (2016).
28. Robertson, A. G. et al. Comprehensive molecular characterization of muscle-invasive bladder cancer. *Cell* **171**, 540–556 (2018).
29. Iyer, G. et al. Multicenter prospective phase II trial of neoadjuvant dose-dense gemcitabine plus cisplatin in patients with muscle-invasive bladder cancer. *J. Clin. Oncol.* **36**, 1949–1956 (2018).
30. Teo, M. Y. et al. DNA damage response and repair gene alterations are associated with improved survival in patients with platinum-treated advanced urothelial carcinoma. *Clin. Cancer Res.* **23**, 3610–3618 (2017).
31. Lu, H. et al. RECQL4 promotes DNA end resection in repair of DNA double-strand breaks. *Cell Rep.* **16**, 161–173 (2016).
32. Ribic, C. M. et al. Tumor microsatellite-instability status as a predictor of benefit from fluorouracil-based adjuvant chemotherapy for colon cancer. *N. Engl. J. Med.* **349**, 247–257 (2003).
33. Sargent, D. J. et al. Defective mismatch repair as a predictive marker for lack of efficacy of fluorouracil-based adjuvant therapy in colon cancer. *J. Clin. Oncol.* **28**, 3219–3226 (2010).
34. Matin, S. F. et al. Incidence of downstaging and complete remission after neoadjuvant chemotherapy for high-risk upper tract transitional cell carcinoma. *Cancer* **116**, 3127–3134 (2010).
35. Liao, R. S. et al. Comparison of pathological stage in patients treated with and without neoadjuvant chemotherapy for high risk upper tract urothelial carcinoma. *J. Urol.* **200**, 68–73 (2018).
36. Hyman, D. M. et al. HER kinase inhibition in patients with HER2- and HER3-mutant cancers. *Nature* **554**, 189–194 (2018).
37. Zammataro, L. et al. Whole-exome sequencing of cervical carcinomas identifies activating ERBB2 and PIK3CA mutations as targets for combination therapy. *Proc. Natl Acad. Sci. USA* **116**, 22730–22736 (2019).
38. Modi, S. et al. Trastuzumab deruxtecan in previously treated HER2-positive breast cancer. *N. Engl. J. Med.* **382**, 610–621 (2019).
39. Le, D. T. et al. Mismatch repair deficiency predicts response of solid tumors to PD-1 blockade. *Science* **357**, 409–413 (2017).
40. Le, D. T. et al. PD-1 blockade in tumors with mismatch-repair deficiency. *N. Engl. J. Med.* **372**, 2509–2520 (2015).
41. Loriot, Y. et al. Erdafitinib in locally advanced or metastatic urothelial carcinoma. *N. Engl. J. Med.* **381**, 338–348 (2019).
42. Slamon, D. J. et al. Use of chemotherapy plus a monoclonal antibody against HER2 for metastatic breast cancer that overexpresses HER2. *N. Engl. J. Med.* **344**, 783–792 (2001).
43. Bang, Y. J. et al. Trastuzumab in combination with chemotherapy versus chemotherapy alone for treatment of HER2-positive advanced gastric or gastro-oesophageal junction cancer (ToGA): a phase 3, open-label, randomised controlled trial. *Lancet* **376**, 687–697 (2010).
44. Li, B. T. et al. Ado-trastuzumab emtansine for patients with HER2-mutant lung cancers: results from a phase II basket trial. *J. Clin. Oncol.* **36**, 2532–2537 (2018).
45. Li, B. T. et al. HER2-mediated internalization of cytotoxic agents in ERBB2 amplified or mutant lung cancers. *Cancer Discov.* https://doi.org/10.1158/2159-8290.CD-20-0215 (2020).
46. Dong, Y. et al. Tumor xenografts of human clear cell renal cell carcinoma but not corresponding cell lines recapitulate clinical response to sunitinib: feasibility of using biopsy samples. *Eur. Urol. Focus* **3**, 590–598 (2017).
47. Tracey, A. T., Murray, K. S., Coleman, J. A. & Kim, K. Patient-derived xenograft models in urological malignancies: urothelial cell carcinoma and renal cell carcinoma. *Cancers* **12**, E439 (2020).
48. Li, B. & Dewey, C. N. RSEM: accurate transcript quantification from RNA-Seq data with or without a reference genome. *BMC Bioinformatics* **12**, 323 (2011).
49. Love, M. I., Huber, W. & Anders, S. Moderated estimation of fold change and dispersion for RNA-seq data with DESeq2. *Genome Biol.* **15**, 550 (2014).
50. Subramanian, A. et al. Gene set enrichment analysis: a knowledge-based approach for interpreting genome-wide expression profiles. *Proc. Natl Acad. Sci. USA* **102**, 15545–15550 (2005).
51. Junqueira, L. C., Bignolas, G. & Brentani, R. R. Picrosirius staining plus polarization microscopy, a specific method for collagen detection in tissue sections. *Histochem J.* **11**, 447–455 (1979).
52. Pratilas, C. A. et al. Genetic predictors of MEK dependence in non-small cell lung cancer. *Cancer Res.* **68**, 9375–9383 (2008).
53. Huber, W. et al. Orchestrating high-throughput genomic analysis with Bioconductor. *Nat. Methods* **12**, 115–121 (2015).

Acknowledgements

This work was supported by the Sidney Kimmel Center for Prostate and Urologic Cancers, the Thompson Family Foundation, Cycle for Survival, P50 CA221745, R01 CA234361, R01 CA229624-01, U54 OD020355, P01 CA221757-01A1, the Kauffhal Family Bladder Cancer Fund and the NIH/NCI Cancer Center Support Grant P30 CA008748. M.S. was funded by a research grant from Puma Biotechnology and Daiichi-Sankio. We thank Nancy Bouvier, Caitlin Bourque, Ramyasree Madupuri and Ritika Kundra of Marie-Josée and Henry R. Kravis Center for Molecular Oncology of Memorial Sloan Kettering Cancer Center for the management of MSK-IMPACT sequencing data; Dr. Elisa De Stanchina and the MSKCC Anti-tumor assessment core for in vivo studies of HER2-targeting agents; and Dr. Margaret Knowles for kindly providing MGHU3 bladder cancer cell line.

Author contributions

K.K., J.A.C. and D.B.S. designed the study. J.A.C. and D.B.S. supervised the project. K.K., A.J.H., V.M., S.J., K.N., C.H., B.G., Y.D., A.E., S.P.G., Z.C., J.J.H., I.S, M.S., E.C. and A.D.S. collected and analyzed lab data. W.H., I.O., J.G. and A.P. performed statistical and